A BILATERAL ELECTRO-HYDRAULIC ACTUATOR SYSTEM TO MEASURE DYNAMIC ANKLE JOINT STIFFNESS DURING UPRIGHT HUMAN STANCE

Shauna Forster

Department of Biomedical Engineering

McGill University

Montréal, Canada

DECEMBER 2003

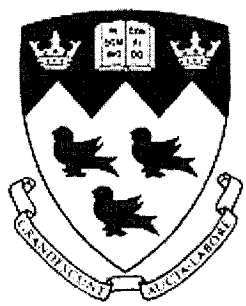

A thesis submitted to McGill University in partial fulfilment of the requirements of the degree of Master of Engineering.

Your file Votre référence
ISBN: 0-612-98526-1
Our file Notre référence
ISBN: 0-612-98526-1

Abstract

The role of the stretch reflex during upright stance remains unclear despite research that has been conducted to date. We have developed a bilateral electro-hydraulic actuator system to measure the dynamic joint stiffness of the human ankle during standing and help understand the role of the stretch reflex in the control of posture. The apparatus consists of two foot pedals that are each connected to an electro-hydraulic rotary actuator. Transducers were incorporated to measure the position and torque of each actuator, the angle of the ankle with respect to the foot plate, and the positions of the knee and hip. The experimental apparatus allows independent perturbations to be applied to each ankle. One subject was studied using the new apparatus and the results showed that reflexes are present during the perturbed standing task.

Résumé

Le rôle du réflexe d'étirement dans le contrôle de la posture est incertain en dépit des recherches effectuées à date. Un système d'activation électro-hydraulique bilatéral a été développé pour mesurer la raideur articulaire à la cheville humaine en position debout et pour déterminer le rôle du réflexe d'étirement. L'appareil consiste en deux pédales pour les pieds qui sont chacune connectées à un mécanisme rotatif hydraulique. Les transducteurs sont incorporés pour mesurer la position et le moment de torsion de chaque pédale, l'angle de la cheville par rapport à la pédale et les positions du genou et de la hanche. L'appareil expérimental permet des perturbations à être appliquées aux chevilles du sujet. Un sujet a été étudié en utilisant le nouvel appareil et les résultats démontrent que les réflexes de raideur sont présents en position debout avec perturbations.

Acknowledgements

I would first like to thank my supervisor, Robert E. Kearney, for his guidance during my time at McGill. The opportunity to develop an experimental apparatus has taught me a great deal in a variety of subject matters and helped expand my knowledge and capabilities. Thank you for this opportunity and thank you for helping me to achieve my goal.

Ross Wagner's continuous help along the way has been greatly appreciated (despite all the remarks about how little mechanical engineers know about electrical stuff). Thank you for being so generous with your time and expertise.

This project would not have been completed without the help of many mechanical engineering undergraduate students. A special thanks to Hank Leung, Ayman Afanah, Fadi Akache, Pascal Fallavollita, Ziad Nabhani, Becky Shaw, Alison Duncan, Fred Arseneault, Alex Whitehouse, and Erin Williamson.

Also, I would like to acknowledge the help of fellow REKlab students Mackenzie Baker, Przemek Bock, and Daniel Ludvig.

I would like to thank my wonderful family for their unconditional love and support, my special guy for always being there for me, and my awesome friends and roommates for providing much needed distractions from my studies.

This work was supported by the Canadian Institutes of Health Research (CIHR).

Table of Contents

Title Page 1
Abstract 2
Résumé 3
Acknowledgements 4
Table of Contents 5
Table of Figures 9
Table of Tables 11
1 Introduction 12
2 Background 14
2.1 Human Posture 14
2.1.1 Sensory mechanisms 14
2.1.2 Strategies 15
2.1.2.1 Hip Strategy 15
2.1.2.2 Ankle Strategy 15
2.2 Muscle Physiology 16
2.2.1 Structure 17
2.2.2 Neuromuscular Junction 18
2.2.3 Muscle Mechanics 19
2.2.4 Activation 19
2.2.4.1 Recruitment 20
2.2.4.2 Rate Encoding 20
2.2.5 Sensory Receptors 21
2.2.5.1 Muscle Spindles 22
2.2.5.2 Golgi Tendon Organs 23
2.3 Nervous System 24
2.3.1 Central Nervous System 24
2.3.1.1 Spinal Cord 25
2.3.1.2 Brain Stem 26

2.3.1.3 Basal Ganglia 27
2.3.1.4 Sensorimotor Cortex 27
2.3.1.5 Cerebellum 28
2.3.2 Peripheral Nervous System 28
2.3.3 Pathways 28
2.4 Motor Control 29
2.4.1 Voluntary Movement 29
2.4.2 Reflexes 29
2.4.2.1 Stretch Reflex 30
2.4.2.2 Inverse Stretch Reflex 31
2.4.2.3 Long Loop Reflex 32
2.4.2.4 H-Reflex 32
2.5 Ankle Joint 32
2.5.1 Bones 32
2.5.2 Muscles 34
2.6 Joint Stiffness 35
2.6.1 Intrinsic and Reflex Contributions 36
2.6.2 Separation of Intrinsic and Reflex Components 36
2.6.3 Parallel Cascade System Identification 37
2.6.3.1 Non-Parametric Model 37
2.6.3.2 Parametric Model 38
2.6.4 Closed-Loop Identification 40
2.7 Postural Control 41
2.7.1 Forceplate Systems 42
2.7.2 Translating and Rotating Platforms 43
2.7.3 Inverted Pendulums 45
2.8 Summary 49
3 Methods 52
3.1 Design Requirements 52
3.2 Experimental Apparatus 54
3.2.1 Actuator and Servo-Valve 55

3.2.2 Safety Mechanisms 56
3.3 Transducers and Signal Conditioning 57
3.3.1 Torque 58
3.3.2 Position 58
3.3.3 EMG 59
3.3.4 Hip and Knee Angles 59
3.3.5 Heel Lift 60
3.3.6. Data Acquisition 60
3.4 Actuator Control 61
3.5 Experimental Protocol 61
4 Performance Evaluation 63
4.1 Pulse Perturbations 63
4.2 Random Perturbations 66
4.3 Frequency Response 68
4.4 Summary 69
5 Experimental Results 71
5.1 Data Analysis 71
5.2 Pulse Trials 72
5.2.1 Case 1 73
5.2.2 Case 2 75
5.2.3 Case 3 76
5.3 Sequence Trials 79
5.3.1 Case 1 80
5.3.2 Case 2 82
5.3.3 Case 3 83
5.4 Dynamic Stiffness 84
5.5 Summary 87
6 Discussion 91
6.1 Results 91
6.3 Future Work 92
6.4 Conclusion 94

7 References 95
8 Appendices 101
Appendix A - Controller Version 1 Block Diagram 102
Appendix B - Controller Version 2 Block Diagram 103
Appendix C - Controller Version 3 Block Diagram 104
Appendix D - Controller Version 4 Block Diagram 105
Appendix E - Actuatory Assembly 106
Appendix F - Data Sheet for Rotary Actuator 107
Appendix G - Data Sheet for Servo-Valve 111
Appendix H - Circuit Diagram for Servo-Valve Module 123
Appendix I - Data Sheet for Torque Transducer 125
Appendix J - Circuit Diagram for Torque Transducer Module 128
Appendix K - Data Sheet for Potentiometer 129
Appendix L - Circuit Diagram for Potentiometer Module 130
Appendix M - Data Sheet for EMG System 131
Appendix N - Data Sheet for EMG Electrodes 133
Appendix O - Data Sheet for Angular Sensors 134
Appendix P - Data Sheet for Ultrasonic Sensor 136
Appendix Q – Actuator Coupling 137
Appendix R – Safety Cam 138
Appendix S - Foot Pedal End 139
Appendix T – Torque Transducer / Foot Pedal Coupling 140
Appendix U – Research Ethics Certificate 141

Table of Figures

Figure 1 Skeletal muscle structure (from [41]) 18
Figure 2 As the stimulus frequency is increased, muscle force goes from a twitch, to unfused tetanus (oscillating at the same frequency as the stimulus), to fused tetanus (from [25]) 21
Figure 3 Muscle spindle and Golgi tendon organ (from [41]) 22
Figure 4 Organization of the motor system (modified from [15]) 25
Figure 5 Section of spinal cord, ventral view (from [41]) 26
Figure 6 Motor areas of the sensorimotor cortex (from [25]) 27
Figure 7 Muscle proprioceptors and their reflex pathways (from [25]) 30
Figure 8 Anterior view of the ankle (from [32]) 33
Figure 9 (a) Plantarflexors of the foot (b) Dorsiflexors of the foot (from [14]) ... 35
Figure 10 Dynamic Ankle Stiffness 36
Figure 11 Parallel cascade identification structure; P, TQ, and EMG_R are experimental data; TQ_I , TQ_R , and $\hat{TQ}$ represent predicted responses; PTQ_{IRF}, TQP_{IRF}, VTQ_{IRF}, and VGS_{IRF} represent non-parametric descriptions; parametric models are then used to fit TQP_{IRF} , and VTQ_{IRF} (from [26]). ... 39
Figure 12 Block diagram of closed-loop system (modified from [40]) 41
Figure 13 Inverted pendulum model, where Φ represents the sway angle, h is the height of the center of mass, and mg is the force of gravity. 46
Figure 14 Inverted pendulum apparatus (from [22]) 49
Figure 15 Photograph of experimental apparatus 54
Figure 16 Schematic of experimental apparatus 55
Figure 17 Pulse response with proportional controller 63
Figure 18 Pulse response with a direction dependant PID controller 65
Figure 19 Position input and actuator outputs for a random stimulus without subject 66
Figure 20 Gain of right actuator controller versus input command voltage 67

Figure 21 Position input and actuator outputs for a random stimulus without subject 68
Figure 22 Frequency responses of the left and right actuators with subject 69
Figure 23 Sample pulse data, 60 s trial for one ankle 72
Figure 24 Pulse trial: left ankle dorsiflexed, right ankle stationary 73
Figure 25 Pulse trial: left ankle stationary, right ankle dorsiflexed 74
Figure 26 Pulse trial: both ankles dorsiflexed 75
Figure 27 Pulse trial: left ankle dorsiflexed, right ankle plantarflexed 76
Figure 28 Pulse trial: left ankle plantarflexed, right ankle dorsiflexed 77
Figure 29 Sample sequence data, 64 s trial for one ankle 79
Figure 30 Sequence trial: left ankle stimulated, right ankle stationary 80
Figure 31 Pulse trial: left ankle stationary, right ankle stimulated 81
Figure 32 Sequence trial: ankles are stimulated with the same signal 82
Figure 33 Sequence trial: ankles are stimulated with opposite signals 83
Figure 34 Example of intrinsic compliance (TQP_{IRF}) and reflex stiffness (VTQ_{IRF}) obtained from Case 2, left ankle, sequence data 85

Table of Tables

Table 1 Parameters of the intrinsic compliance parametric fit given in equation 2 (Section 2.6.3.2); values are the average parameters of the 4 trials plus or minus the standard deviation 85

Table 2 Parameters of the reflex stiffness parametric fit given in equation 3 (Section 2.6.3.2); values are the average parameters of the 4 trials plus or minus the standard deviation 86

Table 3 Relative contributions of intrinsic and reflex to total torque produced (%VAF given by equation 1 in Section 2.6.3.1); values are the average of the 4 trials plus or minus the standard deviation 86

1 Introduction

In everyday life, humans are constantly in motion. We run, walk, talk, write, dance, and perform countless other actions. Some activities involve more complex motions but all require coordination of the musculoskeletal system. The brain sends signals via the nervous system to the muscles causing them to contract or relax appropriately as needed to accomplish the desired task. Although some motions seem complex others may seem very simple. Standing, for instance, is something people do every day without really thinking too much about it.

During upright human stance, the body sways slightly forward and backward. The muscles of the legs and trunk relax and contract to maintain the body's center of mass in a stable position. Normally, these actions are involuntary. The brain controls the body's posture without conscious thought.

The brain receives information about body position from the visual, vestibular and somatosensory systems. It processes this information and then sends signals to the appropriate muscles to control body position. Posture may also be controlled by muscle reflexes [9, 31]. The stretch reflex causes a muscle to contract when it has been stretched. It is hypothesized that the stretch reflex plays an important role in the control of posture.

During quiet stance the body behaves as an inverted pendulum swaying in the sagital plane about the ankle joint. When the body sways forward, the ankle plantarflexors are stretched and respond by contracting to bring the body back to its upright position. Contrarily, when the body sways backward, the ankle dorsiflexors are stretched and contract to bring the body back to its upright position.

One way to determine the role of reflexes during upright stance is to characterize dynamic ankle stiffness. Dynamic stiffness consists of an intrinsic component due to the mechanical properties of the joint, passive tissue, and active muscle, and a reflex component due to the changes in muscle activation mediated by the stretch reflex. For this reason, we have developed an apparatus to measure dynamic ankle stiffness during upright stance in humans.

The new experimental apparatus is a bilateral electro-hydraulic actuator system. It consists of two actuators each attached to a foot pedal. The subject stands with one foot on each pedal, whose axes rotate about the same axes as the ankle joint. Perturbations are applied separately to the subject's left and right ankles. The position and torque of each pedal is measured and electromyographs (EMGs) of the gastrocnemius (GS) and the tibialis anterior (TA) of each leg are recorded. System identification techniques use the data acquired to separate the intrinsic and reflex contributions to dynamic ankle stiffness.

This thesis is divided into six chapters, with chapter one as the introduction. Chapter two covers background information on the nervous system, muscle physiology, and the ankle joint as well as reviewing the literature on postural control and human standing. Chapter three covers the design requirements and construction of the experimental apparatus, in addition to the experimental protocol. Chapter four contains a performance evaluation of the new apparatus. The results of a preliminary study are reported in chapter five and discussed in chapter six along with future work.

2 Background

This chapter describes the basic mechanisms of postural control and reviews the literature related to postural control and stretch reflexes. The physiology of muscle and the neuromuscular system is also described briefly. Information in Sections 2.1-2.5 was taken from the following textbooks: [3], [15], [16], [27], and [43].

2.1 Human Posture

The control of human posture is complex. The central nervous system (CNS) and the peripheral nervous system (PNS) work synergistically to control the musculoskeletal system to maintain a safe body posture. The nervous system takes in sensory information from the body and sends out signals to the muscles to maintain the desired body position. While standing, the muscles of the trunk and legs are continuously contracting and relaxing to prevent the body from swaying excessively.

2.1.1 Sensory mechanisms

In order to determine where the body is with respect to its equilibrium position, the CNS uses inputs from the visual, vestibular, and somatosensory systems. The somatosensory system includes many types of sensory receptors in the body, such as touch, pressure, temperature, pain, and body position. Joint, muscle, and tendon sensory information are referred to collectively as proprioception. The visual, vestibular, and somatosensory systems all have different threshold frequencies for detecting sway [33]. Proprioception contributes most at frequencies greater than 1 Hz [6]. Nashner [33] suggested that

during quiet standing, subjects sway at a frequency near the threshold boundary of the senses being used.

2.1.2 Strategies

When an internal disturbance, such as breathing, or an external disturbance, such as a force applied to the body, unbalances a human's posture, the neuromuscular system must act through the biological mechanisms of the body to restabilize. As outlined above, errors in body position are detected by the visual, vestibular, and somatosensory systems. The central nervous system processes these errors and devises a strategy to regain the desired body positioning. Knee movements are very limited during standing and therefore, two main strategies exist: (1) the hip strategy and (2) the ankle strategy [32].

2.1.2.1 Hip Strategy

In anterior posterior movement, the response strategy chosen by the nervous system depends on the magnitude of the perturbation. For large perturbations in the sagital plane, large trunk rotations are required to maintain posture. These are achieved in a hip strategy that involves large rotations about the hip and smaller rotations about the ankle joint [32]. The hip strategy is also used if there are physical constraints which limit the ankle's ability to exert torque [32]. For example, a support surface that is shorter than the foot.

2.1.2.2 Ankle Strategy

For smaller perturbations in the sagital plane, the ankle strategy is used. Movements to correct posture are limited to the ankle joint, with the hip and knee angles staying relatively constant [32]. Therefore, with the ankle strategy, the

body can be modeled as an inverted pendulum. The ankle strategy is also invoked when the effectiveness of the hip strategy is constrained [32]. The forces that can be exerted by the thigh and hip muscles are limited by the shear force at the support surface [32]. For example, if a subject is standing on ice, the amount of shear force that can be applied to the support surface is limited by the low friction of ice. Under these conditions, subjects will tend to favour the ankle strategy to regain their equilibrium posture.

The ankle and hip strategies are not discrete. They represent a continuum with boundaries delineated by postural stability. With knees fully extended, the ankle-hip plane contains all stable standing postures with the two axes being pure ankle rotation (no hip movement) and pure hip rotation (no ankle movement) [32].

Kuo et al. showed that use of the hip strategy increases when the support surface is sway-referenced, therefore disrupting somatosensory inputs [21]. This finding is interesting because it indicates that disruptions of the somatosensory inputs of the foot induce more sway about the hips than the ankles. Kuo et al. used a multivariate model which integrates sensory feedback and produces different feedback commands for each joint. With this model it was found that vestibular input contributes greatly to hip motion [21].

2.2 Muscle Physiology

In the human body, there are three types of muscle tissue: skeletal muscle, smooth muscle, and cardiac muscle. Skeletal muscle attaches to bones and is responsible for body movements. The structure and function of skeletal muscle is discussed below.

2.2.1 Structure

Skeletal muscle is composed of muscle fibers that are up to 20 cm long and have diameters in the range of 10 to 100 μm [43]. Muscle fibers are composed of myofibrils, which are in turn composed of thick and thin filaments that give skeletal muscle its striated appearance. One unit of the repeating pattern formed by the thick and thin filaments is called a sarcomere. The sarcomeres are separated by Z-disks. The thin filaments are pairs of the contractile protein actin arranged in a helix. Along the groove of the helix lies a protein called tropomyosin and attached to it are the proteins troponin. Each thin filament is attached on one side to the Z-disk. The thick filaments are formed by approximately 250 molecules of the contractile protein myosin [3]. Each myosin molecule has two tails with globular heads. These heads contain ATPases, providing energy for muscle contractions, and are referred to as the cross bridges which link the thick and thin filaments.

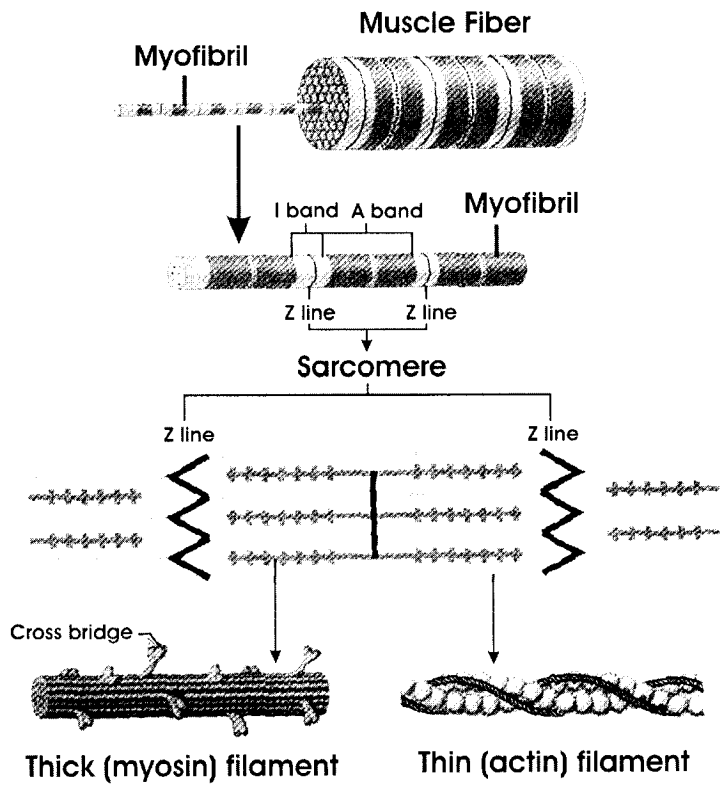

Figure 1 Skeletal muscle structure (from [43])

Each individual muscle fiber is a single cell surrounded by a membrane and containing an aqueous solution of organic and inorganic ions, nuclei, and mitochondria. The myofibrils are enveloped by the sarcoplasmic reticulum. Interweaved among the myofibrils are the transverse tubules (T-tubules) that communicate only with the extracellular space.

2.2.2 Neuromuscular Junction

Muscles are innervated by motor neurons. The synapse between a motor neuron and a muscle fiber is called the neuromuscular junction. The resting membrane potential of a neuron is approximately -70 mV [43]. An action potential involves a brief and rapid increase in membrane potential due to an

increase in permeability to Na^+ ions. The resulting Na^+ influx causes a depolarization and the membrane potential will reach +50 mV [43].

An action potential in the motor neuron causes the release of acetylcholine (ACh) from the presynaptic terminal. When the ACh binds to the receptors in the muscle, a depolarization occurs and causes the action potential to propagate through the muscle fiber via the T-tubules.

2.2.3 Muscle Mechanics

During contraction, action of the cross bridges causes the thick and thin filaments to move past each other, causing the muscle to shorten. This process is known as Huxley's sliding filament theory [27].

Once the action potential propagates into the T-tubules, a release of Ca^{2+} is triggered in the sarcoplasmic reticulum. The Ca^{2+} binds to the troponin and the troponin stops blocking the cross bridge binding sites on the actin. Energized myosin cross bridges on the thick filaments then bind to actin. The cross bridges pull the thin filament over the thick filament. Adenosine triphosphate (ATP) then binds to the myosin and causes the cross bridges to unlink from the actin. The ATP reenergizes the cross bridges and the cycle starts again. When the action potential stops, Ca^{2+} is transported back into the sarcoplasmic reticulum and the cross bridge binding sites on the actin are once again blocked, causing the muscle to relax. The above description of the steps involved in muscle contraction was found in [43].

2.2.4 Activation

Each muscle fiber is activated by one motor neuron. However, a motor neuron can activate many muscle fibers. A motor neuron together with the muscle fibers it activates is called a motor unit. If an action potential occurs in a motor neuron, all the fibers in its motor unit will be stimulated to contract [43].

Tension is the force developed in the muscle when the muscle fibers contract. The external force that acts on the muscle is referred to as the load. Muscle tension depends on the number of muscle fibers activated and the amount of force produced by each muscle fiber [43]. Therefore, force can be modulated in two ways: recruitment and rate modulation [16].

2.2.4.1 Recruitment

Motor units are recruited based on size. The weakest, slow-fatiguing units are recruited first and the largest, fast-fatiguing units recruited last; the reason being that the smallest neurons have the lowest activation thresholds [16]. The size principle allows higher centers to only determine the level of synaptic excitation and not select specific motor units to produce a desired force [16].

2.2.4.2 Rate Encoding

The second method of modulating force is through rate encoding. An increased firing rate by a motor neuron causes an increase in force generated by the muscle fibers [16]. Low frequency stimuli causes individual muscle twitches and, as the frequency increases, the twitches do not have time to decay and they begin to summate. Once unfused tetanus occurs, the muscle force produced maintains a constant level [27].

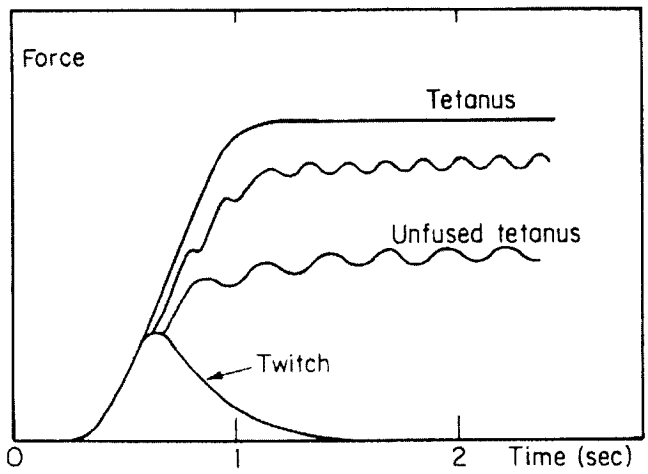

Figure 2 As the stimulus frequency is increased, muscle force goes from a twitch, to unfused tetanus (oscillating at the same frequency as the stimulus), to fused tetanus (from [27])

2.2.5 Sensory Receptors

Afferent input to motor neurons comes from the CNS and from sensory mechanisms in the muscle itself, other surrounding muscles, tendons, joints, and the skin surface [43]. The most important sensory receptors are muscle spindles and Golgi tendon organs.

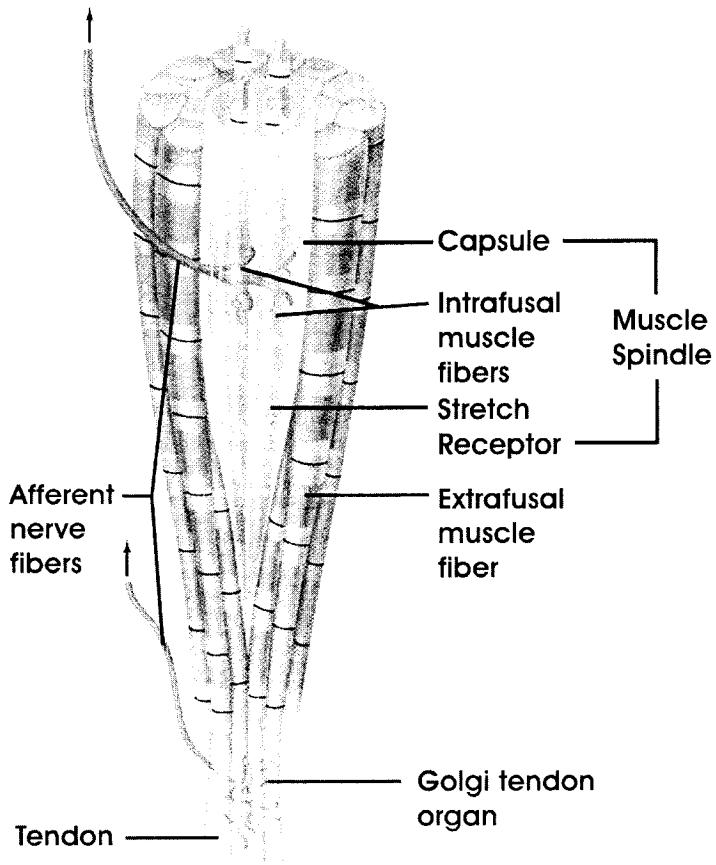

Figure 3 Muscle spindle and Golgi tendon organ (from [43])

2.2.5.1 Muscle Spindles

Muscle spindles are stretch receptors which monitor muscle length. They consist of afferent nerve endings wrapped around a modified muscle fiber and enclosed in connective tissue. Muscle spindles are located in the muscle itself and run parallel to regular muscle fibers. Stretch of the muscle results in an increase in firing rate of the spindles whereas shortening of the muscle reduces the firing rate [43].

Muscle spindles consist of two different types of intrafusal fibers: nuclear bag fibers and nuclear chain fibers. The nuclear bag fiber has an expanded elastic

region in their center and a dense aggregate of nuclei whereas the nuclear chain fibers have a narrower elastic region and fewer nuclei [43]. Both types of fibers have contractile elements at both ends. A spindle normally consists of one or two bag fibers and five to twelve chain fibers [43].

Alpha motor neurons control the extrafusal muscle fibers. When these are active, the muscle shortens and may cause the muscle spindle intrafusal fibers to become slack and stop firing. To prevent this, both ends of the intrafusal fiber are stimulated to contract to maintain tension in the stretch receptors. The intrafusal fibers are activated by gamma motor neurons and therefore this process is referred to as alpha-gamma coactivation [43]. Therefore, the brain can control the sensitivity of the muscles spindles through gamma motor activity.

Muscle spindles have two types of afferent innervation. First, Group Ia afferents are rapidly conducting fibers that terminate around the central elastic regions of the nuclear bag and chain fibers. Second, the Group II afferents conduct more slowly and terminate at the flower-spray receptors located on both sides of the central elastic region [16]. Both types of fibers enter the spinal cord through the dorsal roots. The Group Ia fibers synapse directly and indirectly, through Ia interneurons, to the alpha motorneurons in the ventral horn. The Group II fibers form a polysynaptic connection to the same alpha motorneurons. Group Ia and II fibers have conduction speeds of 90 m/s and 50 m/s respectively [43].

2.2.5.2 Golgi Tendon Organs

Muscle tension is encoded by Golgi tendon organs. These consist of afferent nerve endings that are wrapped around collagen bundles and enclosed in connective tissue [43]. They are located in the tendon near the junction with the

muscle. Golgi tendon organs fire in response to stretch generated when a muscle contracts [43].

Golgi tendon organs are innervated by Group Ib afferents which have a conduction speed of 80 m/s [43]. The fibers enter the dorsal root and form a polysynaptic inhibitory connection with the alpha motorneurons of the same muscle [16]. Therefore, the more the muscle is stretched, the less tension it will generate due to the inhibitory signal.

Muscle spindles are in parallel with the muscle fibers whereas Golgi tendon organs are located in series with the muscle [43]. They are both active during passive stretch and voluntary contraction [16].

2.3 Nervous System

As mentioned above, the CNS and PNS both play crucial roles in neuromuscular control. The CNS consists of the brain and spinal cord; the PNS consists of all nerve fibers that run from the CNS to the body's receptors and effectors. Motor control may involve simple reflex pathways or more complex commands generated in the CNS which propagate through the PNS to the muscles. The CNS and PNS together are comprised of millions of neurons [43].

2.3.1 Central Nervous System

The CNS contains five main structures for motor control: the spinal cord, the brain stem, the basal ganglia, the sensorimotor cortex, and the cerebellum [16]. The organization of these systems is shown in Figure 4 and described in the following sections.

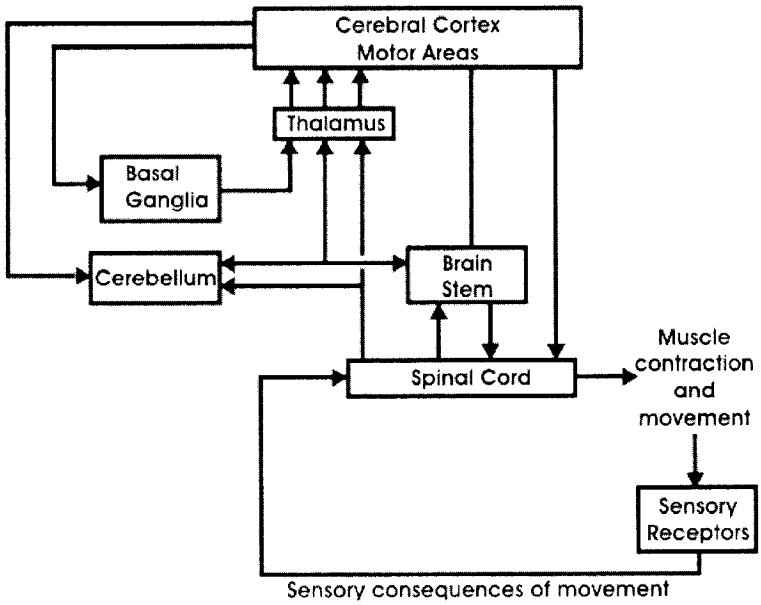

Figure 4 Organization of the motor system (modified from [16])

2.3.1.1 Spinal Cord

The spinal cord is contained in the vertebral column and contains grey matter and white matter. Grey matter is comprised of interneurons, cell bodies and dendrites of efferent neurons, fibers of afferent neurons and glial cells; white matter is comprised of interneuron axons which run longitudinally through the spinal cord [43]. Peripheral afferent nerve fibers enter the spinal cord through the dorsal roots and the efferent nerves leave the cord via the ventral roots [43]

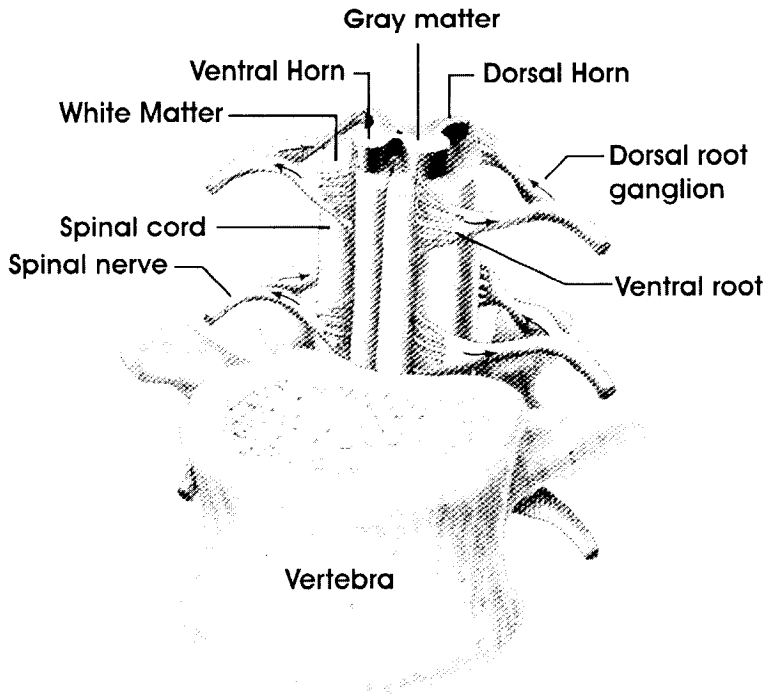

Figure 5 Section of spinal cord, ventral view (from [43])

The spinal cord comprises 31 segments: 8 cervical, 12 thoracic, 5 lumbar, 5 sacral and 1 coccygeal [43]. When the spinal cord is severed just below the brain stem, many important motor abilities are retained. The stretch reflex, described in Section 2.4.2.1, is still present, along with the withdrawal reflex, where a painful stimulus causes the affected limb to withdraw [27].

2.3.1.2 Brain Stem

The brain stem helps regulate the motor circuits of the spinal cord. It coordinates visual, vestibular, and somatosensory information to aid in the control of posture [3].

2.3.1.3 Basal Ganglia

The basal ganglia are a group of specialized nerve cells located in the upper portion of the brain stem. They help the brain execute high-level motor commands and adjust the amplitudes of the motor system to achieve the desired results [3].

2.3.1.4 Sensorimotor Cortex

The area of the cerebral cortex dedicated to motor control is known as the sensorimotor cortex. The sensorimotor cortex projects to the spinal cord through the corticospinal tract and through the brain stem [43]. It helps to plan and coordinate complicated movements [3].

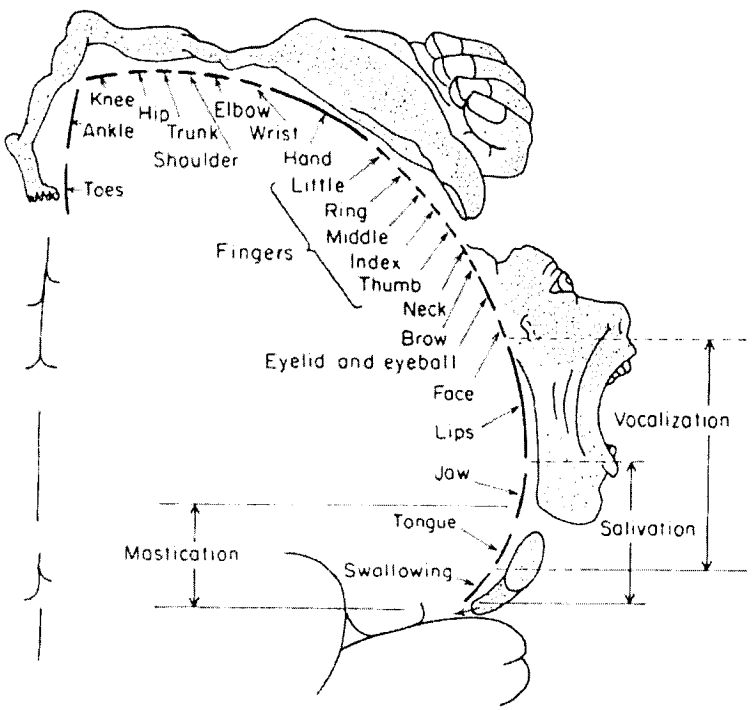

Figure 6 Motor areas of the sensorimotor cortex (from [27])

2.3.1.5 Cerebellum

The cerebellum is located posterior to the brain stem. It compares descending motor commands from the cerebral cortex with sensory information from the spinal cord and brain stem to improve the accuracy of body movements [3].

2.3.2 Peripheral Nervous System

The PNS consists of forty-three pairs of nerves containing both efferent and afferent fibers [43]. Afferent fibers transfer information from sensory receptors to the CNS and efferent fibers carry signals from the CNS to muscles, glands and sense organs [43].

2.3.3 Pathways

Information on posture and movements generated in various areas of the brain is transmitted through two types of descending pathways: corticospinal pathways and brainstem pathways [43]. The corticospinal pathway originates in the sensorimotor cortex and terminates in the spinal cord. Most corticospinal pathways cross the spinal cord and therefore the muscles on one side of the body are controlled by the opposite side of the brain. The brainstem pathways originate in the brainstem and terminate in the spinal cord. Both pathways can send excitatory or inhibitory signals and can synapse on alpha and gamma motorneurons as well as interneurons [43].

2.4 Motor Control

Movements of the body can be broken down into two categories: voluntary movements and reflex movements. Voluntary movements differ from reflex movements in that they have a purpose, they become faster and more efficient with learning, and an external stimulus is not necessary to evoke them [3].

2.4.1 Voluntary Movement

Voluntary movements have three phases: target identification, plan of action, and execution of the movement [3]. These phases are controlled by different areas of the cerebral cortex and motor commands are sent via the descending pathways to the motorneurons.

2.4.2 Reflexes

There are several types of reflexes present in humans. Short latency responses, such as the stretch reflex, tend to peak 50 ms after stimulus whereas medium and long latency responses peak at 80 ms and 100 ms respectively [3].

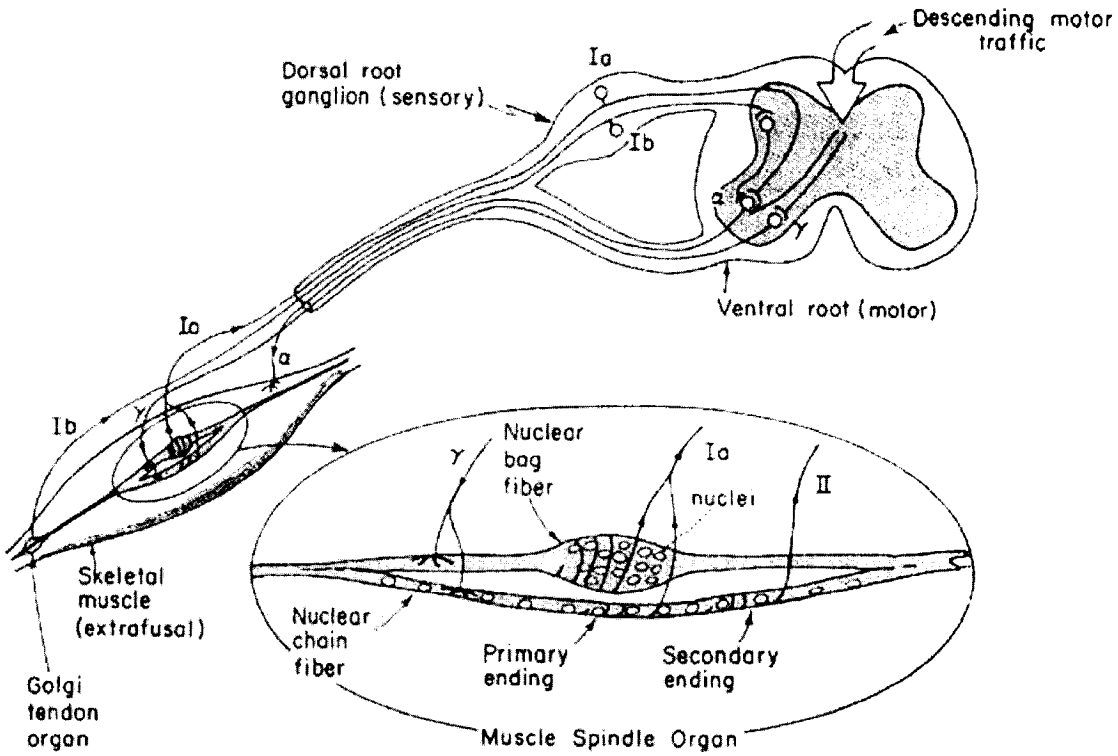

Figure 7 Muscle proprioceptors and their reflex pathways (from [27])

2.4.2.1 Stretch Reflex

The stretch reflex occurs when a muscle is stretched. The muscle spindle fires an afferent signal that directly stimulates the motor neurons causing the muscle to contract. Group Ia afferents form monosynaptic excitatory connections with motorneurons of the stretched muscle and of synergistic muscles [16]. Group Ia afferents also form polysynaptic inhibitory connections to antagonistic muscles; this pathway is referred to as reciprocal inhibition [16]. Group II afferents form polysynaptic excitatory connections with motorneurons of the stretched muscle [16].

The stretch or myotatic reflex has two components: 1) a short, quick, phasic contraction resulting from the dynamic change in muscle length, and 2) a

long, weak, tonic contraction resulting from the static muscle stretch at the new length [16]. The Group Ia afferents respond to both the static and dynamic components of muscle stretch whereas Group II afferents respond less to dynamic stimuli [16].

The stretch reflex can be modulated in several ways. Alpha-gamma coactivation, discussed in section 2.2.5.1, helps to maintain muscle spindle sensitivity during muscle contraction. But, gamma motor neurons can be controlled independently. This process is called fusimotor control and is used to fine tune muscle spindle sensitivity for specific tasks [16]. A second method of modulating the stretch reflex is through presynaptic inhibition [3]. This process involves interneurons that form a presynaptic synapse to Group Ia afferents and decrease the amount of neurotransmitter released by the Ia afferent to the motorneuron [43]. A final method of stretch reflex modulation is through Renshaw cells. These interneurons receive input from motorneurons and inhibit the same motorneuron. They are controlled by descending signals from the CNS. Renshaw cells also suppress the Ia inhibitory interneurons to the antagonistic muscle [16]. This process is called recurrent inhibition [16].

2.4.2.2 Inverse Stretch Reflex

The inverse stretch reflex is a polysynaptic inhibitory reflex [43]. The stretching of a muscle will activate the Golgi tendon organs, which encode muscle tension. The action potentials from the Golgi tendon organs travel along Group Ib afferents to the spinal cord where, through the actions of inhibitory interneurons, they tend to suppress activity of the alpha motorneurons of the same muscle [16]. The Group II projections may also form an excitatory synapse with the motorneurons of the antagonistic muscles [16].

2.4.2.3 Long Loop Reflex

Long loop responses lie somewhere between short latency reflexes and voluntary control. They occur at a supraspinal level and are mediated by the sensorimotor cortex [3]. Long loop reflexes compare the current position of the limb with the desired position, originally set out by the motor cortex, and therefore work to return the limb to the proper position [3].

2.4.2.4 H-Reflex

The Hoffman reflex, or H-reflex, occurs when Group Ia fibers are stimulated electrically through the skin [3]. It is similar to the stretch reflex but without a natural stretch as the stimulus. The electrical stimulation will result in two responses. The first is due to the stimulus travelling directly to the muscle along the motorneuron and the second is due to the stimulus travelling up the Group Ia afferent and evoking a monosynaptic response in the same motorneurons [3].

2.5 Ankle Joint

The bones of the lower leg and foot articulate to form a hinge joint at the ankle. Movements of this joint are controlled by a few large muscles as well as numerous smaller ones in the lower leg and foot.

2.5.1 Bones

The lower leg consists of two bones: the tibia and the fibula. The tibia transmits most of the body weight since the fibula does not extend all the way to

the knee and it articulates at the side of the ankle. At its distal end, the tibia expands to form the medial malleolus and similarly, the fibula expands to form the lateral malleolus. The medial surface of the lateral malleolus as well as the lateral surface of the medial malleolus form an articulation surface for the ankle joint. The talus, a bone on the upper part of the foot, articulates between the medial and lateral malleoli creating a hinge joint which dorisflexes and plantarflexes the foot. The axis of rotation of the ankle joint passes through the lateral and medial malleoli. The talus rests on the calcaneus bone, or heel bone, whose posterior projection is the site of attachment of several plantarflexor muscles. The above description of the ankle joint was obtained from [15].

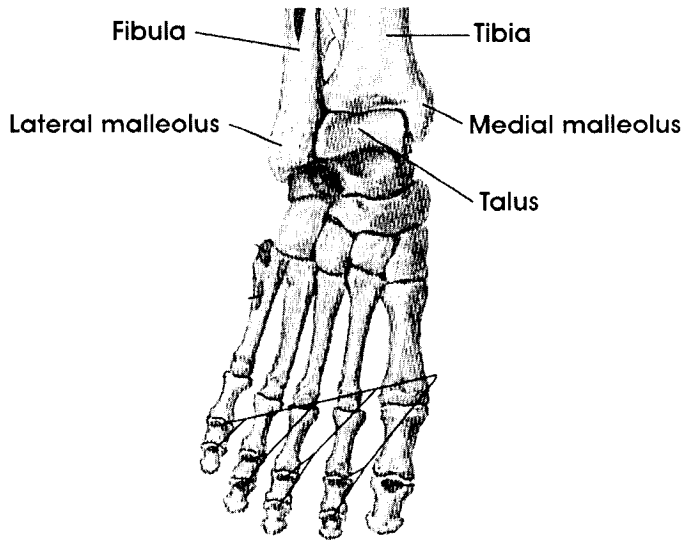

Figure 8 Anterior view of the ankle (from [34])

2.5.2 Muscles

There are three main muscles which act upon the ankle joint: the gastrocemius (GS), the soleus, and the tibialis anterior (TA).

The GS and the soleus both act to plantarflex the foot. The medial and lateral gastrocnemii originate at the medial and lateral femoral condyles respectively. The soleus originates at the posterior surface of the tibia and fibula. They both join to form the Achilles tendon which inserts on the calcaneal surface at the back of the heel [15]. Since the GS originates above the knee it also plays a role in knee flexion whereas the soleus only acts in ankle plantarflexion. Both the GS and soleus are innervated by the tibial nerve [38]. Other small plantarflexor muscles include the flexor hallucis longus, the flexor digitorum longus, the tibialis posterior, the fibularis longus, and the fibularis brevis [15].

The TA, originating from the lateral surface of the head of the tibia and inserting on the medial side of the foot, acts to dorsiflex and invert the foot [15]. The TA is innervated by the deep peroneal nerve [38]. Other small dorsiflexor muscles include the extensor digitorum longus, the fibularis tertius, and the extensor hallucis longus [15].

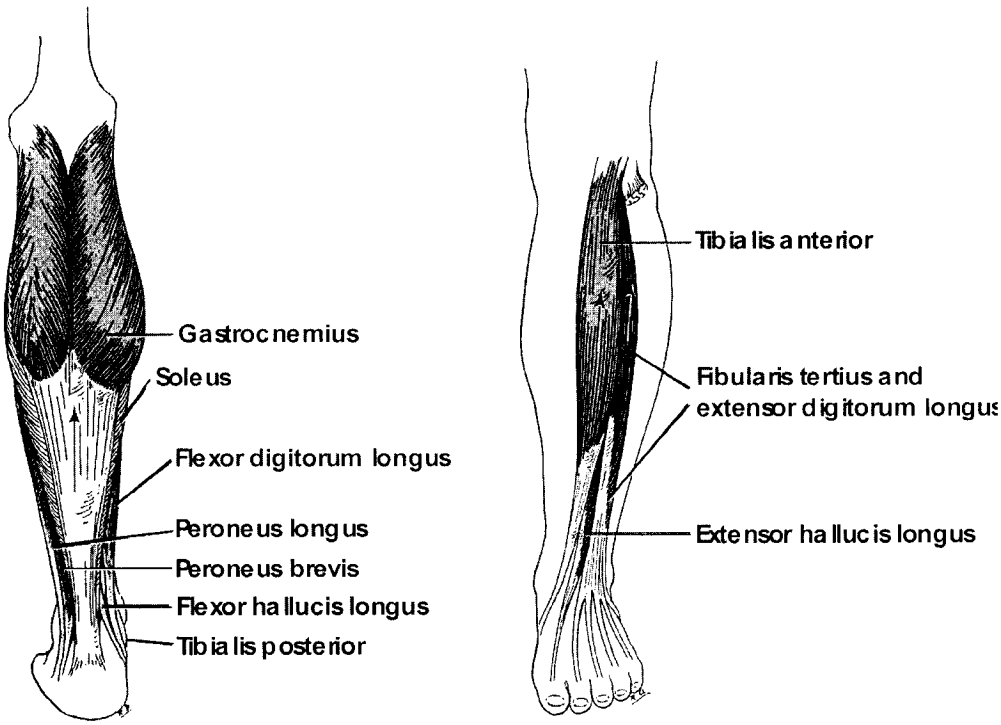

Figure 9 (a) Plantarflexors of the foot (b) Dorsiflexors of the foot (from [15])

The tibialis anterior and posterior, the flexor hallucis longus and digitorum longus, and the extensor hallucis longus all work to invert the foot [15]. Eversion of the foot is achieved by the peroneus longus, brevis, and tertius, as well as the extensor digitorum longus [15].

Flexion of the toes is done by the flexor digitorum longus and hallucis longus whereas the extensor digitorum longus and hallucis longus work to extend the toes [15].

2.6 Joint Stiffness

Dynamic joint stiffness is defined as the relation between the angular position and torque acting about a joint [28]. Joint stiffness is important in

postural control because it resists the external perturbations before the muscles have time to contract voluntarily. Dynamic joint stiffness has two components: intrinsic and reflex.

The intrinsic component of joint stiffness is due to the mechanical properties of the joint, passive tissue, and active muscle; the reflex component is due to changes in muscle activation mediated by the stretch reflex [28].

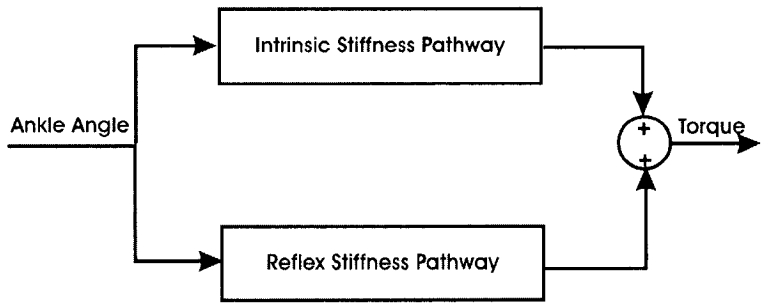

Figure 10 Dynamic Ankle Stiffness

2.6.1 Intrinsic and Reflex Contributions

Mirbaheri et al. [28] used a parallel-cascade system identification method to study the variation of the intrinsic and reflex contributions in supine subjects. They found that intrinsic stiffness increased with contraction level whereas reflex stiffness was maximal during low contractions. Both intrinsic and reflex stiffness increased as ankle position moved from plantarflexion to dorsiflexion.

2.6.2 Separation of Intrinsic and Reflex Components

Several methods are presently used to separate intrinsic and reflex components of muscle torque. These include electrical stimulation [30], anesthesia [10], and system identification techniques [20, 42]. Our laboratory has

made extensive use of a non-linear, parallel cascade identification scheme [20] to determine the relative contributions of intrinsic and reflex mechanisms in normal subjects and neurological patients. However, these experiments have all been conducted with subjects lying prone with no requirement to maintain postural stability.

2.6.3 Parallel Cascade System Identification

The nonlinear, parallel cascade method described by Kearney et al. [20] is described below.

2.6.3.1 Non-Parametric Model

Intrinsic and reflex contributions to total torque are separated using the parallel-cascade identification described in [20]. The method is outlined here and shown in figure 11:

1) Intrinsic dynamics are estimated by a linear impulse response function (IRF) relating position and torque (PTQ_{IRF}). The length of the intrinsic IRF is less than the reflex delay, approximately 40ms, and therefore reflex mechanisms can not influence the estimate. The intrinsic compliance (TQP_{IRF}) is the dynamic inverse of the intrinsic IRF.
2) Reflex dynamics are estimated using a Hammerstein procedure. The position is differentiated and the resulting velocity is passed through a half-wave rectifier. The reflex IRF relates velocity and torque (VTQ_{IRF}). The latency of the reflex IRF provides an estimate of the conduction delay of the reflex pathway. The length of the reflex IRF is chosen so that the IRF decays to zero.

3) The intrinsic and reflex torques are then convolved with the experimental input to obtain the predicted intrinsic and reflex torques. The percentage variance accounted for (%VAF) is used to assess the intrinsic and reflex IRFs, where TQ_{obs} is the observed torque and TQ_{pred} is the torque predicted by the IRF.

$$\%VAF = 100 * (1 - \frac{\sum^{N} (TQ_{obs} - TQ_{pred})^2}{\sum^{N} TQ_{obs}^{\ 2}}) \quad (1)$$

2.6.3.2 Parametric Model

Parametric models are used to describe the intrinsic compliance as well as the reflex stiffness.

The intrinsic compliance is fitted with the damped vibration model:

$$TQP_{IRF}(s) = \frac{P(s)}{TQ_{INT}(s)} = \frac{1}{Is^2 + Bs + K} \quad (2)$$

Where P is the joint angle, TQ_{INT} is the intrinsic torque, I is the inertial parameter, B is the viscous parameter, K is the elastic parameter, and s is the LaPlace variable.

The reflex stiffness is fitted with the following third-order model IRF:

$$VGS_{IRF}(s) = \frac{TQ_{REF}(s)}{V(s)} = \frac{G_R \omega_n^2 p}{(s^2 + 2\xi\omega_n s + \omega_n^2)(s + p)} e^{-s\tau} \quad (3)$$

Where V is the joint angular velocity, TQ_{REF} is the reflex torque, G_R is the reflex gain, ω_n is the second order natural frequency, ξ is the damping parameter, p is the first order cut-off frequency, τ is the reflex delay and s is the LaPlace variable.

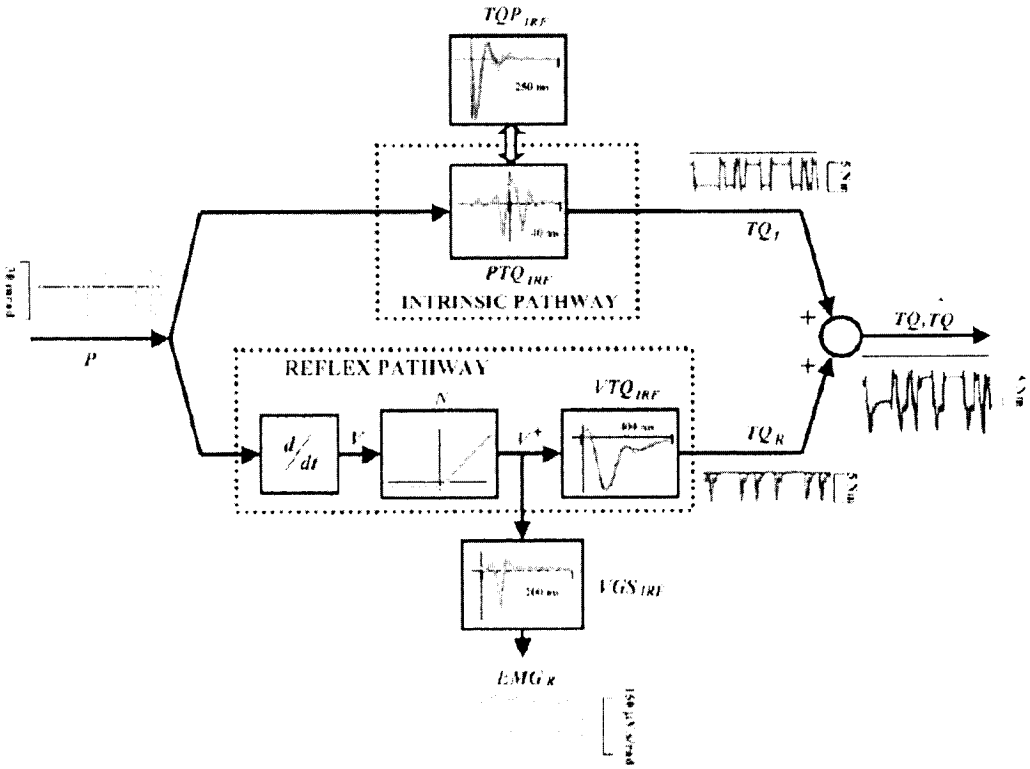

Figure 11 Parallel cascade identification structure; P, TQ, and EMG_R are experimental data; TQ_I, TQ_R, and $\hat{TQ}$ represent predicted responses; PTQ_{IRF}, TQP_{IRF}, VTQ_{IRF}, and VGS_{IRF} represent non-parametric descriptions; parametric models are then used to fit TQP_{IRF}, and VTQ_{IRF} (from [28]).

The parallel cascade identification method was developed for subjects lying prone with their foot attached to a rotary actuator and their leg strapped down so that it remained stationary [20]. The actuator was operated in position control so that the reflex torques generated would not cause changes in ankle joint position. Therefore, the parallel cascade method is an open-loop paradigm. For the upright stance apparatus, the actuators operate in position control but the legs are not fixed and so reflex responses evoked by perturbations to ankle position may cause changes in ankle joint position [42]. Therefore, the data is acquired under closed-loop conditions.

2.6.4 Closed-Loop Identification

Application of open-loop identification methods to data acquired under closed loop conditions can lead to biased results [19]. Since data acquired using the new apparatus is closed-loop, a new closed-loop identification method will need to be used to compute unbiased estimates of intrinsic and reflex contributions to dynamic ankle stiffness [42].

Tung et al. [42] developed an algorithm to estimate the intrinsic stiffness and reflex stiffness contributions in a closed loop system. The method uses IRFs to correlate an unbiased reference signal to the position and torque signals containing feedback; the IRFs are used to predict signals without feedback and the system is then identified using open-loop methods [42]. The closed-loop block diagram is shown in Figure 12 and the algorithm is outlined below:

1) An IRF, h_{act} relating the input, INP, to torque, TQ, is used to estimate the actuator dynamics. Similarly, forward path dynamics, h_{pos}, are estimated by relating INP to position, Φ.
2) INP is convolved with h_{act} and h_{pos} to obtain the projected torque, TQ_p, and the projected position, Φ_p, respectively.
3) Intrinsic dynamics, h_{IS}, are estimated in terms of an IRF relating Φ_p to TQ_p (with the IRF length less than the value of the reflex delay).
4) Intrinsic torque, TQ_I, is computed by convolving h_{IS} with INP. Residual torque, TQ_{IR}, is computed by subtracting TQ_I from TQ.
5) The reflex pathway consists of a differentiator, a delay, a half-wave rectifier, followed by reflex IRF, h_{RS}, relating the half-wave rectified velocity input to the TQ_{IR} output.
6) The reflex torque, TQ_R, is estimated by convolving h_{RS} with the rectified velocity.

7) The net predicted torque, TQ, is the sum of TQ_I and TQ_R. The %VAF is computed as in eq. (1) of Section 2.6.3.1.
8) The reflex-residual torque, TQ_{RR}, is computed by subtracting TQ_R from TQ. The entire estimation procedure is repeated with TQ_{RR} as the output torque.
9) The procedure is repeated until the %VAF fails to improve in successive iterations.

The projected position and torque estimates provide unbiased input-output data to better identify the intrinsic stiffness contributions [42]. With more accurate intrinsic torque estimates, the reflex torque estimates are improved as well. A simulation study of the closed-loop system showed that closed-loop estimations were more accurate than those computed using the open-loop method [42].

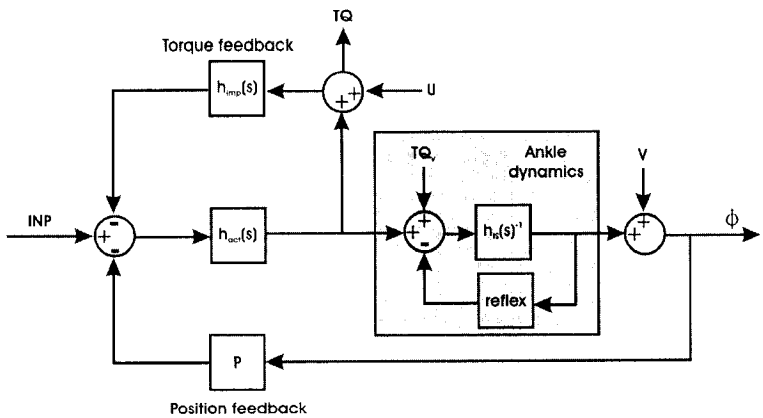

Figure 12 Block diagram of closed-loop system (modified from [42])

2.7 Postural Control

Human posture has been studied extensively over the years, but there is still no consensus about how it is controlled. There are still questions about whether control is a feedback or feedforward process and whether or not the

stretch reflex plays a significant role. Various devices have been used to study the mechanisms of posture. These range from stationary forceplates to rotating or translating platforms to inverted pendulums.

2.7.1 Forceplate Systems

One method of studying posture is to have the subject stand on a stationary forceplate and then measure ground reaction forces and center of pressure (COP) movements. Often, kinematic data of the body is obtained using an optoelectronic system. This involves the subject wearing reflective markers on specific target points on their body while an optoelectronic camera records the 3D movements of these targets.

Winter et al. [44, 45] had subjects stand with each foot on a stationary forceplate and recorded kinematic data for the 14 segment 3D model. They found that the COP and the center of mass (COM) are in phase during quiet stance [44]. The COM is the controlled variable and the COP is the controlling variable. The COP oscillates to either side to the COM to keep it in the desired position. These results indicate that the body acts as an inverted pendulum. Also, they found no evidence of feedback control [44] and concluded that postural control is passive and cannot be reactive since the velocities and accelerations of the body during quiet stance are all below the sensory thresholds [45].

Dault et al. [6] used a dual forceplate system to measure the vertical ground reaction forces of each leg. Subjects were asked to stand with three different stances: 1) shoulder width stance, 2) shoulder width stance on two seesaws, 3) and tandem stance on two seesaws. These tests were conducted with the addition of a cognitive task. It was found that when executing well learned postural control strategies, such as the shoulder-width stance, the addition of a cognitive task had little effect on postural control. However, with the other two

stances, the addition of the cognitive task resulted in an increase in COP frequency and a decrease in COP amplitude.

Gatev et al. [12] used one forceplate and an optoelectronic system to obtain kinematic and kinetic data for subjects standing with normal shoulder width stance and narrow stance. They found a correlation between the center of gravity (COG) and COP during anterior posterior motion. During narrow stance, ankle angular motion and mediolateral sway both increased. During regular stance they found that EMG activity of the gastrocnemius had a phase lead of 250 to 300 ms over the COP and COG. They suggested that stance was controlled using a feedforward process.

Patla et al. [35] used a single forceplate and an 18 marker record of body kinematics. Postural disturbances were in the form of voluntary arm movements by the subject. They found that the initial response of the body to a perturbation is to stabilize the joints and not to control the position of the COM. Once the joint moments are in equilibrium the body will attempt to regain control of the COM. Therefore, following a perturbation, postural control is initially passive and then active.

Collins and DeLuca [5] used a random-walk model to analyze the COP movements obtained from forceplate data during quiet stance. They found evidence of open-loop control for short term stability and closed-loop control for long term stability.

2.7.2 Translating and Rotating Platforms

An alternative to the stationary forceplate is a translating or rotating platform or forceplate.

A hydraulically driven translating force platform was used by Brown et al. [4]. This setup allowed various backward displacements, velocities, and waveforms to be tested while kinematic, ground reaction force and moment, and EMG data were obtained.

Huang et al. [13] used a translating platform driven by an AC servomotor to create lateral perturbations during various movement and loading conditions. Kinematic data was obtained using an optoelectronic system and ground reactions were obtained from the forceplate data.

Nardone et al. [31] used a platform that was capable of imposing positive and negative rotations or forward and backward translations. EMGs of the soleus, lateral and medial GS, and the TA were studied under these four conditions. They found that a stretch to the triceps surae evokes a short latency response (SLR) in the soleus and a medium latency response (MLR) in the gastrocnemii whereas a stretch to the tibialis anterior evokes only a medium latency in TA. However, the MLRs decreased dramatically when the subjects were allowed to grasp a handrail. This indicates that the MLRs are very sensitive to "postural set".

Sinha and Maki [39] pointed out that many studies have shown that subjects lean slightly forward when expecting a perturbation to occur. They hypothesized that forward lean acts to increase the stiffness of ankle. They used a translating platform with two forceplates to measure the ground reaction forces of each foot during random anterior posterior perturbations. Their findings showed that during forward lean, the intrinsic stiffness increased and played an important role in postural stability, but that the reflex gain decreased.

A study conducted by Fitzpatrick et al. [11] determined the loop gain of reflexes during standing. Small, imperceptible perturbations were applied to the subjects at waist level with the subject standing on a platform that could be either rigid or compliant. Cross correlation and spectral analysis were used to estimate

the open loop gain. To compute the reflex loop gain, external perturbations gave rise to EMG activity, whereas to compute the muscle/load transfer function, vestibular stimulation was applied to modify muscle activity. It was found that the loop gain during standing was near unity, which was considered to be too low to explain stable standing as a feedback loop. It was suggested that there is some form of feedforward process at work.

The stretch reflex is a functional reflex which responds differently to various tasks. Brown et al. [4] found that the latency of the stretch reflex in the GS was related to the platform acceleration and that the magnitude of the muscle response was not affected by the type of displacement waveform. Allum et al. [2] found that stretch reflexes in the soleus were much more sensitive to rotational perturbations in the pitch plane than in the roll plane. Even perturbations invoking similar stretches to a muscle will result in different responses. Nardone et al. [31] compared two types of perturbations that stretch the triceps surae, upward tilt and backward translation. The type of perturbation did not affect the latency of the response in the triceps surae; however, the duration and amplitude of the responses were larger during the backward translation [31].

2.7.3 Inverted Pendulums

During upright stance, with no external perturbations, researchers have found that the subject will sway in the anterior posterior direction as an inverted pendulum about the ankle joint [9, 23, 25, 29, 32, 35, 44]. The inverted pendulum model of the human body is shown in Figure 13.

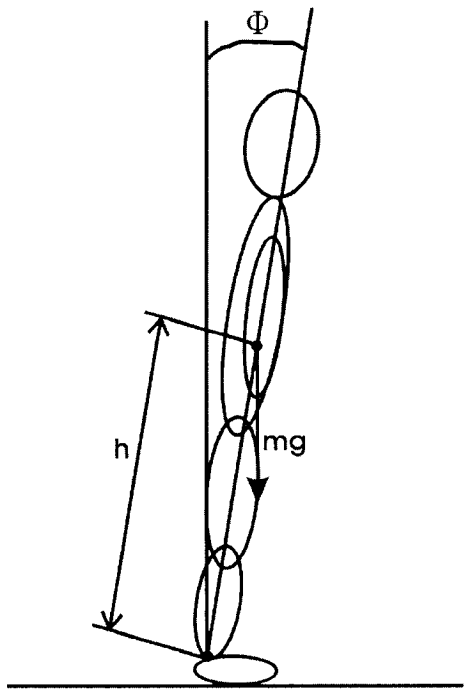

Figure 13 Inverted pendulum model, where Φ represents the sway angle, h is the height of the center of mass, and mg is the force of gravity.

Fitzpatrick et al. [8] used the inverted pendulum model to define load stiffness (K) as follows (mg and h are defined in Figure 13):

$$K = \frac{1}{2} mgh \qquad (4)$$

where ankle torque equals K multiplied by sway angle. They found that ankle stiffness is always greater than the load stiffness and that the former is larger when standing with eyes open than with them closed and is greatest when the subject is asked to "stand still" as opposed to "standing at ease" [8].

Some researchers have had subjects balance an inverted pendulum that was equivalent mass to the human body in order to study human posture [8, 9, 10, 23, 24, 25]. These setups involve the subject standing on foot pedals whose axes of rotation are in line with those of the subjects' ankles. Attached to the rotating foot pedals is an inverted pendulum of equivalent mass and COG to the subject.

The subject's body is fixed in a vertical position so that their ankle movements work to balance the inverted pendulum attached to the foot pedals.

In two of their studies, Fitzpatrick et al. compared perturbed and unperturbed stance under two tests conditions: 1) with the subject standing with each foot on a rotating pedal, balancing their own body, and 2) with the subject standing on the same rotating foot pedals with their body fixed and their ankle rotations balancing the inverted pendulum [8, 9]. Perturbations in the first case were applied by a servo-motor attached to a belt worn around the subject's waist, and in the second case were applied using the same servo-motor attached to the inverted pendulum. It was concluded that during normal standing and during the equivalent standing task, the reflex characteristics were very similar, indicating that vestibular feedback plays a very small role in postural control [9]. By excluding vision in the inverted pendulum balancing task, it was shown that sensory information from the legs was enough to maintain upright posture [8]. Tests conducted with a random perturbation were compared to tests done with a predictable sine wave perturbation. The results were similar indicating that for upright stance with small perturbations, there is little voluntary response [9]. The reflex response had a coherent frequency response up to 5Hz, and when subjects attempted to "stand still" the coherence increased, as did the reflex gain [9]. Another interesting finding was that the soleus was activated before ankle movement, indicating some form of predictive control [9].

In a following study, Fitzpatrick et al. [10] tested the effects of segmentation of the human body on postural control. By testing subjects whose whole bodies were splinted and only rotations about the ankle joint were allowed, they showed that the lack of segmental movements increased sway. They also studied postural control with no visual or vestibular inputs, as well as no sensory inputs from the feet or ankles. This was done by balancing an equivalent body, with eyes closed, and feet anaesthetized. With only proprioception from the leg muscle receptors affecting posture, the amplitude of sway was approximately 2.4

times that of normal standing (with all sensory inputs) and that this feedback alone was enough to stabilize posture. The muscle proprioceptors used were thought to be the group I and II muscle spindle afferents as well as the group Ib Golgi tendon organs.

Loram and Lakie [23, 24, 25] had subjects balance an inverted pendulum (shown in Figure 14) to study sway size and amplitude, as well as intrinsic stiffness. They used a piezo-electric translator to apply dorsiflexing perturbations which were imperceptible to most subjects. Their results showed that subjects could reduce the sway size without significantly changing the ankle impedance [23]. If subjects were asked to "stand still" rather than "stand at ease", sway size decreased. They also noted that sway frequency remained relatively constant whether or not visual feedback was being used. They concluded that sway size is not controlled by ankle impedance, since during all trials, impedance remained relatively constant [23]. Instead, they suggested that when subjects are asked to "stand still" their sway size decreases due to a decrease in torque noise through a predictive, damping process. Loram et al. found no evidence of stretch reflex during standing [25]. They concluded that the magnitudes of internal and external perturbations during quiet stance are not large enough to elicit a stretch reflex response. To estimate intrinsic stiffness they fit a second order damped vibration model to the footplate torque and showed that intrinsic stiffness provides only 91% of the stiffness necessary to maintain stability [25]. They argued that intrinsic stiffness is not neurally controlled but rather is a biomechanical constant.

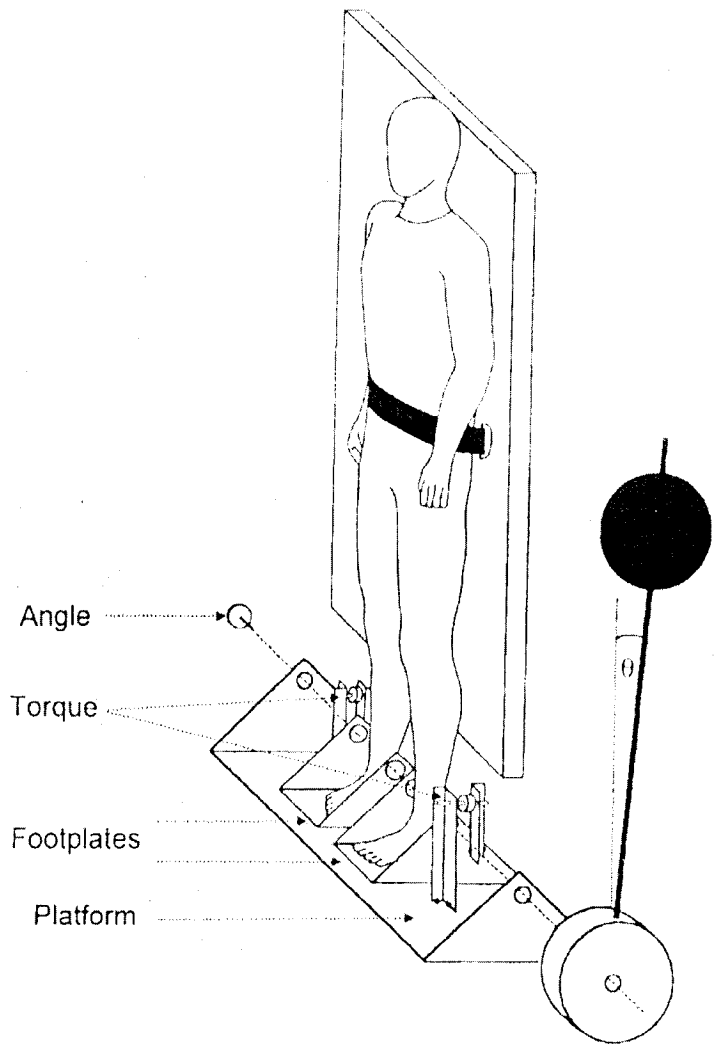

Figure 14 Inverted pendulum apparatus (from [24])

2.8 Summary

The human neuromuscular system controls body posture and movement. Sensory inputs from the visual, vestibular, and somatosensory systems are processed by the CNS to determine errors in position and to generate commands to correct these. The brain generates motor commands which are then sent via the

spinal cord to the PNS. These commands elicit muscle contraction through motor neurons that synapse with muscle fibers. Muscle contractions occur when the individual filaments in the muscle fibers slide over each other causing the muscle to shorten. Contractions of the GS and soleus cause the hinge joint at the ankle to plantarflex. TA contractions cause the ankle to dorsiflex. Muscle length is encoded by the muscle spindle fibers. These signals synapse directly with the motor neurons. Therefore, when the muscle is stretched, the stretch reflex mediated by the muscle spindles causes the muscles to contract. Muscle tension is encoded by the Golgi tendon organs. These signals inhibit the muscle contraction and excite the antagonist muscle to contract, thus creating an inverse stretch reflex.

The study of dynamic stiffness in supine subjects indicates that reflex stiffness can contribute torques similar in magnitude to those generated by intrinsic stiffness [20] and that stretch reflexes are present in ankle flexors [18] and extensors [17]. It seems logical that reflex stiffness would also be present during upright stance and that the ankle stretch reflex would play a role in the control of posture. However, the evidence to support this idea is not strong and the role of the stretch reflex in the control of posture is still unclear.

Although some have found no evidence of the stretch reflex during upright stance [25, 44], others have determined that ankle reflexes make substantial contributions to upright posture [9, 10, 31]. Nardone et al. found that during stance disturbed by small translations and rotations of the support surface, SLRs were present in the soleus, and MLRs were present in the GS and TA [31]. Fitzpatrick et al. found that proprioception from the legs was enough to maintain upright posture [10].

The control of posture has been thought to be passive [44], initially passive and then active [12], both open-loop and closed-loop [5], and feedforward [11, 35], but, the evidence that the stretch reflex is present during upright stance

[9, 10, 31] indicates that some form of feedback control is used. Since reflex responses evoked by perturbations to ankle position may cause changes in ankle position [42], it is conceivable that by using an appropriate closed-loop identification for postural studies the feedback mechanisms will become apparent.

Kearney et al. [17, 18] have characterized stretch reflexes in the GS and TA in prone subjects and used system identification techniques to separate the intrinsic and reflex contributions to ankle stiffness [20]. However, there is an apparent need for more conclusive evidence of the presence and role of the stretch reflex during upright stance. Applications of closed-loop algorithms [42] to identify dynamic stiffness during standing may help to clarify the nature of postural control and whether it is in fact a feedback system.

Knowledge of dynamic joint stiffness and how the neuromuscular system controls posture and movement has many important implications. In the medical field, this information will help to characterize neuromuscular diseases such as multiple sclerosis. Also, patients suffering from spinal cord injuries and parapalegia will benefit from new advances in functional electrical stimulation (FES) to enable them to stand and walk. Detailed knowledge of neuromuscular control will also affect the fields of robotics and biomechanics.

3 Methods

This section covers the design requirements and the final design of the experimental apparatus. It also outlines the methods of data acquisition and experimental control. Finally, the experimental protocol and data analysis are reviewed.

3.1 Design Requirements

The design problem was to create a device that would enable the study of human ankle dynamics during standing. In addition to the study of basic intrinsic and reflex mechanisms, the apparatus must support the study of these mechanisms during different functional requirements, such as with and without vision, with and without external support, with changes in the base of support, and with loads applied to the subject.

This led to the following design requirements:

1) The system must be capable of imposing random perturbations to ankle position over a range of motion of ±6° (0° being when the foot pedal is horizontal). These perturbations will disturb the subject's posture and stretch the GS and TA muscles to elicit reflex responses.
2) The system must have a frequency response that is greater than the range of frequencies present during postural sway to prevent any high frequency dynamics of the ankle from being filtered out by the low pass characteristics of the actuator system. A bandwidth of 20 Hz is felt to be more than adequate.
3) The maximum torque required for each actuator was calculated to be 350 Nm and a maximum speed of 20 rad/s [22]. During active contraction, a maximum torque of 150 Nm can be reached. Maximum passive torque

was determined by simulating the ankle-body system with a stochastic input position of amplitude ±0.1 rads and frequency 50 Hz. The torque velocity and passive torque were maximum, 20 rad/s and 200 Nm respectively, for the high ankle stiffness case (k=1000 Nm/rad). Therefore, the maximum total torque, consisting of active and passive components, is 350 Nm, and the maximum velocity is 20 rad/s.

4) The apparatus must be able to measure the torque and position of each actuator during perturbations to enable the computation of dynamic stiffness. Accuracies of ±0.1 Nm for torque and ± 0.01 rads for position are required.
5) The position of the foot with respect to the actuator must also be measured to account for the possibility of heel lift which would alter the angle of the ankle with respect to foot pedal.
6) The knee and hip angles need to be measured to determine whether the body is in fact acting as an inverted pendulum. The study of dynamic joint stiffness does not depend on the body acting as an inverted pendulum but movements of the knee cause changes in length of the GS and therefore the knee angle must be monitored.
7) The position of the feet and ankles during standing must also be considered since the subject should adapt a comfortable shoulder width stance. Consequently, the distance between the feet must be adjustable for 15 to 40 cm; this range was determined to be wide enough to include comfortable shoulder width stance for subjects of various sizes.
8) The rotation of the actuator shaft must be in line with the axis of rotation of the ankle joint. Therefore the height of the foot pedal from the axis of rotation must also be adjustable. A range of 3 to 5 cm (in increments of 0.5 cm) from the bottom of the foot to the axis of rotation was selected based on the maximum and minimum heights from thirty subjects already tested in our laboratory.
9) The safety of the subject must be ensured at all times. During experiments, the subject's balance is constantly being disrupted. If at any

point the subject becomes unstable and is unable to regain their balance, there must be a system in place to prevent them from falling. Also, mechanisms are required to prevent the foot pedals from exceeding the maximum range required for stability of the subject.

3.2 Experimental Apparatus

The experimental apparatus was designed by Hank Leung [22] as an honours project for the department of Mechanical Engineering of McGill University. The main goal was to have a subject stand with each foot on a separate rotating platform to measure the dynamic ankle stiffness during upright stance. Stress and vibration analyses were conducted by a Mechanical Engineering undergraduate project group [1], who then made modifications to the original design and did the mechanical fabrication. The final assembly is shown in Figure 15.

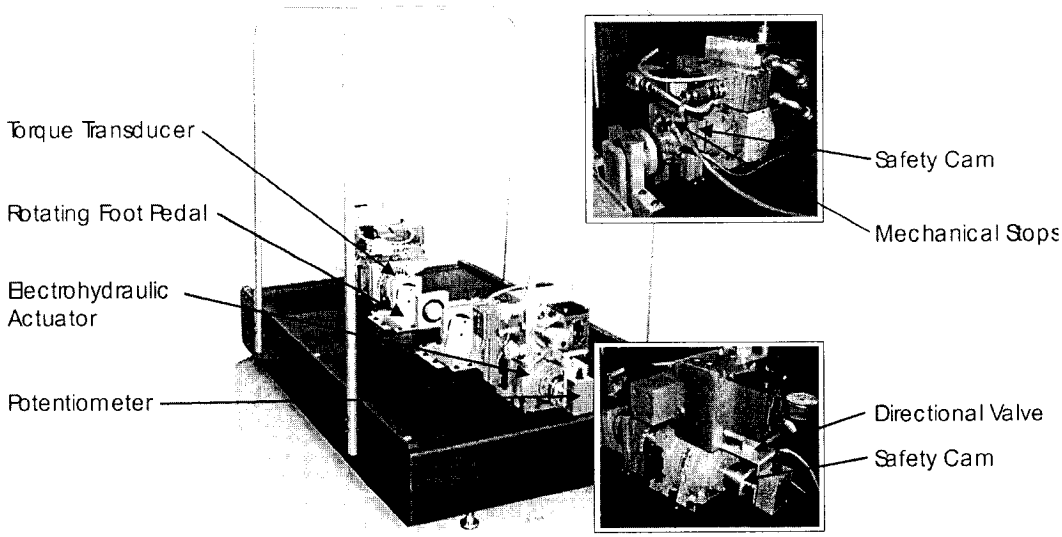

Figure 15 Photograph of experimental apparatus

The schematic in Figure 16 shows the basic components of the experimental apparatus. The apparatus is symmetrical with each side consisting of a potentiometer coupled to a safety cam mechanism (described in 3.2.2), then to the actuator whose shaft is coupled to a second safety cam (also described in 3.2.2), and then to a torque transducer which is connected to the foot pedal.

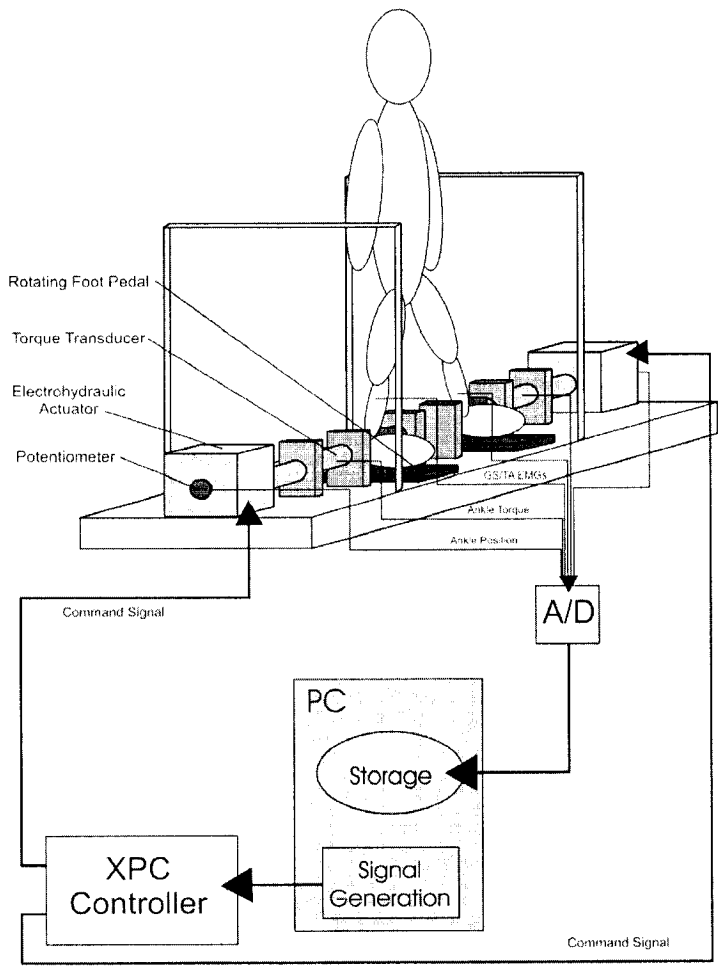

Figure 16 Schematic of experimental apparatus

3.2.1 Actuator and Servo-Valve

The actuator apparatus consists of two high pressure rotary actuators (Rotac 26R-2 1V), each controlled by a proportional servo-valve (Moog D681-

4718). The actuator assembly is shown in Appendix E. The single vane actuators operate at a maximum pressure of 20690 kPa and can generate a maximum torque of 583.1 Nm (see data sheets in Appendix F).

The servo-valves are two-stage, four-way proportional valves with 10% overlap, deadband compensation, and linear flow characteristics. The input command signal is ±10 V and power supplied is 24 VDC. The rated flow is 60 L/min and the response time for a 0-100% stroke is 11.0 ms (see data sheet in Appendix G).

The servo-valves are both equipped with a fail-safe valve that moves the spool to its centered position if the electrical power is shut off. Without a failsafe mechanism, the actuator would move to its end position if the power was cut and compromise the stability of the subject. With the fail-safe mechanisms, the actuators stop moving when the power is cut and therefore the foot pedals remain stationary and the subject remains stable.

Custom built electronic modules are used to send the supply voltage and the command signal to the servo-valves. The supply voltage is obtained from a 24V, 7.2 A power supply (Power-One part #HE24-7.2-ASVMII) with overvoltage protection (Power-One part #OVP-24) and input to the servo-valve module through 3-pin Amphenol connectors. The command signal is generated on a host PC (described in section 3.4) and sent to the module via a BNC cable. The electronics were designed to drive the 8m long cable connecting the modules to the servo-valves. The circuit diagram for these modules is shown in Appendix H.

3.2.2 Safety Mechanisms

To prevent injury of the subject, five safety mechanisms are used:

1. The actuator shafts both have a cam which limits rotation to ±20°. When the rotation exceeds this range, the cam mechanically activates a directional valve which blocks the hydraulic pressure to the actuator. This mechanism can be seen in the bottom right inset of Figure 15 and in Appendix E.
2. Two other steel cams rotate with the actuator shafts and block the rotation when the cam comes in contact with bolts used as mechanical stops. These stops are set at the start of each experiment and prevent the foot pedal displacement from exceeding ±5° from neutral. This mechanism can be seen in the top right inset of Figure 15.
3. The servo-valves are equipped with fail-safe mechanisms so that if power to the actuator is lost, a solenoid will cause the spool to move into its centered position, therefore preventing movement of the actuator.
4. There are handrails (seen in Figure 15) to the left and right of the subject allowing him or her to grab on to them if ever they feel unstable.
5. A full body harness (Jelco 740) is worn by the subject. The harness is attached to steel crossbars in the ceiling by carabiners and two daisy chains (typically used for mountain climbing). The individual pockets of the daisy chain are rated at 3 kN and the overall chain is rated at 16 kN. The carabiners are each rated at 7 kN.

3.3 Transducers and Signal Conditioning

Torque and angular position data is acquired using analog sensors. These signals are conditioned using custom made electronic modules and then sampled using a dynamic signal acquisition card. EMG data is acquired using a four

channel EMG system and then sampled using the dynamic signal acquisition card. Hip and knee angle, as well as heel lift, is also monitored.

3.3.1 Torque

Torques are measured using two flanged reaction torque sensors (Lebow 2110-5k). These transducers have a capacity of 565 Nm and a torsional stiffness of 103941 Nm/rad. The transducers have a maximum nonlinearity of ±0.1% of the rated output and a repeatability of ±0.05% of the rated output (see data sheet in Appendix I). Torque signals are conditioned using custom built electronic modules which allow the gain and offset to be set as desired (see circuit diagram in Appendix J). The modules have a strain gage conditioner (Analog Devices 2B31J) comprising of an instrumentation amplifier, followed by a low-pass filter, and an adjustable transducer excitation. The modules have a gain of 2000 up to a cutoff frequency of 2 kHz and provide a calibrated sensitivity of 0.05 V/Nm. The root mean square (RMS) noise level of the torque transducer module is 2.1 mV or 0.042 Nm. Dorsiflexion torques are assigned a positive polarity and plantarflexion torques a negative polarity.

3.3.2 Position

The angular position of each foot pedal is measured using a conductive plastic 5 kΩ rotary potentiometer (Maurey Instruments 112-P19). The potentiometer has a linearity of ±0.5% over a theoretical electrical travel of 340° ±5° and a theoretical resolution of infinity (see data sheet in Appendix K). The signals from the potentiometers are conditioned using custom built circuit (see circuit diagram in Appendix L) comprising an instrumentation amplifier (Analog Devices AMP02FP) that permits gain and offset adjustments. These modules were calibrated to have a sensitivity of 10 V/rad. The RMS noise level of the

potentiometer module is 0.1 mV or 0.1 mrads. Dorsiflexion is assigned a positive polarity and plantarflexion a negative polarity.

3.3.3 EMG

Electromyograms (EMGs) of the gastrocnemius (GS) and the tibialis anterior (TA) muscles are measured using a four channel EMG system (Bagnoli-4 EMG system, Delsys Inc.) (see data sheet in Appendix M). Electrodes are placed over the lateral GS muscle and over the TA muscle, parallel to the muscle fiber with a fifth ground electrode placed on the patella. The surface electrodes are made of two pure silver bars housed in polycarbonate plastic (see data sheet in Appendix N). They are attached to the subject using medical grade adhesive. The main amplifier unit filters the EMG signals to a bandwidth of 20 to 450 Hz and amplifies the signals with gains of 100, 1000, or 10000. The system also checks for line interference and amplifier saturation. The negative absolute value of the GS EMG signal and the positive absolute value of the TA EMG signal are computed to indicate that GS EMG produces negative (or plantarflexing) torques whereas TA EMG produces positive (or dorsiflexing) torques.

3.3.4 Hip and Knee Angles

Three angular sensors (MicroStrain Inc. FAS-G-M) are attached to the subject's skin on the right tibia, femur, and pelvis, using medical grade, two-sided tape. The right hip and knee angles are computed using the absolute angles of the tibia, femur, and pelvis. These angles are monitored to determine whether the body is acting like an inverted pendulum. The knee angle is particularly significant since any knee movement causes a change in length of the GS, which in turn affects the reflex characteristics of this muscle.

The FAS-G sensor combines an angular rate gyro, two orthogonal DC accelerometers, 12 bit A/D converter, multiplexer, microcontroller, and D/A converter to provide an analog voltage linearly proportional to inclination in dynamic and static environments. The sensors operate over a 360° range. A digital serial output can be programmed to provide either compensated angles or raw sensor data. The digital output modes and software filter parameters are user programmable. All programmed parameters are stored in nonvolatile memory. The angular sensors are accurate to ±1°, with an angular resolution of ±0.1°, a nonlinearity of 0.23% of the full range, a repeatability of 0.10° (see data sheet in Appendix O).

3.3.5 Heel Lift

The right foot pedal is equipped with an ultrasonic sensor (Baumer Electric UNDK 30U6113/S14) to measure heel lift. It is mounted under the foot pedal and a small hole in the foot pedal allows the sound pulse to bounce off the subject's heel. The ultrasonic sensor uses a special transducer which alternates between transmission and reception of sound waves. The sonic wave is emitted and then reflected off the subject's heel and back to the receptor. The time elapsed between emitting and receiving is proportional to the distance of the heel from the sensor. The sensor has an analog output of 0 to 10 V which can be set to either rise or fall proportional to the target distance. The scanning range is 20 to 200 mm with a resolution of 0.3 mm (see data sheet in Appendix P).

3.3.6. Data Acquisition

Torque, position and EMG data for each leg are sampled at 1 kHz using a dynamic signal acquisition card (National Instruments 4472). The NI 4472 card

is equipped with a digital anti-alias filter which passes only the signal components with frequencies below the Nyquist frequency or 500 Hz.

3.4 Actuator Control

The experimental code was developed using MATLAB (The MathWorks, Inc.). The servo-valve controller was developed using SIMULINK (The MathWorks, Inc.) and compiled on the host computer using the Real-Time Workshop Toolbox for MATLAB. It uses a MATLAB-based xPC real-time digital signal processing system. The target computer is equipped with a 16 bit, 8 channel A/D card (Computer Boards PCIM-DAS1602/16) and a 16 bit, 6 channel D/A card (Computer Boards PCIM-DDA06/16). The host loads the DSP code to the target using Ethernet.

For these experiments, a controller using position feedback was created in SIMULINK. Before being input to the controller, the left and right position signals are filtered using a 64 channel programmable filter/amplifier system (Frequency Devices Model 9064). The filters are 8-pole 6-zero constant delay low-pass filters whose cutoffs are set to 400 Hz. The desired position signals are generated in the host computer and uploaded to the xPC target computer using a buffer.

Design of the controller is covered in Section 4 and the controller block diagrams are shown in the Appendix A through D.

3.5 Experimental Protocol

Matlab and its xPC real-time digital signal processing system are used to generate the command signals to the servo-valves. Subjects are trained to stand

quietly while undergoing small amplitude stochastic perturbations. Each ankle is driven by independent perturbations to minimize their effect on the body lean.

Reflex stiffness is sensitive to the properties of the input perturbations. Inputs with low root mean square (RMS) velocities are known to stimulate stretch reflexes [20]. There are two types of command signals used for the pilot experiments:

1) Pulse Signals: The pulse signal has an amplitude of 0.03 rads and duration of approximately 40 ms. This permits the reflex and intrinsic components to be dissociated on the basis of latency since, due to the reflex delay, the intrinsic response are completed before the reflex response begins [28]. The entire trial lasts 60 s and contains 10 pulses. Both dorsiflexing and plantarflexing pulses are used.
2) Pseudorandom Binary Sequence (PRBS): The PRBS inputs have a peak to peak amplitude of 0.03 rads and a switching rate of 125 ms. These input characteristics provide a low enough RMS velocity to avoid suppressing the reflex response [20]. The trial duration is 64 s.

Three separate cases are tested, with each two command signals.

Case 1: One foot pedal remains stationary and horizontal while the other moves according to the command signal. This protocol will verify whether a stretch in one ankle elicits a symmetric response in the opposite, un-stretched ankle.

Case 2: Both foot pedals move according to the command signal. This protocol will verify whether the responses in both ankles are symmetric.

Case 3: One foot pedal moves according to the command signal and the other foot pedal moves according to the negative of the command signal. This protocol will verify whether the reflex responses in both ankles are independent or if they are attenuated when the motion of both ankles is opposite.

4 Performance Evaluation

The dynamic performance of the new bipedal electro-hydraulic actuator system was evaluated using random and pulse inputs and the frequency response of both actuators was determined.

4.1 Pulse Perturbations

Initially, a proportional position feedback was used to control both actuators (see controller block diagram in Appendix A). A pulse perturbation of amplitude 0.03 rads and 40 ms duration was input to both actuators. Figure 17 shows the input command signal and the resulting positions of the left and right foot pedals with a subject.

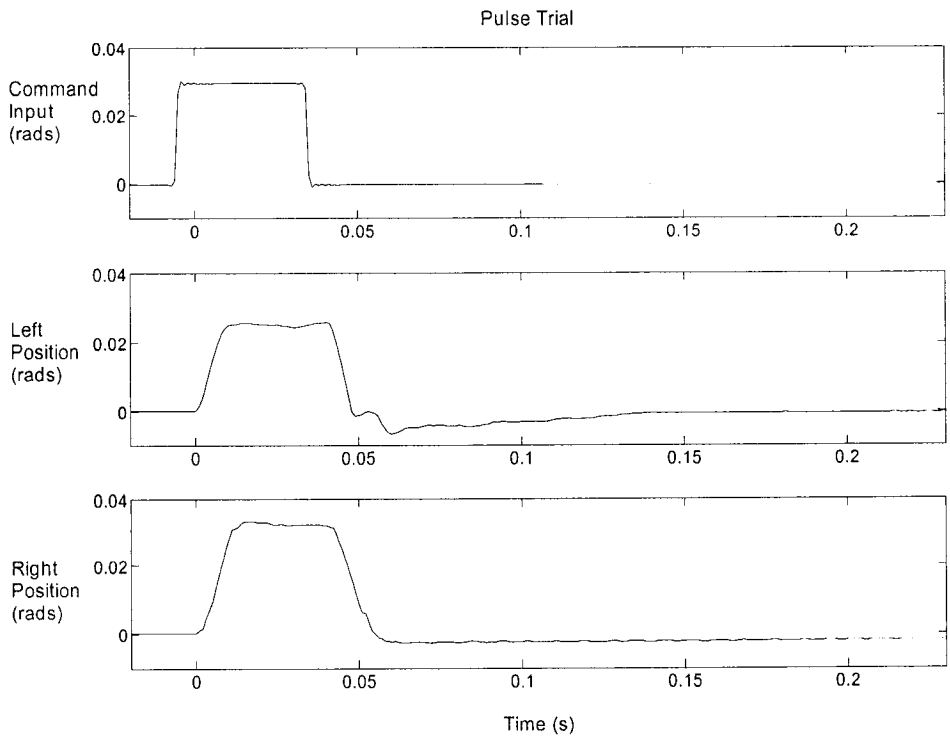

Figure 17 Pulse response with proportional controller

The rise times of both pulses were approximately 15 ms and the pulse lengths were 50 ms. It is evident in Figure18 that the left actuator response had a large overshoot on the return. The right actuator had an overshoot as well and took almost a second to return to the desired zero position. These results were not acceptable since this overshoot could elicit a second reflex response.

Next, a PID (proportional, integral, and derivative) controller with position feedback was used (see controller block diagram in Appendix C). With this controller, it was easy to reduce the steady-state error and settling time of the pulse responses. It was also found that overshoot occurred at the rising and falling edge of the pulse response. With the PID controller it was possible to minimize one of these overshoots but not both at once. It was determined that the actuator dynamics varied with the direction of rotation. This was particularly noticeable in the right actuator.

The final controller developed was a PID controller with position feedback and different proportional gains for the positive and negative rotations (see controller block diagram in Appendix D). Using the same command signal as in Figure 17, the pulse responses using the new direction dependant PID controller are shown in Figure 18.

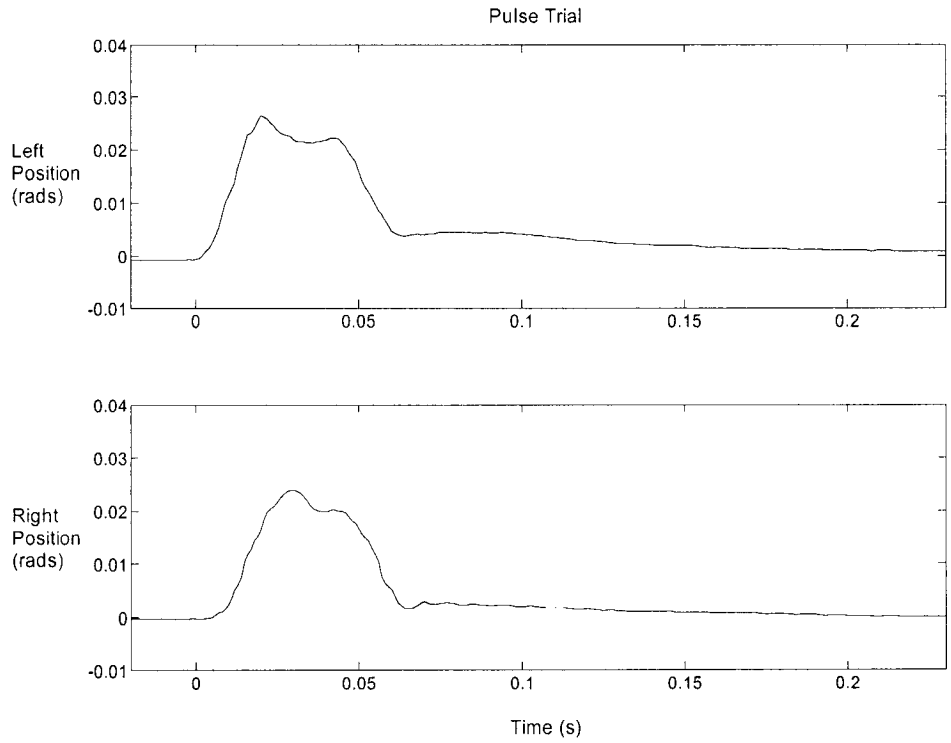

Figure 18 Pulse response with a direction dependant PID controller

With the new controller, the left pulse response had an average rise time of 22 ms, pulse length of 65 ms, and a settling time of 0.35 s. The right pulse response had an average rise time of 22 ms, pulse length of 58 ms, and settling time of 0.21 s. The above responses do not look as nice as those shown in Figure 18 but there is no overshoot which is advantageous. The pulses with overshoot shown in Figure 17 would elicit undesired reflex responses. Although the rise time and settling times are longer with the new controller, the lack of overshoot is crucial for the desired reflex measurements.

The problems in designing a suitable controller come from the complex, nonlinear, and non-identical dynamics of the two actuators. In the future, identification done on the actuator dynamics will lead to improvements in the controller design and better overall performance.

4.2 Random Perturbations

A random perturbation with peak to peak amplitude of 0.05 rads and a bandwidth of 0 to 20 Hz was applied to both actuators with no subject. Initially, proportional position feedback was used to control both actuators (see controller block diagram in Appendix A). Figure 19 shows the input command and the corresponding left and right position outputs. It can be seen that the left and right position records vary a great deal. The correlation coefficient (R) between the left and right position signals is 0.70.

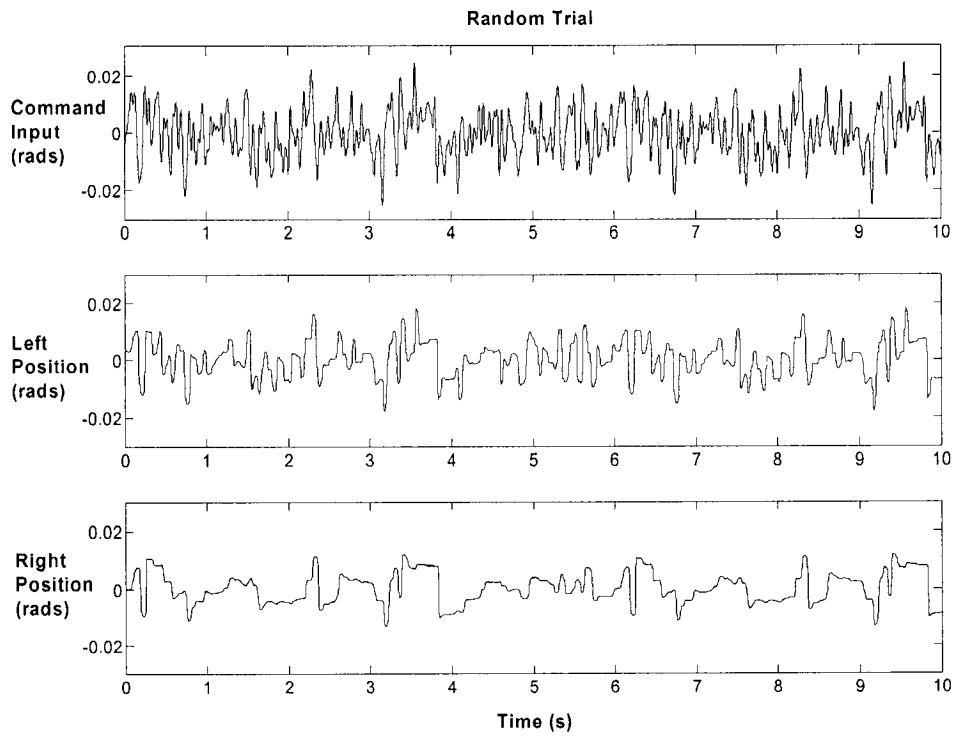

Figure 19 Position input and actuator outputs for a random stimulus without subject

Upon further investigation it was found that the right actuator did not respond to command inputs below 0.1 V. The servo-valves have a 10% overlap and the electronics have a deadband compensation. According to the manual, a

signal over 0.1 V is required for the electronics to compensate for the 10% overlap. For some unknown reason, the internal electronics adjustments done in the factory were different for the two actuators and the left valve responds to commands below 0.1 V whereas the right valve does not. To solve this problem, a nonlinearity was added to the Simulink block diagram (see controller block diagram in Appendix B) to increase the gain of the right actuator for small command voltages. The command voltage range for the actuators is -10 to +10 V, but is usually less than 1 V. The gain of the left actuator was changed to a constant 1.7 and the gain of the right actuator was changed to vary with the input amplitude as shown in Figure 20.

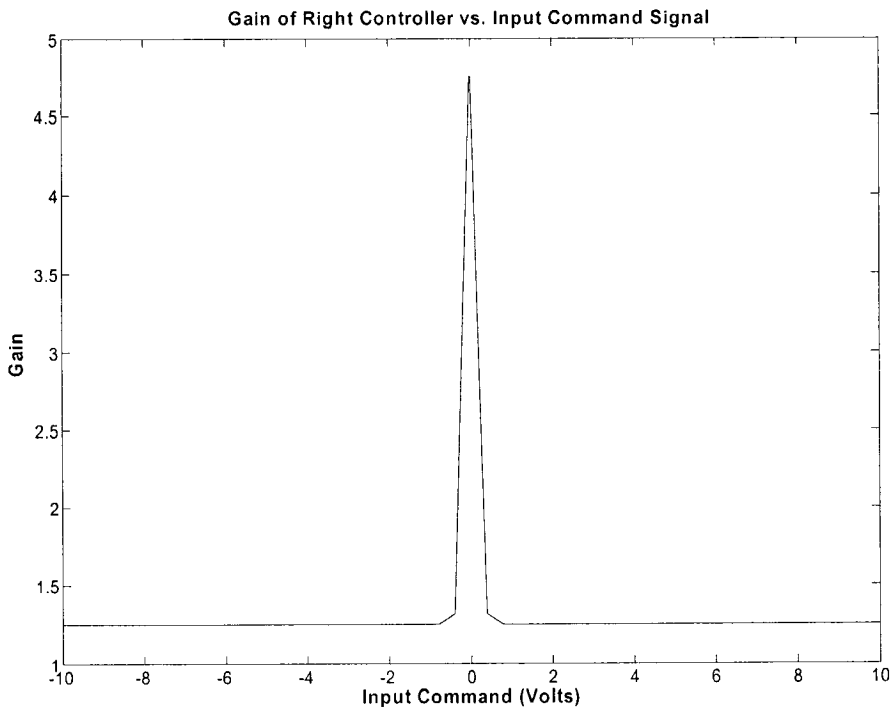

Figure 20 Gain of right actuator controller versus input command voltage

The same random perturbations used above were applied to both actuators using the new controller. The results are shown in Figure 21. The right and left position records are more similar. The correlation coefficient (R) between the left

and right position signals is 0.87 as compared to 0.70 from the data of Figure 19. It is evident from the position records of both actuators that the low-pass dynamics of the actuators have eliminated some of the high-frequency content of the command input.

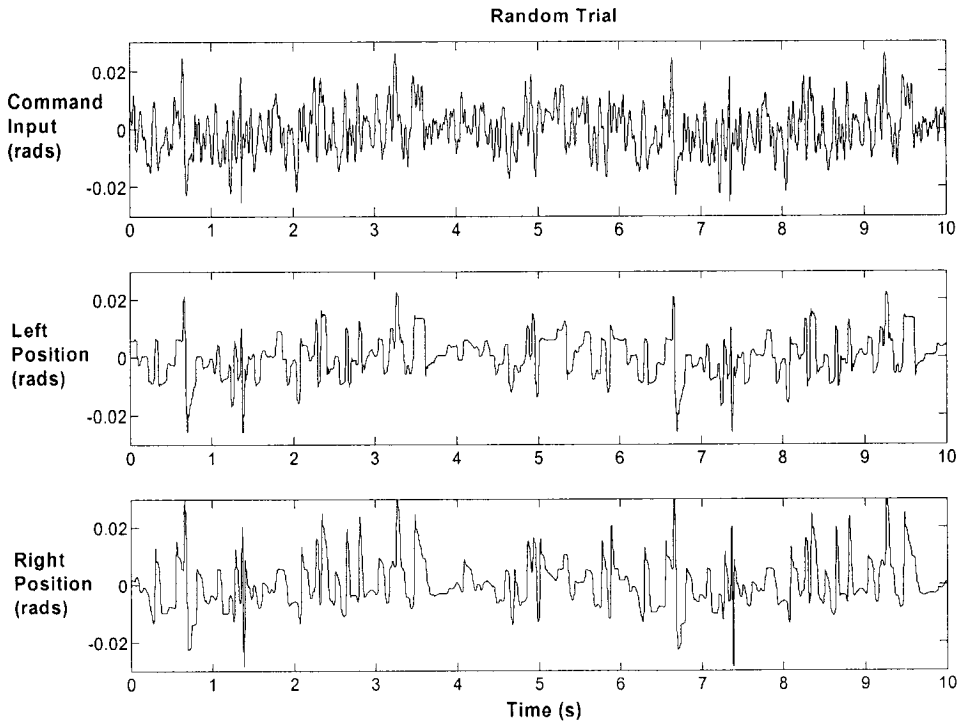

Figure 21 Position input and actuator outputs for a random stimulus without subject

4.3 Frequency Response

The frequency response of the actuator with a subject was computed using an input perturbation with peak to peak amplitude of 0.05 rads and bandwidth 0 to 20 Hz. The input and output positions signals were sampled at 1000 Hz for 60 s and then decimated by 20. The gain, phase, and coherence plots were generated using the Matlab spectrum function with a NFFT length of 64. The frequency

responses of both the left and right actuators with a subject are shown in Figure 22.

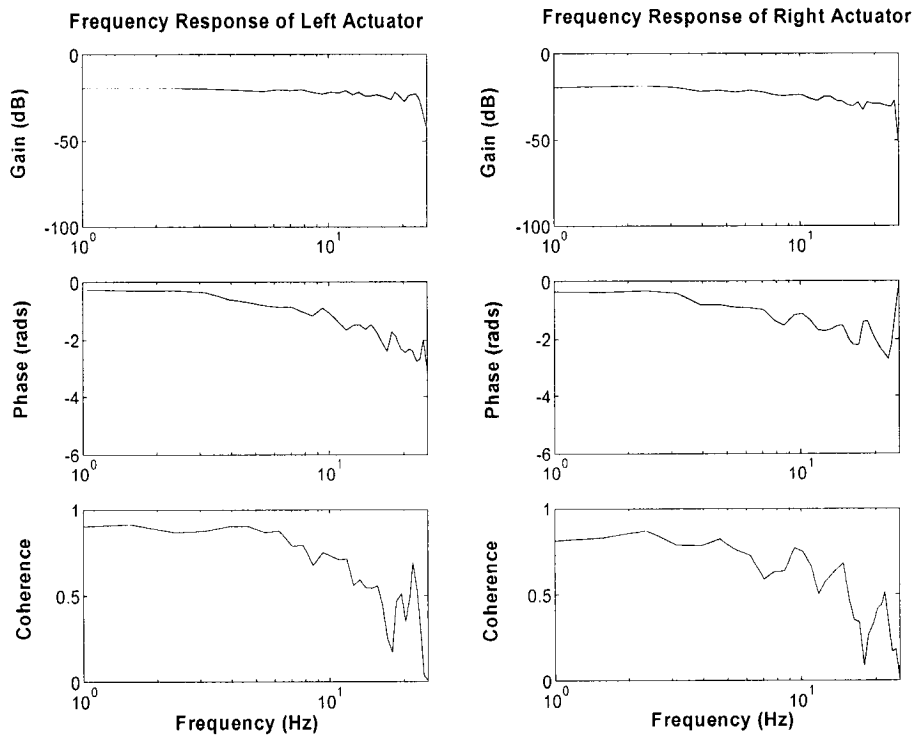

Figure 22 Frequency responses of the left and right actuators with subject

The coherence squared was greater than 0.5 for frequencies up to approximately 16 Hz for both actuators. The gain was flat up to 23 Hz. At 20 Hz, the gain was approximately -25 dB for the left actuator and -30 dB for the right actuator.

4.4 Summary

With the direction dependant PID controller and a command pulse perturbation of 0.03 rads amplitude and 40 ms length, the corresponding left and right position responses had rise times of 22 ms and pulse lengths of

approximately 60 ms. Although these responses are not ideal, the fact that there was no overshoot is important in evoking that desired reflex responses and therefore this actuator performance should be adequate for reflex identification.

For the random tests, a different controller was designed and used. The results of the random performance analysis showed that the output positions for the left and right actuators had a correlation coefficient of 0.87.

The design requirements specified that the system should have a frequency response that is greater than the range of frequencies present during postural sway. A bandwidth of 20 Hz was chosen as the acceptable range. It can be seen from the frequency response shown in Figures 22 that the gain of both actuators was flat until 23 Hz, the phase began to fluctuate at 23 Hz, and the coherence was greater than 0.5 up to a frequency of 16 Hz. These results are acceptable, but not ideal.

The results of the dynamic performance of the actuators are not as good as expected. The dissimilar and complex dynamics of the two actuators led to difficulties in controller design. Future work will be required to identify the actuator dynamics and to improve the controller design and performance.

5 Experimental Results

A pilot study was conducted to determine whether the new apparatus was capable of eliciting reflex responses in standing subjects. The experiments described in Section 3.5 were performed on one subject. These included pulse and PRBS input perturbations. Pulse perturbations of 40 ms duration were used to stretch and return the ankle to its original position before the reflex torque is generated [26]. This allowed the reflex torque to be measured without any intrinsic component. PRBS inputs were used to identify the intrinsic and reflex stiffness components. These inputs had a low RMS velocity to avoid suppressing the reflex response [20] and contained power over a wide enough bandwidth to identify the stiffness dynamics [28].

5.1 Data Analysis

All data analysis was performed after the completion of the experiments. Data was sampled at a 1000 Hz after anti-alias filtering to a cut-off of 500 Hz. The data was then scaled appropriately. The position and torque records were detrended by subtracting their mean values. The EMG data was rectified accordingly.

The pulse signals were generated using a 6 s vector that was continuously repeated. For the results presented in Sections 5.2, the 60 s trials were separated into 9 or 10 repeated segments. The average of the segments was computed and a plot of position, torque, and EMG averages was obtained. For the pulse data, the magnitude of the reflex torque and the reflex torque delay were computed using custom pulse analysis software (Kearney, 1995).

The sequence signals were generated using a 16 s vector that was repeated 4 times for a total trial length of 64 s. Plots of position, torque, and EMG can be seen in Section 5.3.

Four separate trials were selected to be analyzed using the parallel cascade identification (Section 2.6.3). These included the left and right ankle data from PRBS Cases 2 and 3. The data was decimated by 10 before computing the intrinsic compliance and reflex stiffness IRFs, and the parametric model parameters. The results are shown in Section 5.4.

5.2 Pulse Trials

The pulse trials described in section 3.5 were performed on one subject. A typical pulse trial record is shown in Figure 23.

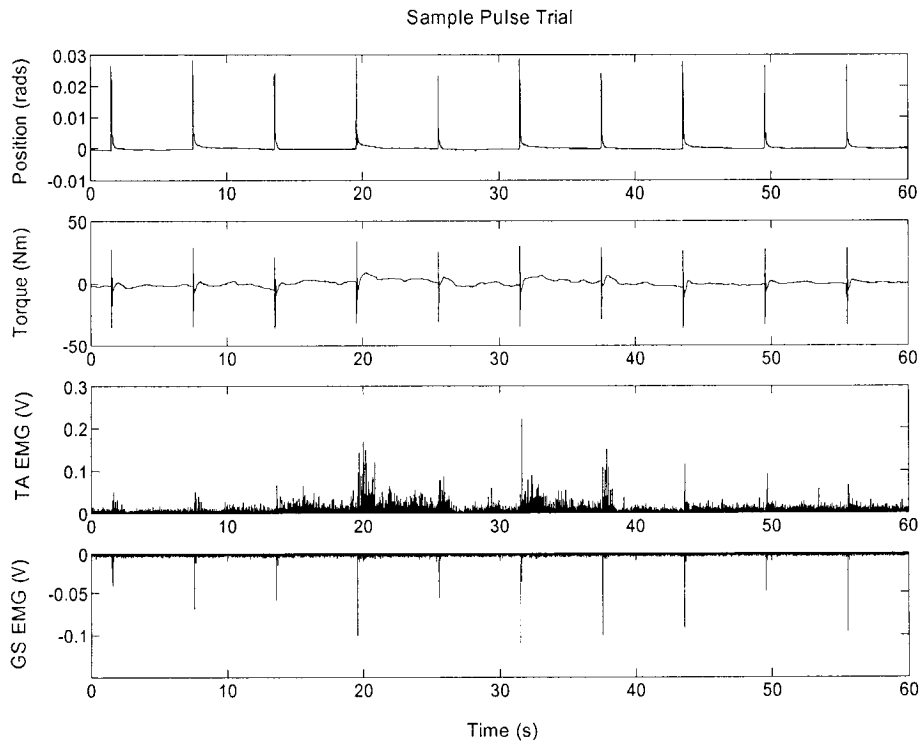

Figure 23 Sample pulse data, 60 s trial for one ankle

5.2.1 Case 1

The pulse perturbation was applied to one ankle while the other ankle remained stationary. Figure 24 shows the average position, torque, and EMG records of both legs for the 60 s trial when the left ankle was stimulated and Figure 25 shows the results when the right ankle was stimulated.

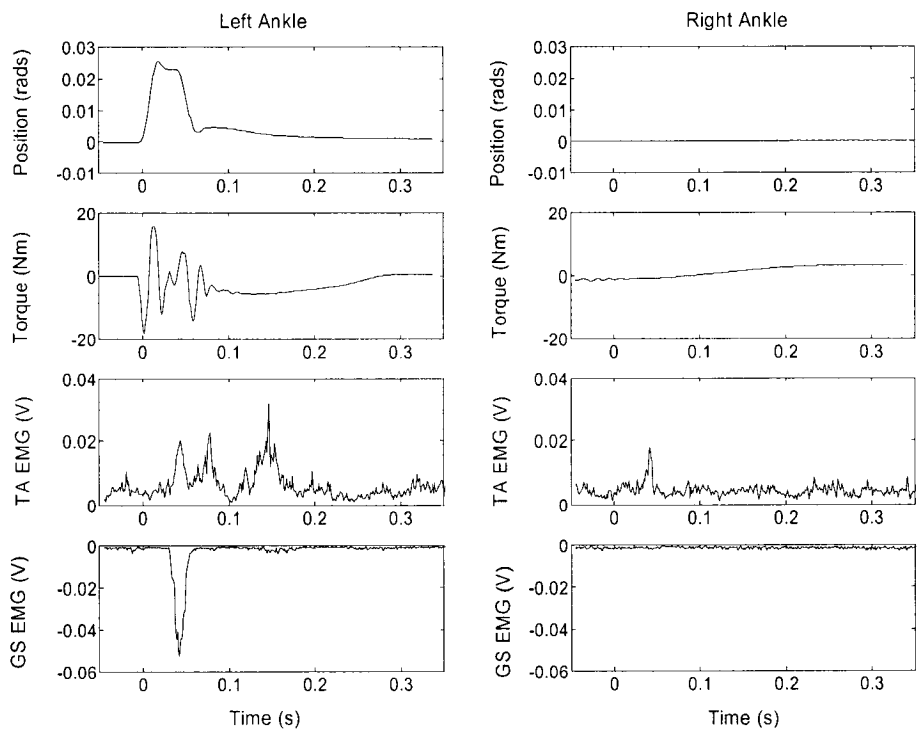

Figure 24 Pulse trial: left ankle dorsiflexed, right ankle stationary

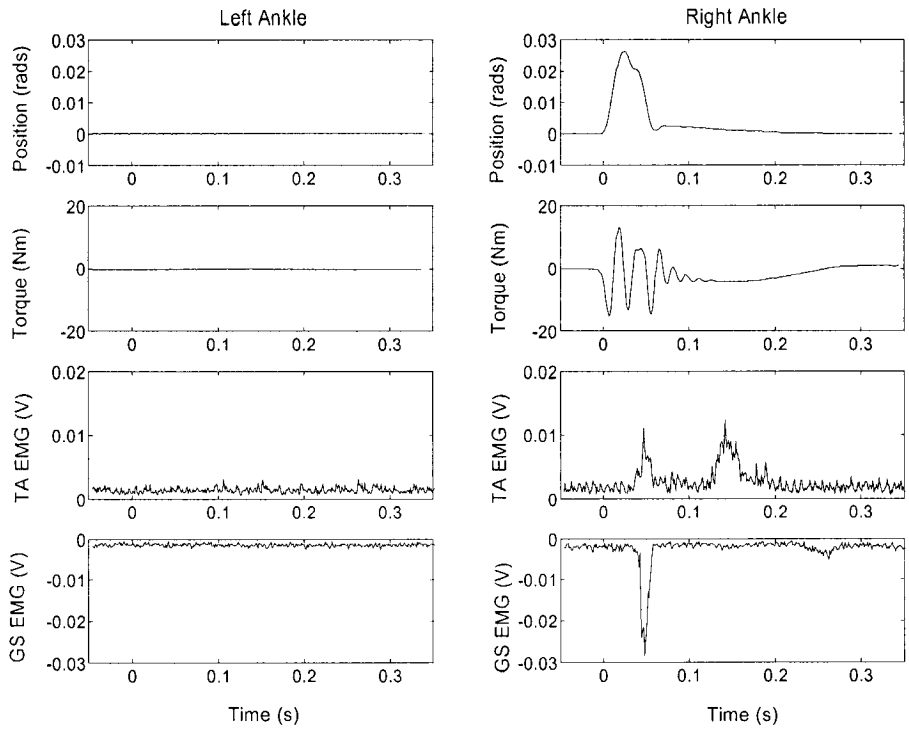

Figure 25 Pulse trial: left ankle stationary, right ankle dorsiflexed

The results in both Figures 24 and 25 showed that there was no EMG response evoked in the stationary ankle. In the dorsiflexed ankle, there was a spike in the GS EMG at a latency of 32 ms for Figure 24 and 25 ms for Figure 27. Some TA EMG activity was present in the stimulated ankle at latencies of 32 ms in Figure 24 and 39 ms and 123 ms in Figure 25. A spike in the TA EMG of the right ankle in Figure 24 occurred at a latency of 148 ms.

The torque response showed an initial component attributed to intrinsic mechanics and correlated with ankle position and its derivatives. Once the ankle had returned to its original position and the intrinsic component has subsided the reflex torque response could be seen. The reflex torque produced in the left ankle in Figure 24 had a magnitude of -5.8 Nm and a maximum at 141 ms. The reflex torque produced in the right ankle in Figure 25 had a magnitude of -4.3 Nm and a maximum at 144 ms.

5.2.2 Case 2

The same 0.03 rads, 40 ms pulse perturbation was applied to the left and right ankles. Figure 26 shows the average position, torque, and EMG records of both legs for the 60 s trial.

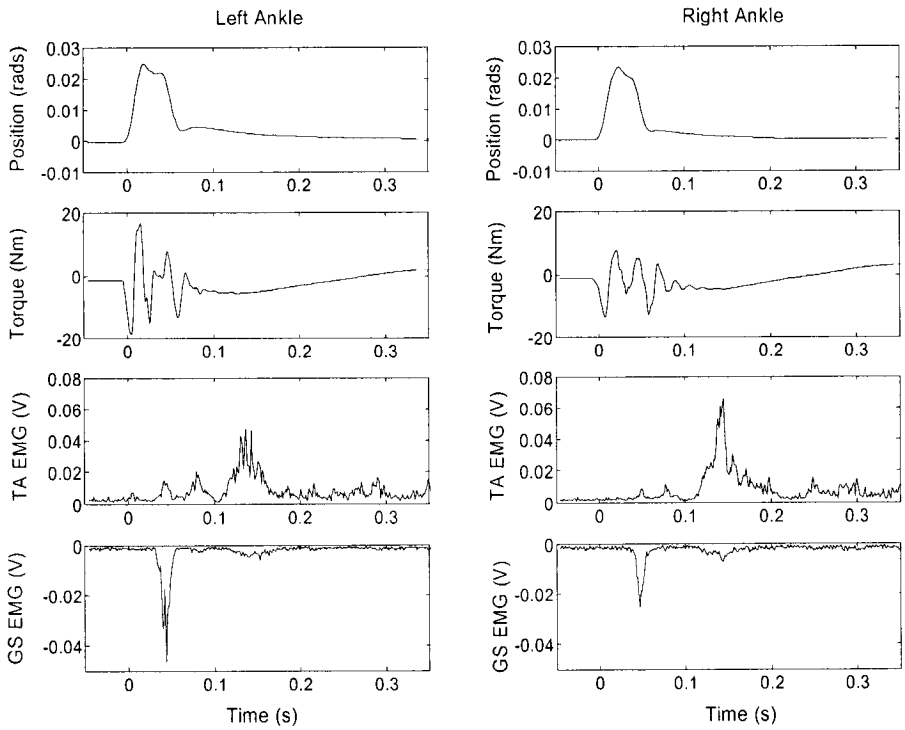

Figure 26 Pulse trial: both ankles dorsiflexed

GS response in the left ankle occurred at 29 ms and in the right ankle at 38 ms. Some TA activity was present at a latency of 32 ms in the left ankle and 40 ms in the right ankle. The reflex torque produced in the left ankle had a magnitude of -4.5 Nm and peaked at 122 ms. The reflex torque produced in the right ankle had a maximum magnitude of -3.4 Nm at 132 ms.

5.2.3 Case 3

A dorsiflexing pulse perturbation was applied to the one ankle and a similar amplitude plantarflexing pulse perturbation was applied to the other. This was done once with the left ankle being dorsiflexed and once with the right ankle being dorsiflexed. Figure 27 and 28 shows the average position, torque, and EMG records of both legs for both 60 s trials.

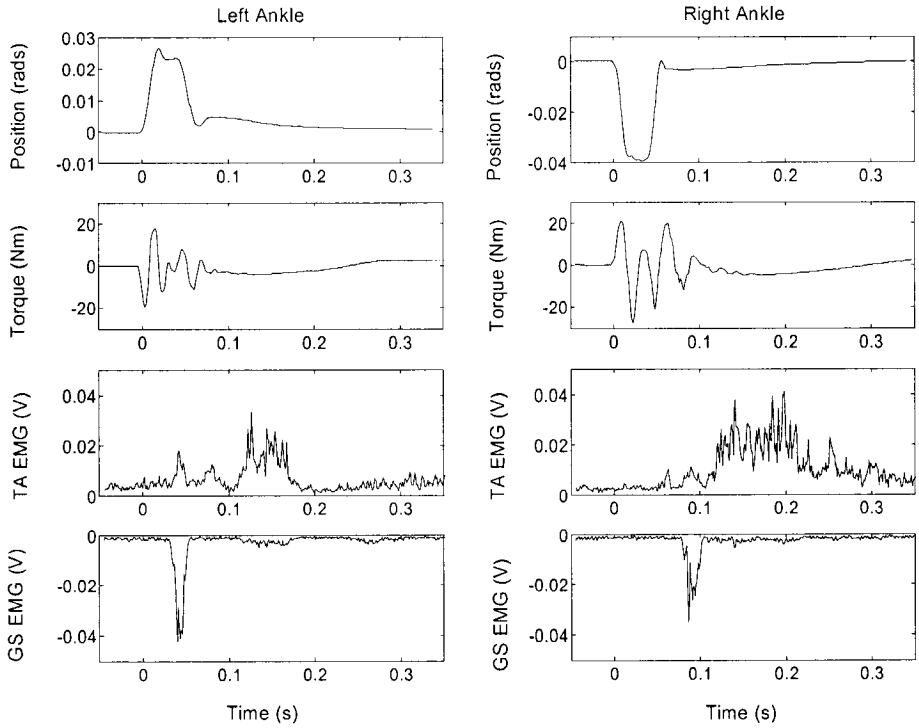

Figure 27 Pulse trial: left ankle dorsiflexed, right ankle plantarflexed

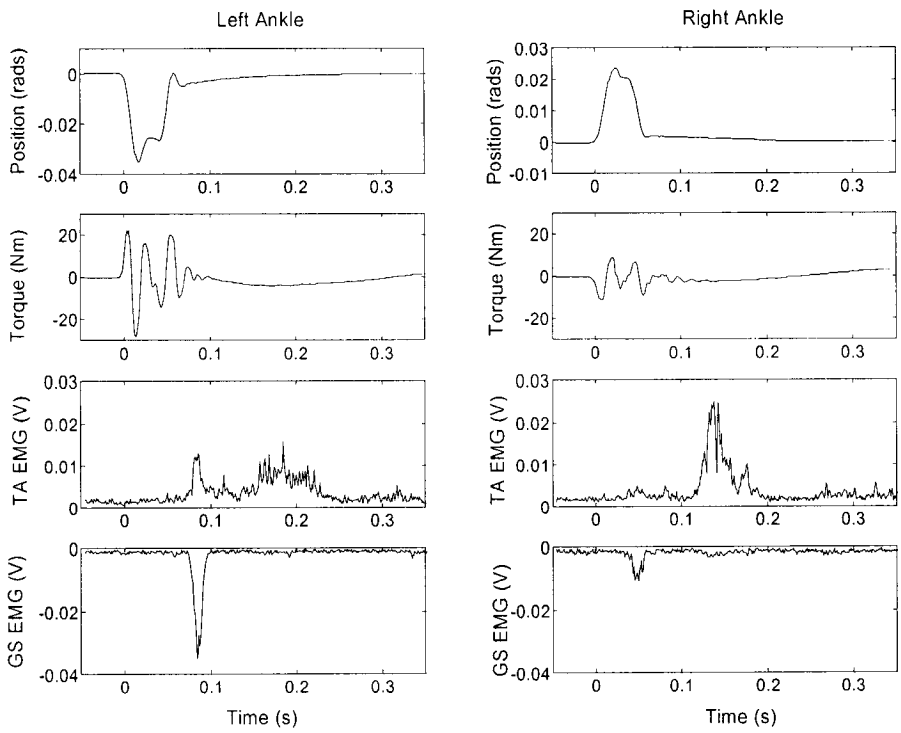

Figure 28 Pulse trial: left ankle plantarflexed, right ankle dorsiflexed

For the trial shown in Figure 27, the average GS response in the left ankle occurred 32.5 ms after the onset of the dorsiflexing pulse. The average GS response in the right ankle occurred at 79.4 ms after the onset of the plantarflexing pulse, which is at a 32.5 ms delay after the positive (dorsiflexing) edge of the plantarflexing pulse. EMG responses in the TA occurred at 29 ms in the left leg and 61 ms in the right leg. The reflex torque produced in the left ankle had a maximum magnitude of -3.9 Nm at 142 ms. The reflex torque produced in the right ankle had a maximum magnitude of -5.4 Nm at 177 ms.

For the trial shown in Figure 28, the average GS response in the right ankle occurred at 36.0 ms after the onset of the dorsiflexing pulse. The average GS response in the left ankle occurred 72.1 ms after the onset of the plantarflexing pulse, which was at a 32.5 ms delay after the positive (dorsiflexing) edge of the plantarflexing pulse. EMG responses in the TA occurred at 79 ms in

the left leg and 123 ms in the right leg. The reflex torque produced in the left ankle had a magnitude of -3.8 Nm at a delay of 182 ms. The reflex torque produced in the right ankle had a magnitude of -2.0 Nm at a delay of 130 ms.

In all five trials, a reflex torque was generated in the stimulated ankle which ranged from -2 Nm to -6 Nm. In Case 1 trials, the stationary ankle had no torque or EMG responses. Therefore, we can conclude that a stretch in one ankle does not elicit a symmetric response in the opposite ankle. In Case 2 trials, both ankles were dorsiflexed and exhibited similar torque and GS EMG responses. In Case 3 trials, both ankles showed torque and EMG responses. The plantarflexed ankle responded 32 ms to 53 ms after the dorsiflexed ankle. These delays corresponded to the onset of the positive (dorsiflexing) edge of the plantarflexing pulse. These results showed that each ankle responds to GS stretch independent of the stimulus in the opposite ankle.

5.3 Sequence Trials

The sequence trials described in section 3.5 were performed on one subject. A typical trial record is shown in Figure 29.

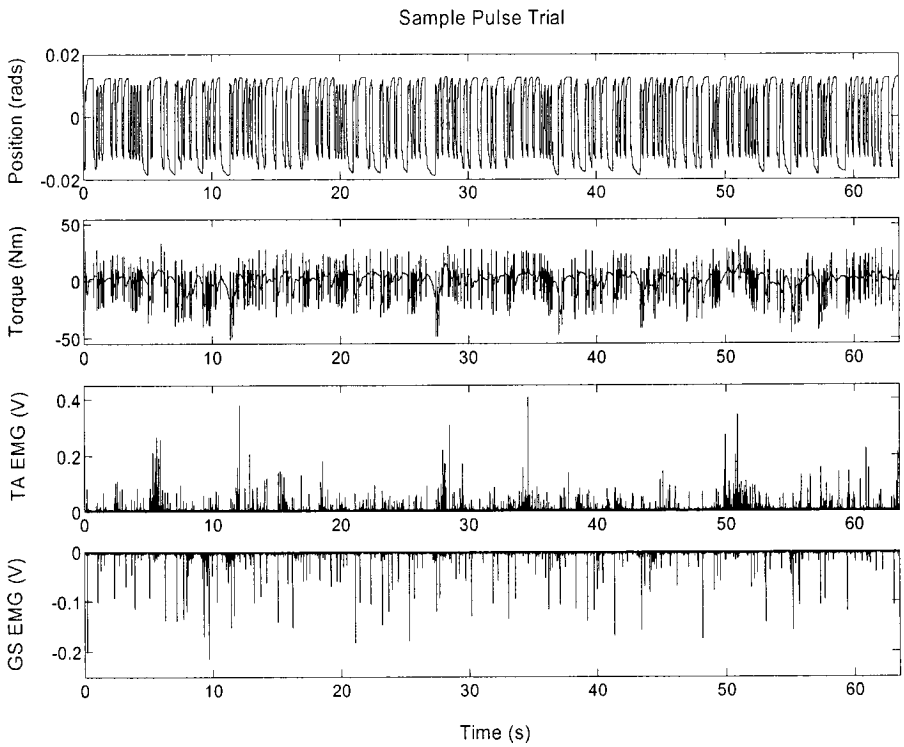

Figure 29 Sample sequence data, 64 s trial for one ankle

5.3.1 Case 1

The sequence perturbation was applied to one ankle while the other ankle remained stationary. Figure 30 shows the average position, torque, and EMG records for both legs for the first 4 s of the 64 s trial when the left ankle was stimulated and Figure 31 shows the results when the right ankle was stimulated.

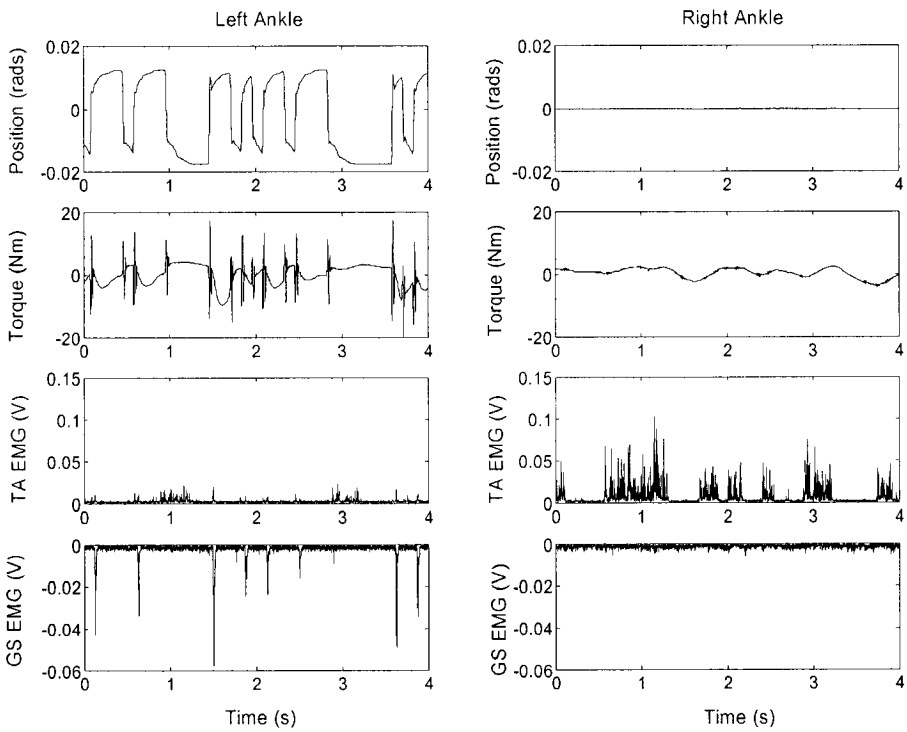

Figure 30 Sequence trial: left ankle stimulated, right ankle stationary

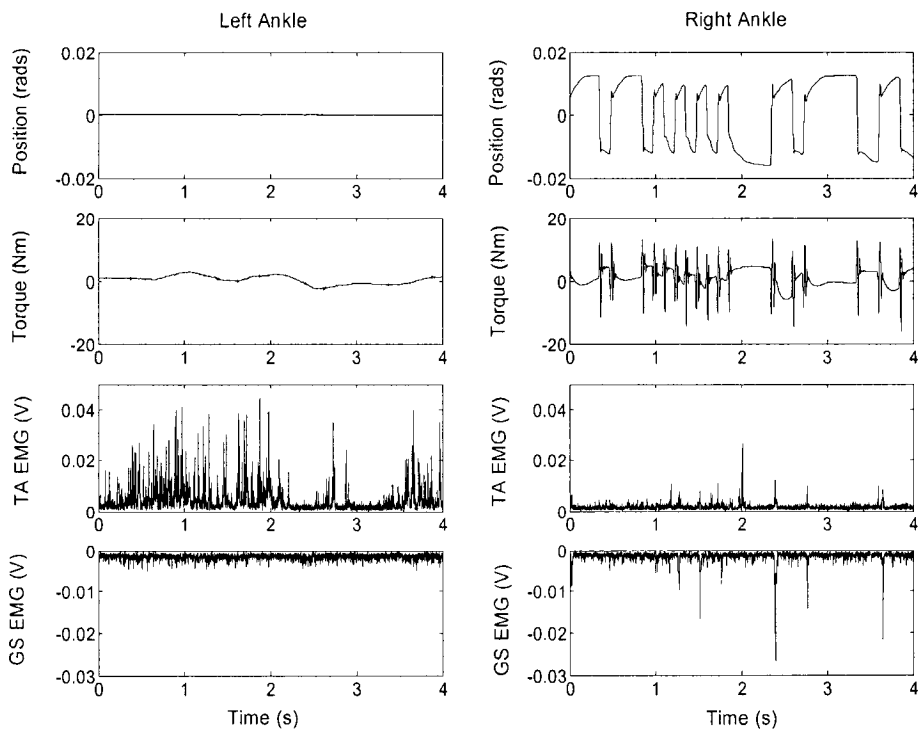

Figure 31 Pulse trial: left ankle stationary, right ankle stimulated

The results in Figures 30 and 31 showed that there was no GS EMG response in the stationary ankle. However, much TA activity was present in the stationary ankle compared to the stimulated ankle. In the stationary ankle, torques generated range from -4 Nm to +3 Nm. In the stimulated ankle, the torque responses were similar to those during the pulse trials where, after a dorsiflexing change in position, an initial component attributed to intrinsic mechanics was visible, followed by a reflex torque. Small, positive reflex torques were generated after ankle plantarflexion. These could be mediated by a stretch reflex in the TA. Reflex torques generated in the stimulated ankle range from -10 Nm to + 1.5 Nm.

5.3.2 Case 2

The same pseudo-random binary sequence input was applied to both the left and right ankles. Figure 32 shows the average position, torque, and EMG records of both legs for the 64 s trial.

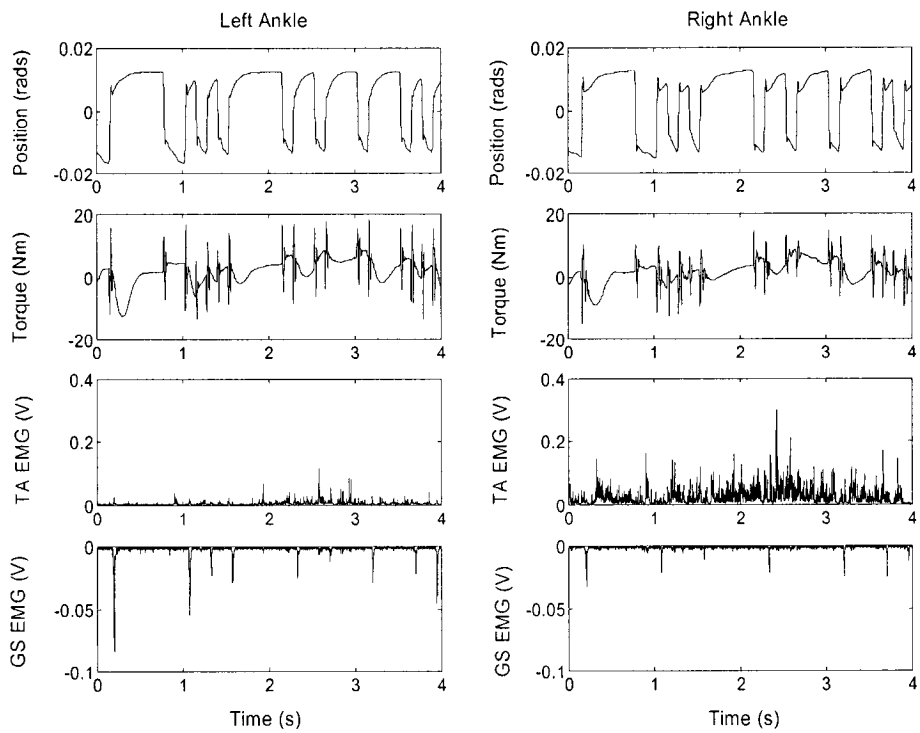

Figure 32 Sequence trial: ankles are stimulated with the same signal

The results in Figure 32 showed EMG activity in all muscles. However, the EMG activity in the left and right legs was not symmetric. Reflex torques generated range from -12 Nm to +2 Nm and the responses in the left and right ankles were similar.

5.3.3 Case 3

The sequence signal was applied to the left ankle and the negative or opposite of that signal was applied to the right ankle. Figure 33 show the average position, torque, and EMG records of both legs for the 64 s trial.

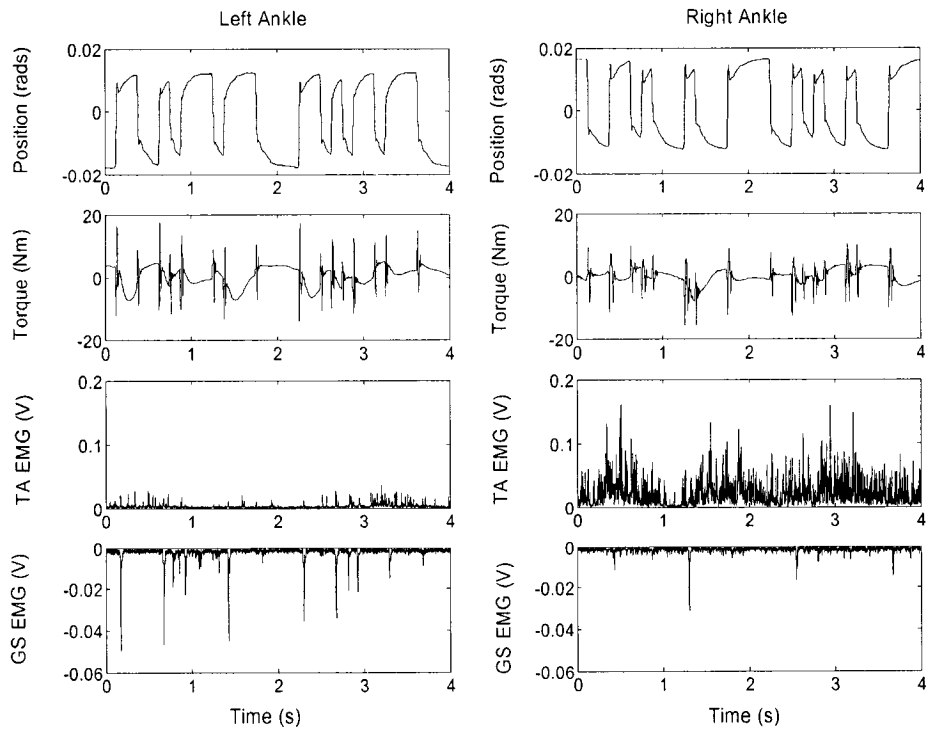

Figure 33 Sequence trial: ankles are stimulated with opposite signals

The results in Figure 33 were similar to those of Figure 32. The EMG activities in the left and right legs were not symmetric. Reflex torques generated range from -6 Nm to +3 Nm.

In all four trials, reflex torques could be seen in the stimulated ankles. These ranged from -12 Nm to +3 Nm. The positive reflex torques were generated after a plantarflexing stretch whereas the negative reflex torques were generated

after a dorsiflexing stretch. In the Case 1 trials, the stationary ankle had small torque variations and activity in the TA. In the Case 2 trials, both ankles were stimulated with the same input and exhibited similar torque responses. More activity was present in the right TA and a few spikes in GS EMG were present in both ankles. In the Case 3 trials, responses were similar to those of Case 2. The results showed EMG responses in the GS and negative reflex torques following ankle dorsiflexion. Small, positive reflex torques were generated after plantarflexion, but these did not seem to correspond to bursts in TA activity. None of the torque records displayed large, low frequency components that might be expected if there was significant sway.

5.4 Dynamic Stiffness

The left and right ankle data from Cases 2 and 3 of the sequence trials were modeled using the non-parametric and parametric models described in Section 2.6.3. Sample intrinsic compliance and reflex stiffness IRFs and their parametric fits are shown in Figure 34.

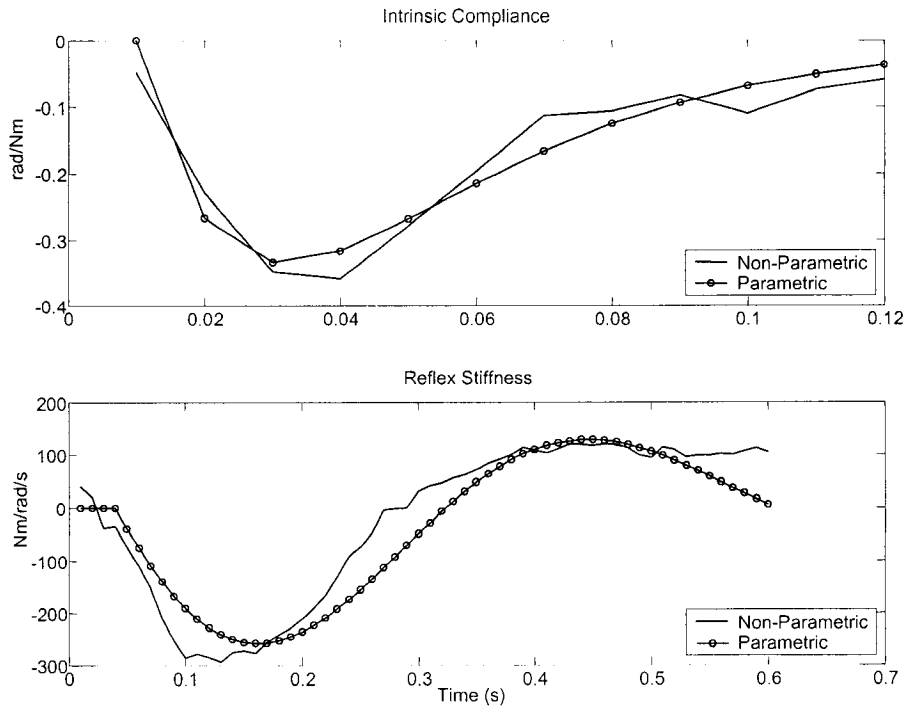

Figure 34 Example of intrinsic compliance (TQP_{IRF}) and reflex stiffness (VTQ_{IRF}) obtained from Case 2, left ankle, sequence data

Intrinsic and reflex parameters from the parametric models described in Section 2.6.3.2 were obtained for 4 sequence trials. Table 1 and 2 show the average intrinsic and reflex parameters of these for trials plus or minus the standard deviation.

Intrinsic Parameters	
K (Nm/rad)	96.7 ± 34.5
B (Nm/rad/s)	1.8 ± 0.3
I (Nm/rad/s^2)	0.04 ± 0.01

Table 1 Parameters of the intrinsic compliance parametric fit given in equation 2 (Section 2.6.3.2); values are the average parameters of the 4 trials plus or minus the standard deviation

Reflex Parameters	
G_R (Nm/rad/s)	20.5 ± 6.0
ω_n (rad/s)	11.0 ± 1.3
Z	0.29 ± 0.20
p (rad/s)	>1000
Delay (s)	0.04 ± 0.01

Table 2 Parameters of the reflex stiffness parametric fit given in equation 3 (Section 2.6.3.2); values are the average parameters of the 4 trials plus or minus the standard deviation

Table 3 shows the amount of the measured torque that can be attributed to the intrinsic stiffness model, the reflex stiffness model, or the total (intrinsic plus reflex). The results are the averages from 4 trials.

Percentage Variance Accounted For	
Intrinsic Torque (%VAF)	23.0 ± 7.1
Reflex Torque (%VAF)	18.0 ± 10.8
Total Torque (%VAF)	37.3 ± 5.9

Table 3 Relative contributions of intrinsic and reflex to total torque produced (%VAF given by equation 1 in Section 2.6.3.1); values are the average of the 4 trials plus or minus the standard deviation

The intrinsic and reflex parameters in Tables 1 and 2 had values of reflex gain and intrinsic stiffness similar in magnitude to those previously reported in supine subjects tested in our lab [24].

The results in Table 3 showed that reflex torque accounts for 18% of the measured torque as compared to 23% accounted for by the intrinsic torque. However, the total torque predicted by the model only accounted for 37%VAF of the measured torque. This indicates that the parallel-cascade model, designed to

analyze ankle dynamics in supine subjects, may not be suitable for ankle dynamics during standing, or, there is substantial noise present in the angular torque due to body sway.

5.5 Summary

Five pulse experiments were performed. The first two had one ankle being dorsiflexed while the other remained stationary. The third trial had both ankles being dorsiflexed simultaneously. And the last two trials had one ankle being dorsiflexed while the other was being plantarflexed. For all cases, the command pulse was of amplitude ±0.03 rads and length 40 ms to stretch and return the ankle to its original position before the reflex torque was generated [26]. This allowed the reflex torque to be measured without any intrinsic component.

For the case where only one ankle was being stimulated, there was no EMG activity in the GS of the stationary ankle. For all dorsiflexing pulses, the corresponding EMG records showed spikes in the GS activity with latencies ranging from 25 ms to 40 ms after the pulse onset. For the case where two opposite pulses are applied to the ankles, the results showed that the spike in the GS EMG for the dorsiflexed ankle occurred approximately 33 ms after the onset of the dorsiflexing pulse. The spike in the GS EMG for the plantarflexed ankle occurred approximately 33 ms after the positive (dorsiflexing) edge of the plantarflexing pulse. The GS showed an EMG response at a latency of 29 ms to 36 ms after onset of the stretching stimulus.

The EMG records showed spikes in TA activity with latencies ranging from 30 ms to 110 ms after the pulse onset. Because of the varying latencies of activity in the TA, it was difficult to determine if it is attributed to cross-talk from the GS, or if it was short and medium latency responses of the stretch reflex.

Further work needs to be done with plantarflexing inputs to determine whether the TA stretch reflex is used during upright stance.

The reflex torques generated in the pulse trials were in the range of -2 Nm to -6 Nm. The latency of the reflex torque responses were in the range of 122 ms to 182 ms after the pulse onset.

The resulting torque and EMG responses from the pulse trials indicated that stretching of the GS during upright stance produces a spike in GS EMG activity and generates reflex torque. The responses in one ankle appeared to be independent of stimulus in the opposite ankle.

Four experiments were performed using a pseudo-binary random sequence. The first two had one ankle stimulated and the other stationary. The third trial had both ankles stimulated with the same input signal. And the fourth trial had one ankle stimulated with a sequence perturbation and the other ankle stimulated with the opposite perturbation. The sequence inputs had a peak to peak amplitude of 0.03 rads and a switching frequency of 125 ms.

In all four trials, reflex torques were seen in the stimulated ankles. The torque responses are similar to those during the pulse trials where, after a dorsiflexing change in position, an initial component attributed to intrinsic mechanics was visible, followed by a reflex torque. Small, positive reflex torques were generated after ankle plantarflexion. Reflex torque magnitudes ranged from -12 Nm to +3 Nm. During the Case 1 trials, the stationary ankle generated torques in the range of -2 to +2 Nm but these were not accompanied by any GS EMG activity. However, TA activity was present in the stationary ankle. The results of the Case 2 and 3 trials were similar in that EMG activity in both legs was not alike.

The results from the PBRS trials are similar to those of the pulse trials in that they showed ankle responses depend only on the stimulus of the same ankle and not that of the opposite leg. The results also indicated that stretch reflexes in the GS are present during upright stance. Further investigation needs to be done to determine whether the small torque responses generated during plantarflexion are due to a stretch reflex in the TA.

The results of both the pulse and sequence trials showed that the GS was active during upright stance. Some TA activity was evident in both trials but whether this was due to crosstalk or is in fact a reflex response can not be determined at this time. For the pulse trials, the latencies of the GS responses are similar with those previously reported for the stretch reflex [17, 18, 28].

The responses in one ankle appear to be independent of the stimulus in the other ankle. Therefore, it is expected that when different input perturbations are applied to each ankle, as in Case 1 and Case 3 trials, the resulting responses are asymmetric. However, during Case 2 trials, when the same input command was applied to each ankle the responses were not necessarily symmetric. During the pulse trial, reflex torques of different magnitude were generated in both ankles and the EMG responses were similar for the GS but not for the TA. During the sequence trial, the reflex torques generated were symmetric, spikes in the GS occurred at similar latencies; however, the TA responses were not similar. The asymmetry of responses could have occurred for several reasons: 1) the input perturbations generated from the actuators were not identical, or 2) the dynamic stiffness of both the subject's ankles were not identical.

The system identification that was done on the sequence trial data showed that the predicted intrinsic torque accounted for 23% of the total torque, whereas the predicted reflex torque accounted only for 18% of the total torque. The model parameters for intrinsic compliance and reflex stiffness were in the same range as those of previous studies [26]. However, the total torque accounted for by the

model was only 37% of the total measured torque. This indicates that the model does not correctly identify dynamic stiffness during upright stance or, there is substantial noise present in the angular torque due to body sway. A closed-loop identification is needed to compute the intrinsic and reflex components of dynamic stiffness.

6 Discussion

This thesis presented original work of the author including: 1) assisting in the fabrication of the new apparatus, 2) developing control systems, 3) analysing the performance of the apparatus, and 4) conducting a pilot study to show that reflex responses are elicited in subjects tested on the new experimental apparatus.

6.1 Results

The results of the performance analysis showed that the actuators did not function as desired. The dynamics of the actuators are complex and nonlinear. The responses of the two actuators were not identical and pulse responses in the individual actuators were not symmetric and seemed to depend on the direction of rotation. Identification needs to be done to determine what the actuator dynamics are so that a more appropriate controller can be developed.

Controllers were designed to compensate for the actuator dynamics and adequate system responses were obtained for the requirements of the pilot study. The pilot study used pulse and sequence input perturbations to acquire data for one subject. Reflex torques ranging in magnitude from -12 Nm to +1.5 Nm were generated. Spikes in GS EMG activity were present following ankle dorsiflexion.

Results showed that stimulating one ankle did not evoke responses in the opposite, stationary ankle. When both ankles were stimulated with the same input, torque responses were similar, but EMG responses still varied between the two legs. When the ankles were stimulated with opposite signals, they responded independently to their own stimulus and no attenuation of responses was seen.

Open-loop identification done on the sequence data showed that reflex stiffness accounted for 18% of the total torque. However, the total torque accounted for by the model was low, indicating that the model does not correctly identify dynamic stiffness during upright stance or that there is substantial noise in the angular torque data due to the body's ability to sway. Therefore, a closed-loop identification will be required.

6.3 Future Work

Further knowledge in the field of motor and postural control has many uses. First, neuromuscular disease may cause changes in muscle stiffness. These changes are normally characterized using clinical tests which have little mechanical correlation [19]. With further research, tools to evaluate muscle tone can be developed to provide an objective measure of the mechanical properties. Second, information on how the body controls its movements will lead to advances in the fields of telerobotics, human-machine interfaces, and robotics. Finally, knowledge of how the neuromuscular system works will be of great benefit to the field of rehabilitation engineering. Advances in functional electrical stimulation (FES) will help spinal cord injury patients to stand and walk.

The new experimental apparatus will be used to measure dynamic ankle joint stiffness, and the relative contributions of reflex and intrinsic mechanisms, in humans during upright stance.

The apparatus was designed with future studies in mind. Eventually, trials will be run with and without vision, with and without additional support in the form of a handle in front of the subject, with the ankle at different positions to reduce the base of support, and with different loads applied to the back of the subject to increase the effective gain of the stretch reflex needed for stability.

Another area of interest that may be investigated is the attentional demand required for standing. Several studies have already looked into the attention required to maintain a stable posture [36, 41]. Some have asked questions to the subjects while increasing the difficulty of the standing task [36]. Others have reintegrated sensory mechanisms during a trial and observed how the body stabilization was affected [41].

The data acquisition system must be set up to measure the hip and knee angles during the experiments. The experiments conducted will focus on ankle dynamics and will not require the body to act as an inverted pendulum. Therefore hip and knee angles are not necessary, but it will be interesting to see if trunk movements occur during larger amplitude perturbations. Also, any movement of the knee will cause a change in length of the gastrocnemius. Significant knee movement is not expected during upright stance [32] but should it occur a custom fitted orthosis will be used to lock the knee in an extended position.

A method of system identification must be developed to separate the intrinsic and reflex components of dynamic joint stiffness. In the past, our laboratory has made use of a nonlinear parallel cascade identification scheme [20] to determine the relative contributions to dynamic stiffness. This method is an open-loop identification and the experiments have all been conducted with subjects lying prone with no requirement of maintaining a stable posture. For the upright stance, a closed-loop identification will be needed since the responses evoked by ankle perturbations will cause changes in ankle position [42]. Tung et al. [42] developed an algorithm to estimate the intrinsic stiffness and reflex stiffness contributions in a closed loop system. Again, this method was used to estimate the contributions to dynamic ankle joint stiffness in prone subjects. For the upright stance, a new closed-loop identification method may be needed since the latencies and characteristics of the muscle reflexes in upright stance are not well understood and may not be the same as those evoked when subjects are lying prone.

6.4 Conclusion

A new experimental apparatus device has been designed and built in order to enable the characterization of dynamic ankle stiffness in humans during upright stance. Using Matlab and SIMULINK, the control system has been designed and tested. The device is capable of applying pulse, random, and pseudo-random binary sequence perturbations to each ankle separately. The results of a pilot study show that reflex responses generated in the gastrocnemuis are present during upright stance.

7 References

1. Afanah, A., Akache, F., Fallavollita, P., Nabhani, Z. *Ankle testing device: Final report.* Mechanical Engineering Project Report, McGill University, Department of Mechanical Engineering, 2002
2. Allum, J.H.J, Bloem, B.R., Carpenter, M.G., Hulliger, M., Hadders-Algra, M. *Proprioceptive control of posture: a review of new concepts.* Gait and Posture, Vol. 8, pp214-242, 1998
3. Brooks, V.B. The Neural Basis of Motor Control. Oxford University Press, 1986
4. Brown, L.A., Jensen, J.L., Korff, T., Woollacott, M.H. *The translating platform paradigm: perturbation displacement and waveform alters the postural response.* Gait and Posture, Vol. 14, pp256-263, 2001
5. Collins, J.J., De Luca, C.J. *Open-loop and closed-loop control of posture: a random-walk analysis of center-of-pressure trajectories.* Experimental Brain Research, Vol. 95, pp308-318, 1993
6. Dault, M.C., Geurts, A.C.H., Mulder, T.W., Duysens, J. *Postural control and cognitive task performance in healthy participants while balancing on different support-surface configurations.* Gait and Posture, Vol. 14, pp248-255, 2001
7. Fisekovic, N., Popovic, D.B. *New controller for functional electrical stimulation systems.* Medical Engineering and Physics, Vol. 23, pp391-399, 2001

8. Fitzpatrick, R.C., Taylor, J.L., McCloskey, D.I. *Ankle stiffness of standing humans in response to imperceptible perturbation: reflex and task-dependent components.* Journal of Physiology, Vol. 454, pp533-547, 1992
9. Fitzpatrick, R.C., Gorman, R.B., Burke, D., Gandevia, S.C. *Postural proprioceptive reflexes in standing human subjects: bandwidth of response and transmission characteristics.* Journal of Physiology, Vol. 458, pp69-83, 1992
10. Fitzpatrick, R., Rogers, D.K., McCloskey, D.I. *Stable human standing with lower-limb muscles afferents providing the only sensory input.* Journal of Physiology, Vol. 480(2), pp395-403, 1994
11. Fitzpatrick, R., Burke, D., Gandevia, S.C. *Loop gain of reflexes controlling human standing measured with the use of postural and vestibular disturbances.* Journal of Neurophysiology, Vol. 76, pp3994-4007, 1996
12. Gatev, P. Thomas, S., Kepple, T., Hallett, M. *Feedforward ankle strategy of balance during quiet stance in adults.* Journal of Physiology, Vol. 514(3), pp915-928, 1999
13. Huang, Q.-M., Hodges, P.W., Thorstensson, A. *Postural control of the trunk in response to lateral support surface translations during trunk movement and loading.* Experimental Brain Research, Vol. 141, pp552-559, 2001

14. Hunt, K.J., Gollee, H., Jaime, R.-P. *Control of paraplegic ankle joint stiffness using FES while standing.* Medical Engineering and Physics, Vol. 23, pp541-555, 2001

15. Jenkins, D. B. Hollinshead's Functional Anatomy of the Limbs and Back (8th edition). W. B. Saunders Company, 2002

16. Kandel, E.R., Schwartz, J.H., Jessell, T.M. Principles of Neural Science (3rd edition). Elsevier Science Publishing Co. Inc., 1991

17. Kearney, R.E., Hunter, I.W. *System identification of human triceps surae stretch reflex dynamics.* Experimental Brain Research, Vol. 51, pp117-127, 1983

18. Kearney, R.E., Hunter, I.W. *System identification of human stretch reflex dynamics: tibialis anterior.* Experimental Brain Research, Vol. 56, pp40-49, 1984

19. Kearney, R.E., Hunter, I.W. *System identification of human joint dynamics.* Critical Reviews in Biomedical Engineering, Vol. 18, pp55-87, 1990

20. Kearney, R.E., Stein, R.B., Parameswaran, L. *Identification of intrinsic and reflex contributions to human ankle stiffness dynamics.* IEEE Transactions on Biomedical Engineering, Vol. 44(6), pp493-504, 1997

21. Kuo, A.D., Speers, R.A., Peterka, R.J., Horak, F.B. *Effect of altered sensory conditions on multivariate descriptors of human postural sway.* Experimental Brain Research, Vol. 122, pp185-195, 1998

22. Leung, H. D*esign and development of an experimental apparatus to measure dynamic ankle joint stiffness of humans in upright stance.* Honour's thesis, McGill University, Department of Mechanical Engineering, 2001.

23. Loram, I.D., Kelly, S.M., Lakie, M. *Human balancing of an inverted pendulum: is sway size controlled by ankle impedance?* Journal of Physiology, Vol. 532(3), pp879-891, 2001

24. Loram, I.D., Kelly, S.M., Lakie, M. *Human balancing of an inverted pendulum: position control by small, ballistic-like, throw and catch movements.* Journal of Physiology, Vol. 540(3), pp1111-1124, 2002

25. Loram, I.D., Lakie, M. *Direct measurement of human ankle stiffness during quiet standing: the intrinsic mechanical stiffness is insufficient for stability.* Journal of Physiology, Vol. 545(3), pp1041-1053, 2002

26. Ludvig, D., Baker, M., Cathers, I., Kearney, R.E. Task-dependence of ankle stretch reflex. Proceedings of the 25th Annual EMBS Conference, September 2003, Cancun, Mexico

27. McMahon, T.A. Muscles, Reflexes, and Locomotion. Princeton University Press, 1984

28. Mirbagheri, M.M., Barbeau, H., Kearney, R.E. *Intrinsic and reflex contributions to human ankle stiffness: variation with activation level and position.* Experimental Brain Research, Vol. 135, page423-436, 2000

29. Morasso, P.G., Schieppati, M. *Can muscle stiffness alone stabilize upright standing?* Journal of Neurophysiology, Vol. 82, pp1622-1626, 1999

30. Mrachacz-Kersting, N., Sinkjaer, T. *Reflex and non-reflex torque responses to stretch of the human knee extensors.* Experimental Brain Research, April 2003

31. Nardone, A., Corrà, T., Schieppatti, M. *Different activations of the soleus and gastrocnemii muscles in response to various types of stance perturbation in man.* Experimental Brain Research, Vol. 80, pp323-332, 1990

32. Nashner, L.M., McCollum, G. *The organization of human postural movements: a formal basis and experimental synthesis.* The Behavioral and Brain Sciences, Vol. 8, pp135-172, 1985

33. Nashner, L.M., Shupert, C.L., Horak, F.B., Black, F.O. *Organization of posture controls: an analysis of sensory and mechanical constraints.* Progress in Brain Research, Vol. 80, pp411-418, 1989

34. Netter, F. H. Atlas of Human Anatomy (2nd edition). Novartis, 1989

35. Patla, A.E., Ischac, M.G., Winter, D.A. *Anticipatory control of center of mass and joint stability during voluntary movement from a standing posture: interplay between active and passive control.* Experimental Brain Research, Vol. 143, pp318-327, 2002

36. Redfen, M.S., Jennings, J.R., Martin, C., Furman, J.M. *Attention influences sensory integration for postural control in older adults.* Gait and Posture, Vol. 14, pp211-216, 2001

37. REKlab Manual http://www.bmed.mcgill.ca/reklab/REKLAB_manual/manual.htm

38. Richardson, M. L. Lower Extremity Muscle Atlas, University of Washington, http://www.rad.washington.edu/atlas2/

39. Sinha, T., Maki, B.E. *Effect of forward lean on postural ankle dynamics.* IEEE Transactions on Rehabilitation Engineering, Vol.4(4), pp348-359, 1996

40. Soetanto, D., Kuo, C.-Y., Babic, D. *Stabilization of human standing posture using functional neuromuscular stimulation.* Journal of Biomechanics, Vol. 34, pp1589-1597, 2001

41. Teasdale, N., Simoneau, M. *Attentional demands for postural control: the effects of aging and sensory reintegration.* Gait and Posture, Vol. 14, pp203-210, 2001

42. Tung, J.Y., Kearney, R.E. *Closed-loop estimation of intrinsic and reflex contributions to ankle stiffness.* Proceedings of the 2nd Joint EMBS/BMES Conference, October 2002, Houston, TX, pp.2550-2551

43. Vander, A., Sherman, J., Luciano, D. Human Physiology: The Mechanisms of Body Function (8^{th} edition). McGraw Hill, 2001

44. Winter, D.A., Patla, A.E., Prince, F., Ishac, M. Gielo-Perczak, K. *Stiffness control of balance in quiet standing.* Journal of Neurophysiology, Vol. 80, pp1211-1221, 1998

45. Winter, D.A., Patla, A.E., Ishac, M., Gage, W.H. *Motor mechanisms of balance during quiet standing.* Journal of Electromyography and Kinesiology, Vol. 13, pp49-56, 2003

8 Appendices

A) Controller Version 1 Block Diagram

B) Controller Version 2 Block Diagram

C) Controller Version 3 Block Diagram

D) Controller Version 4 Block Diagram

E) Actuator Assembly

F) Data Sheet for Rotary Actuator

G) Data Sheet for Servo-Valve

H) Circuit Diagram for Servo-Salve Module

I) Data Sheet for Torque Transducer

J) Circuit Diagram for Torque Transducer Module

K) Data Sheet for Potentiometer

L) Circuit Diagram for Potentiometer Module

M) Data Sheet for EMG System

N) Data Sheet for EMG Electrodes

O) Data Sheet for Angular Sensors

P) Data Sheet for Ultrasonic Sensor

Q) Actuator Coupling

R) Safety Cam

S) Foot Pedal End

T) Torque Transducer / Foot Pedal Coupling

Appendix A - Controller Version 1 Block Diagram

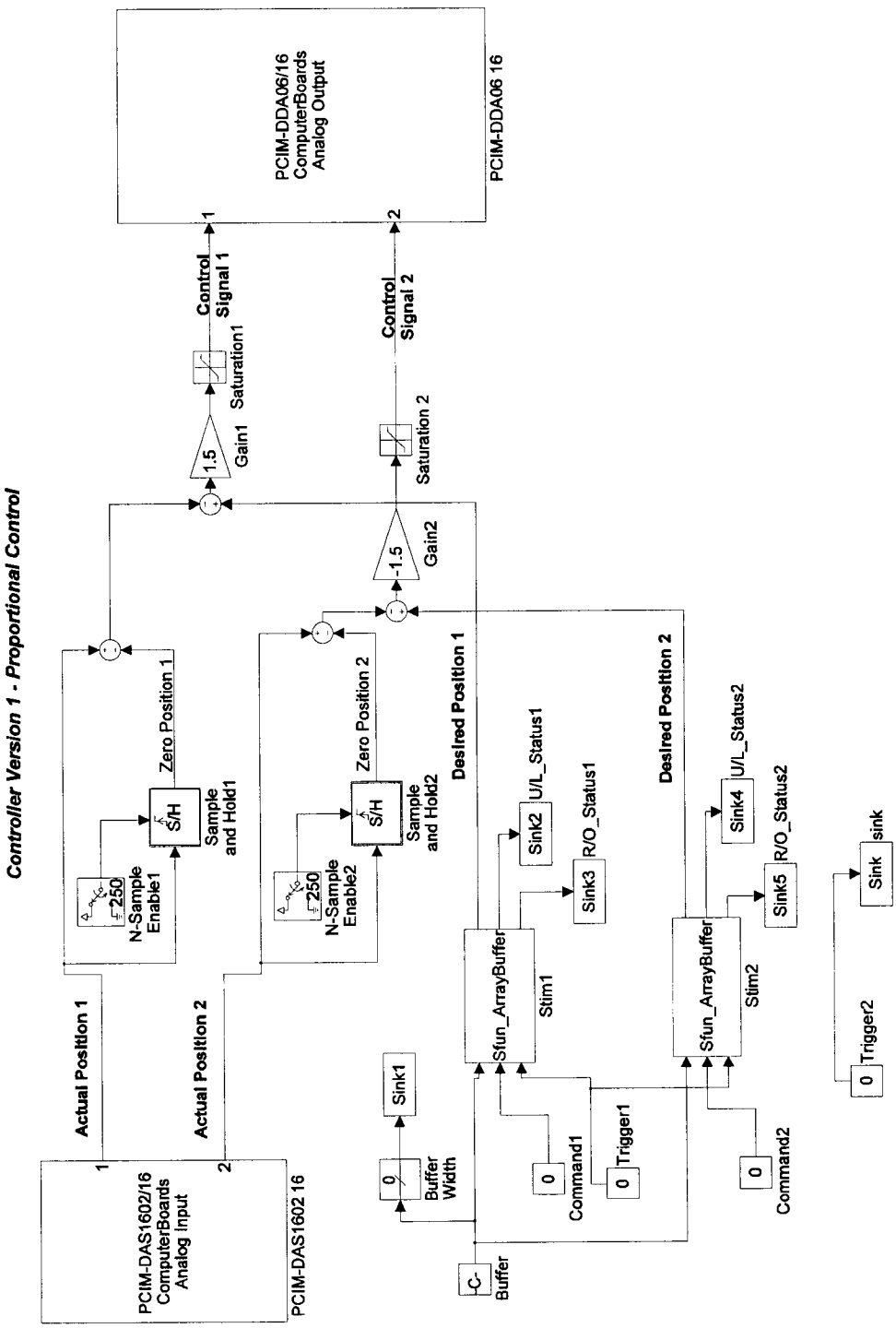

Appendix B - Controller Version 2 Block Diagram

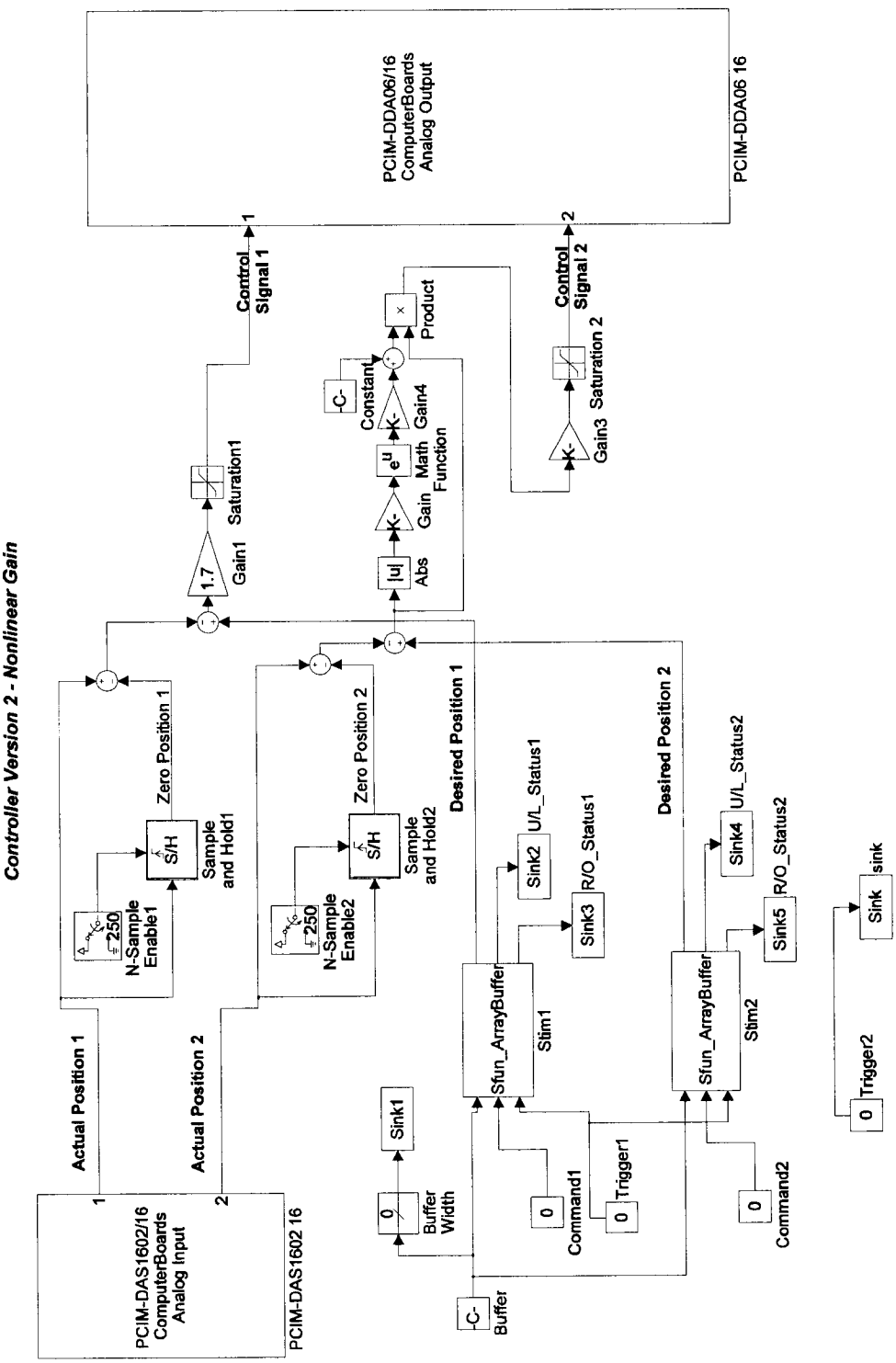

Appendix C - Controller Version 3 Block Diagram

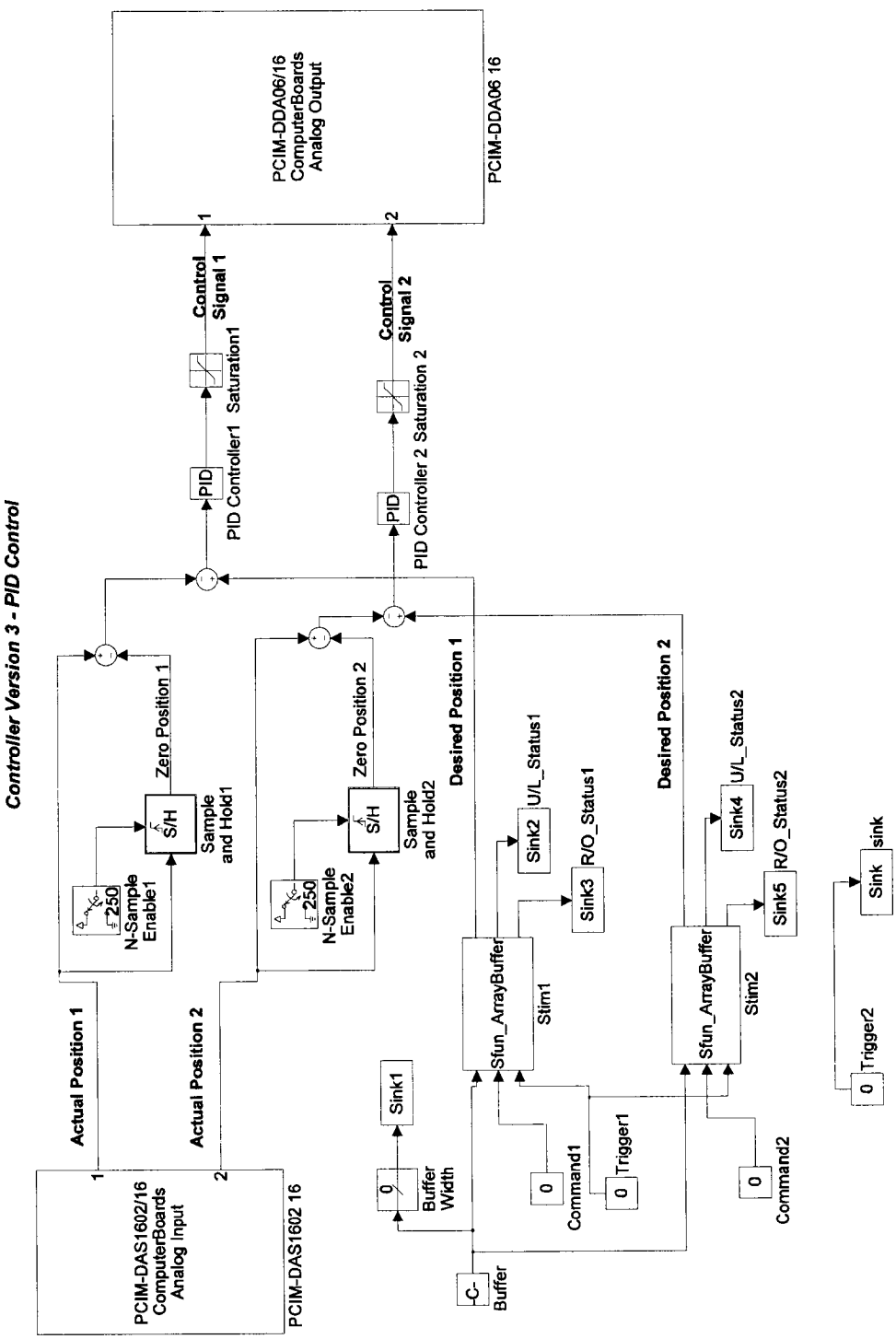

Appendix D - Controller Version 4 Block Diagram

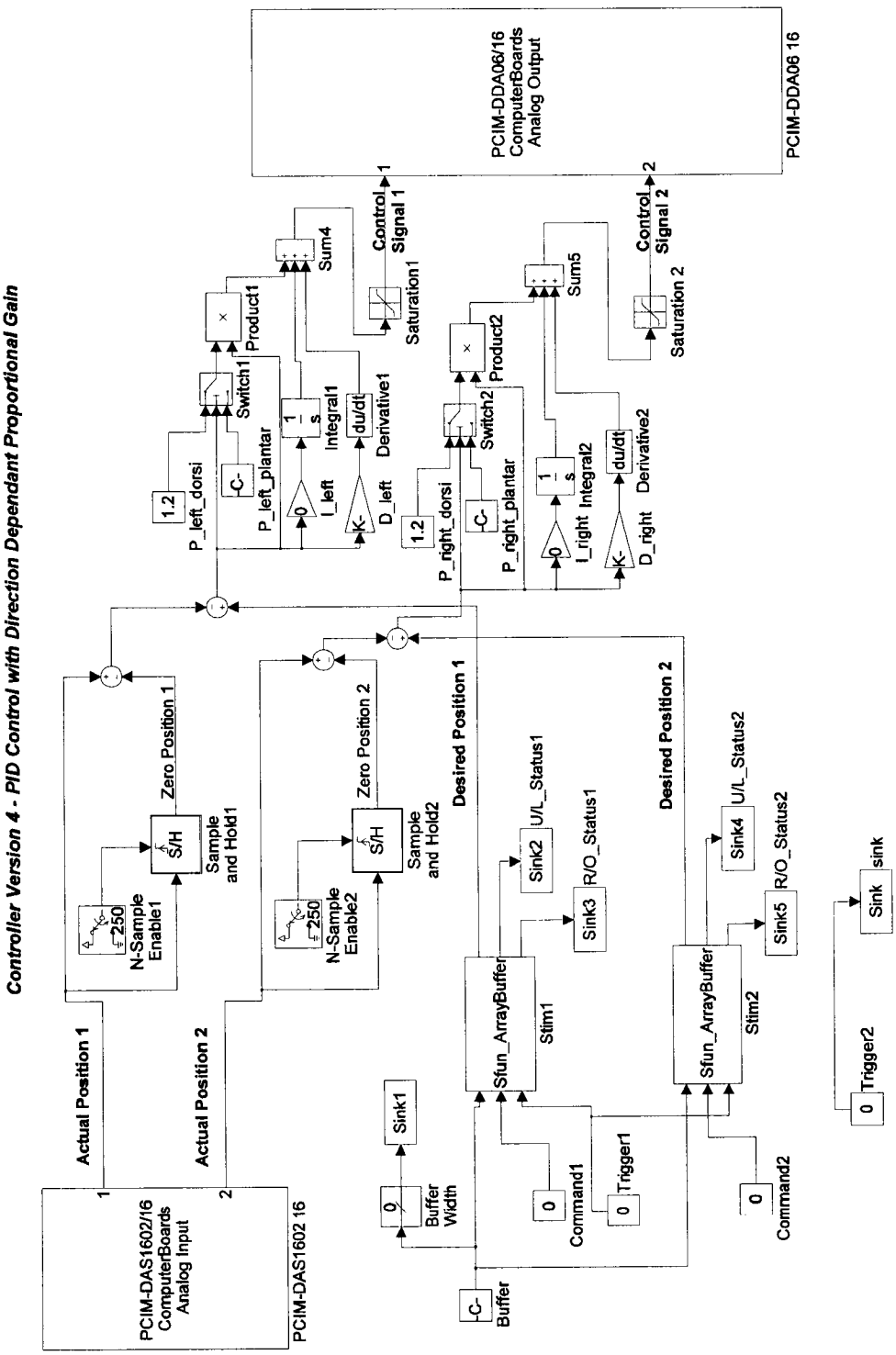

Appendix E - Actuatory Assembly

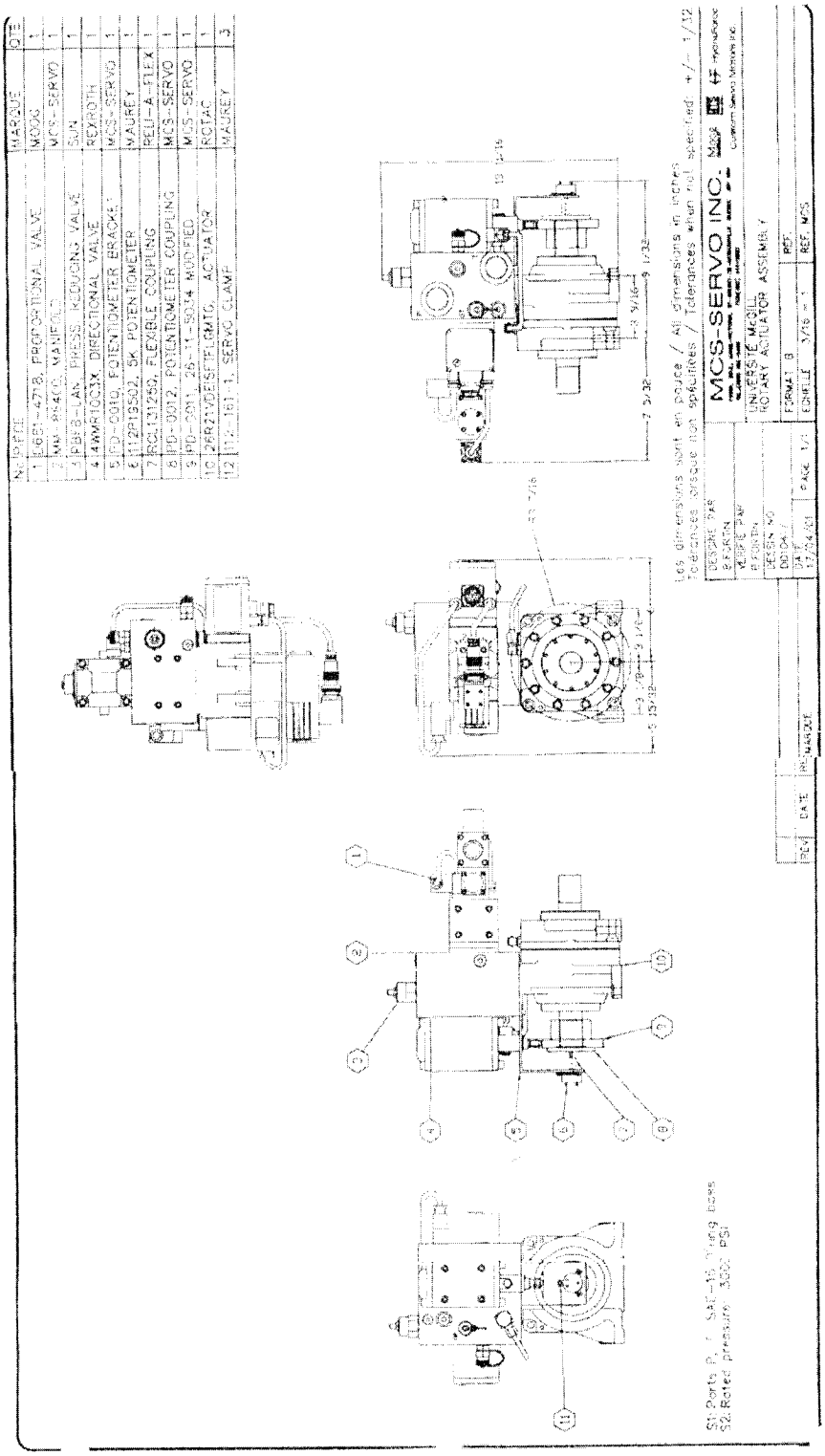

Appendix F - Data Sheet for Rotary Actuator

(model #26R21VDEISFTFLGMTG)

Micro-Precision TEXTRON

26-R MODELS

HIGH PRESSURE 3000 PSI MAX

Rotary Actuators

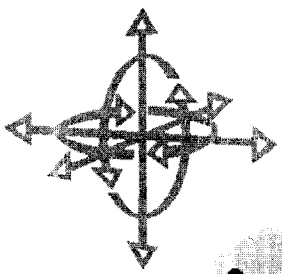

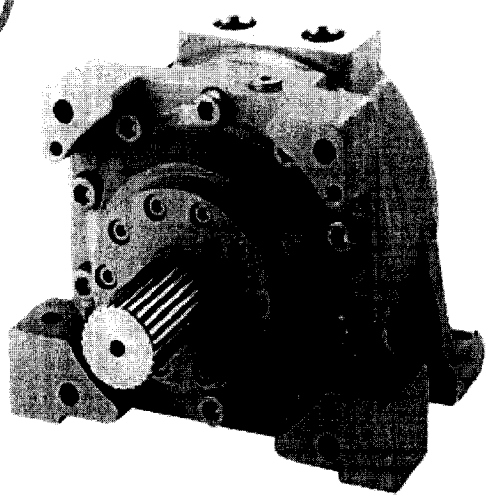

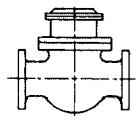

VALVE OPEN—CLOSE

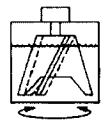

MIX—STIR

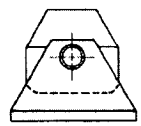

TURNOVER—DUMP

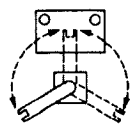

LOAD—POSITION—UNLOAD

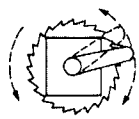

CONTINUOUS ROTATION

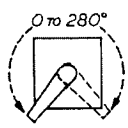

TURN—OSCILLATE

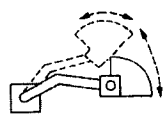

MATERIAL HANDLING

High-Pressure Solid Shaft

PROVIDING the "**MUSCLE**" **for your**
lifting, turning, indexing, opening, closing, clamping, mixing, bending, testing, steering. . . **applications.**

26R-1

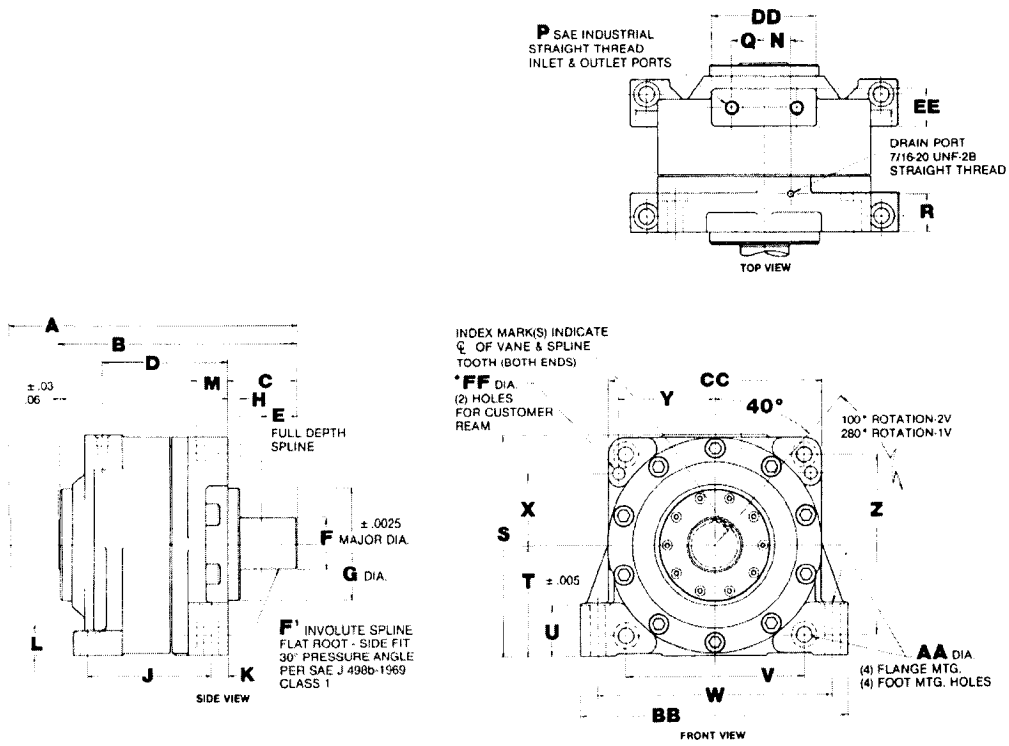

NOTE: Connection of drains will add significant life to shaft seals. *Their use is highly recommended.*

*NOTE: FOR FLANGE MTD. UNITS THESE HOLES SHOULD BE TRANSFER DRILLED AND REAMED AT INSTALLATION FOR INSERTION OF DOWEL PINS. (THIS WILL AID IN PREVENTING "RACKING" OF ACTUATOR ON MOUNTING BOLTS DUE TO TORSIONAL FORCES)

***1 2000 PSI maximum is recommended for severe duty applications, such as operating at maximum torque at high cycle rates for extended periods. Please consult factory for applications beyond 2000 PSI. 3000 PSI can be used on intermittent shockless actuations.**

NOTE: See cut away view on page 26R-4.

NOTE: See pages OA-5 and OA-6 for optional manifolds and shaft couplings.

DIMENSIONS IN INCHES (METRIC)

	26R-2	26R-5	26R-10	26R-17	26R-31	26R-62	26R-124
A	10.03 (256)	12.06 (306.3)	14.19 (360.4)	16.57 (420.9)	18.58 (471.9)	24.39 (619.3)	31.22 (792.9)
B	8.02 (203.7)	9.84 (249.9)	11.50 (292.1)	13.51 (343.2)	15.01 (381.3)	19.44 (493.8)	25.06 (636.5)
C	2.62 (66.5)	2.86 (72.6)	3.41 (86.6)	3.87 (98.3)	4.38 (111.3)	6.02 (152.9)	7.51 (190.8)
D	3.50 (88.9)	4.96 (123.4)	5.63 (143)	6.61 (167.9)	7.50 (198.1)	9.87 (250.7)	12.80 (325.1)
E	1.62 (41.1)	1.75 (44.4)	2.12 (53.6)	2.50 (63.5)	3.00 (76.2)	4.25 (107.9)	5.25 (133.4)
F*	1.3335 (33.871)	1.6685 (42.380)	2.2268 (56.561)	2.6735 (67.907)	3.2735 (83.147)	4.0935 (103.975)	4.8435 (123.025)
F'	26T (20/40P)	26T (16/32P)	26T (12/24P)	26T (10/20P)	32T (10/20P)	32T (8/16P)	38T (8/16P)
G	1.3000PD 3.38 (85.9)	1.6250PD 4.25 (108)	2.1667PD 5.00 (127)	2.6000PD 6.00 (1524)	3.2000PD 7.00 (177.8)	4.0000PD 9.13 (231.9)	4.7500PD 10.50 (266.7)
H	.50 (12.7)	.57 (14.5)	.64 (16.3)	.76 (19.3)	.76 (19.3)	1.02 (25.9)	1.27 (32.3)
J	3.56 (90.4)	4.62 (117.3)	5.37 (136.4)	6.69 (169.9)	7.75 (196.9)	9.31 (236.5)	12.19 (309.6)
K	.63 (16)	.86 (21.8)	1.01 (25.7)	1.07 (27.2)	1.04 (26.4)	1.51 (38.4)	2.01 (51.1)
L	.56 (14.2)	.81 (20.6)	.94 (23.9)	1.12 (28.4)	1.50 (38.10)	1.69 (42.9)	2.06 (52.3)
M	.75 (19.1)	1.25 (31.8)	1.50 (38.1)	1.75 (44.5)	2.00 (50.8)	2.68 (68.1)	4.00 (101.6)
N	.77 (19.6)	1.01 (25.7)	1.19 (30.2)	1.47 (37.3)	1.68 (42.7)	2.17 (55.1)	2.44 (62)
P	⅜-16	⅜-16	⅜-14	1⅛-12	1⅜-12	1⅞-12	1⅞-12
Q	.88 (22.4)	1.06 (26.9)	1.25 (31.8)	1.62 (41.1)	2.06 (52.3)	2.62 (66.5)	2.75 (69.9)
R	1.29 (32.8)	1.80 (45.7)	1.82 (46.2)	2.17 (55.1)	2.42 (61.5)	2.79 (70.9)	3.67 (93.2)
S	6.00 (152.4)	8.00 (203.2)	9.76 (247.9)	11.26 (286)	13.76 (349.5)	17.13 (435.1)	20.50 (520.7)
T**	3.000 (76.20)	4.000 (101.60)	4.875 (123.83)	5.625 (142.88)	6.875 (174.63)	8.562 (217.47)	10.25 (260.35)
U	1.50 (38.1)	1.94 (49.3)	2.25 (57.2)	2.62 (66.5)	3.19 (81.0)	3.90 (99.1)	4.88 (123.9)
V	4.88 (123.9)	6.38 (162.1)	8.00 (203.2)	9.25 (234.9)	11.25 (285.8)	14.00 (355.6)	16.75 (425.5)
W	6.25 (158.8)	8.25 (209.6)	10.25 (260.4)	11.87 (301.5)	14.87 (377.7)	18.37 (466.6)	21.25 (539.8)
X	1.78 (45.2)	2.44 (61.9)	2.94 (74.7)	3.50 (88.9)	4.44 (112.8)	5.44 (138.2)	6.31 (160.3)
Y	2.61 (66.3)	3.41 (86.6)	4.28 (108.7)	4.94 (125.5)	6.06 (153.9)	7.44 (188.9)	8.81 (223.8)
Z	4.88 (123.9)	6.38 (162.1)	8.00 (203.2)	9.25 (234.9)	11.25 (285.8)	14.00 (355.6)	16.75 (425.5)
AA	.41 (10.4)	.53 (13.5)	.69 (17.5)	.81 (20.6)	.94 (23.9)	1.06 (26.9)	1.31 (33.3)
BB	7.12 (180.8)	9.62 (244.3)	11.75 (298.5)	13.62 (345.9)	17.00 (431.8)	21.00 (533.4)	24.50 (622.3)
CC	5.75 (146.1)	7.62 (193.5)	9.50 (241.3)	11.00 (279.4)	13.50 (342.9)	16.75 (425.5)	19.75 (501.7)
DD	3.38 (85.85)	3.94 (100.1)	4.50 (114.3)	5.75 (146.1)	6.62 (168.1)	9.00 (203.2)	9.62 (244.3)
EE	1.62 (41.1)	1.81 (45.9)	2.00 (50.8)	2.50 (63.5)	2.50 (63.5)	2.75 (69.9)	4.12 (104.8)
FF	.23 (5.8)	.34 (8.6)	.47 (11.9)	.72 (18.3)	.84 (21.3)	.84 (21.3)	.84 (21.3)

*± .0025 in. (±0.064 mm)
**.005 in. (0.13 mm)

NOTE: See how to order on page 26R-4.

SINGLE VANE 280° ROTATION (±1°)						
MODEL	TORQUE IN-LBS (N•m)			VOLUMETRIC DISPLACEMENT IN³ (cm³)		APPROX. WEIGHT LB (Kg)
	1000 PSI (69.0 BAR)	2000 PSI (137.9 BAR)	3000 PSI (206.9 BAR)	PER 280°	PER RAD	
26R2	1720 (194.4)	3440 (388.7)	5160 (583.1)	9.35 (153.25)	1.91 (31.3)	32 (15)
26R5	3900 (440.7)	7800 (881.4)	11700 (1322.1)	21.20 (347.47)	4.34 (71.13)	67 (30)
26R10	9100 (1028.5)	18200 (2056.6)	27300 (3084.9)	49.50 (811.31)	10.12 (165.87)	115 (52)
26R17	15200 (1717.6)	30400 (3435.2)	45600 (5152.8)	82.60 (1353.81)	16.90 (276.99)	207 (94)
26R31	27500 (3107.5)	55000 (6215)	82500 (9322.5)	149.50 (2450.31)	30.59 (501.55)	334 (152)
26R62	56000 (6328)	112000 (12656)	168000 (18984)	304.00 (4982.56)	62.20 (1019.46)	680 (309)
26R124	110000 (124.30)	220000 (24860)	330000 (37290)	598.00 (9801.22)	122.00 (1999.58)	1221 (554)

DOUBLE VANE 100° ROTATION (±1°)						
MODEL	TORQUE IN-LBS (N•m)			VOLUMETRIC DISPLACEMENT IN³ (cm³)		APPROX. WEIGHT LB (Kg)
	1000 PSI (69.0 BAR)	2000 PSI (137.9 BAR)	3000 PSI (206.9 BAR)	PER 100°	PER RAD	
26R2	3650 (412.5)	7300 (824.9)	10950 (1237.4)	6.67 (109.32)	3.82 (62.61)	33 (15)
26R5	8240 (931)	16450 (1858.9)	24700 (2791.1)	15.10 (247.49)	8.66 (142.27)	70 (32)
26R10	19300 (2180.9)	38600 (4361.8)	57900 (6542.7)	35.40 (580.21)	20.24 (331.73)	124 (56)
26R17	32200 (3638.6)	64400 (7277.2)	96600 (10915.8)	59.00 (967.01)	33.80 (553.96)	225 (102)
26R31	58300 (6587.9)	116600 (13175.8)	174900 (19762.7)	106.80 (1750.45)	61.20 (1003.07)	363 (165)
26R62	118500 (13390.5)	237000 (26781)	355500 (40171.5)	217.00 (3556.63)	124.40 (2038.92)	730 (331)
26R124	232000 (2621+)	464000 (52432)	696000 (78648)	427.00 (6998.53)	244.00 (3999.16)	1318 (598)

TEST PARAMETERS — OIL					
MODEL	MAX BREAK IN PSI (BAR)	BY-PASS LEAKAGE-MAX ALLOWABLE			
		CUBIC IN. PER MIN. AT 3000 PSI (206.9 BAR)		CUBIC CM. PER MIN. AT 3000 PSI (206.9 BAR)	
		1V	2V	1V	2V
26R2	150 (10.3)	6	8	98.3	131.1
26R5	140 (9.6)	6	8	98.3	131.1
26R10	150 (8.9)	8	10	131.1	163.9
26R17	120 (8.3)	8	10	131.1	163.9
26R31	110 (7.6)	10	12	163.9	196.7
26R62	100 (6.9)	10	12	163.9	196.7
26R124	90 (6.2)	12	15	196.7	245.9

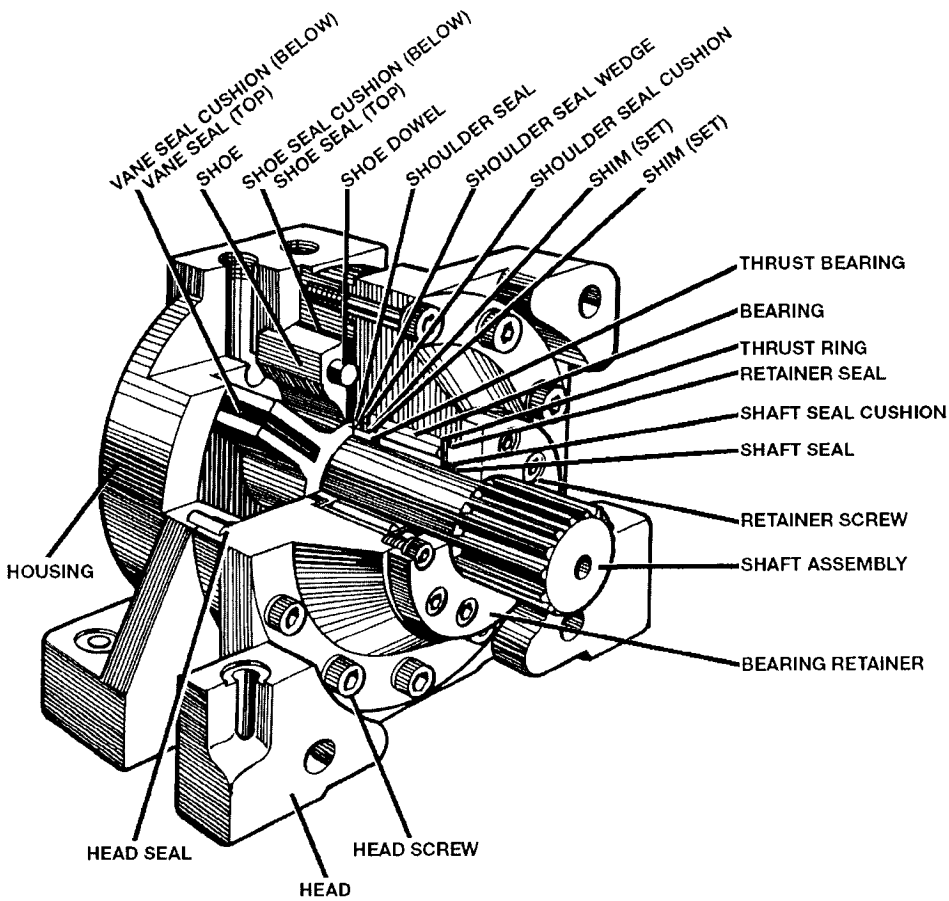

HOW TO ORDER

Sample: 26R 62 2V DE IS FT./FLG. OIL

Model

Size

Number of Vanes
1V—Single Vane
2V—Double Vane

Shaft Extension
SE—Single Extension
DE—Double Extension

Shaft Type
IS—30° Involute Spline
Z—Special

Mounting
Foot/Flange
Special

Fluid Medium
Oil, Other

If you require a special shaft extension, special mounting, air bleeds, special rotation control, or other special requirements, please enclose a drawing showing these requirements. Each number and letter has a specific meaning as shown in the sample.

Appendix G - Data Sheet for Servo-Valve

(model #D681-4718 type P60HDUW4NET2-G)

MOOG

D680 Series
Mini Direct Drive Valve Piloted
Servo-Proportional Control Valves
with Integrated Electronics
ISO 4401 Size 05 to 08

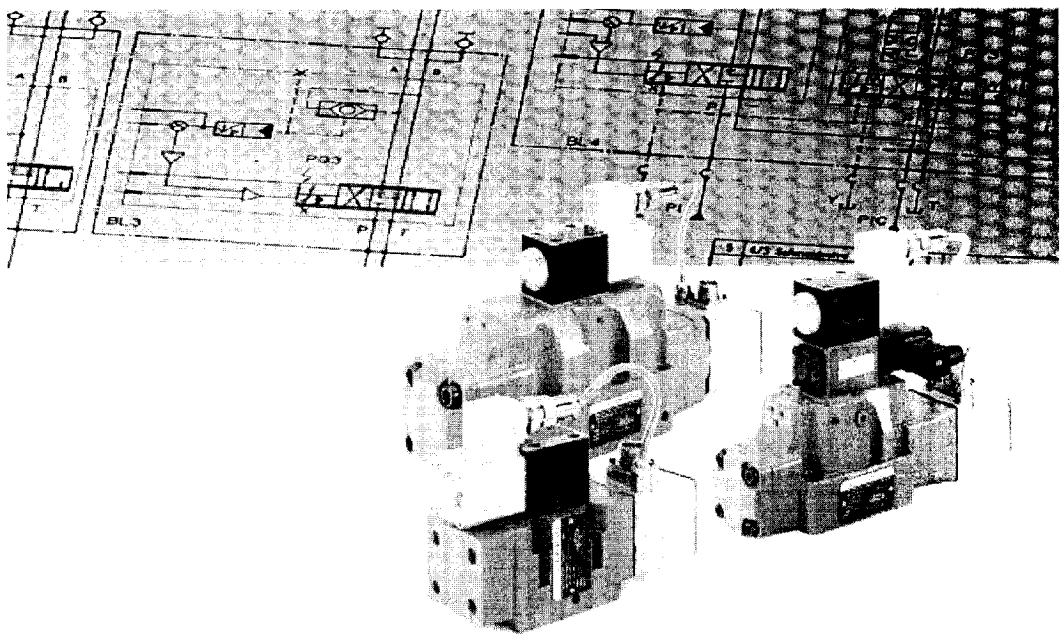

OVERVIEW

Section	Page
Overview	2–3
Technical Data	4–5
Electronics	6-9
Performance Specs.	10-17
Fail-Safe Versions	18-21
Ordering Information	22

MOOG SERVO-PROPORTIONAL CONTROL VALVES

For over 25 years Moog has manufactured proportional control valves with integrated electronics. During this time over 150,000 valves have been delivered. These proportional control valves have been proven to provide reliable control of including injection and blow molding equipment, die casting machines, presses, heavy industry equipment, paper and lumber processing and other applications.

D680 SERIES SERVO-PROPORTIONAL CONTROL VALVES

The D680 Series Direct Drive Piloted Servo-Proportional Control Valves are throttle valves for 2-, 3-, 4- and 5-way applications. These valves are suitable for electrohydraulic position, velocity, pressure or force control systems including those with high dynamic response requirements.

The D680 Series, is a line of direct-drive piloted valves that complement the company's D660 Series ServoJet models.

Like all Moog DDVs, this DDV pilot has a permanent magnet linear force motor that operates the spool directly.

The D680 Series offers these improvements:

- Reduced pilot stage leakage to save energy
- Dynamic performance less dependent on system pressure levels
- Faster step and frequency response to increase system dynamics

The D680 Servo-Proportional Control Valves are equipped with the company's newly developed integrated 24V DC electronics with a pulse-width modulated current driver.

The line's many safety characteristics include enabled signal for the supply voltage, release confirmation, supply voltage monitoring and failsafe spool position confirmation. The two-stage D680 comes in three sizes, which correspond to ISO 4401 sizes 05, 07 and 08. Flow ranges are from 8 gpm to 145 gpm [30 to 550 l/min] at 150-psi [10 bar] drop, while the valves are designed to operate with up to 5,000-psi [345 bar] system pressure.

Fail-safe Option
D680 valves are available with either a mechanical or electrically controlled fail-safe option. Certain conditions must exist for the fail-safe to work reliably. See the type designation section for fail-safe (page 22) and technical data for fail-safe versions (page 18) for more information.

Our quality management system is certified in accordance with DIN EN ISO 9001.

CE The valve series described in this catalogue have succesfully passed EMC tests required by EC Directive. Please refer to the respective references in the electronics section.

This catalogue is for users with technical knowledge. To ensure that all necessary characteristics for function and safety of the system are given, the user has to check the suitability of the products described herein. In case of doubt please contact Moog.

FEATURES & BENEFITS

Flexible Design Elements Optimize the Valve to Your Application
The D680 Series Proportional Control Valves are of two-stage design. By combining a fast first stage, a suitable spool drive area and integrated electronics, an optimum proportional valve can be offered.

Highest Flow Capability for High Velocity Applications
The D07 and D08 (NG 16 to NG 25) D680 Series valves offer the highest flow per body size.

Reduced Spool Drive Area for Improved Dynamic Response
The D08 (NG 25) D683 and D684 Series valves are available with a stub shaft spool for higher valve dynamic.

Fail-Safe Versions for Defined Spool Position at Loss of Power
Mechanical and electrically controlled fail-safe versions provide defined safe spool position by a spring and/or a poppet valve, and/or by external hydraulic supply cut off.

High Dynamics and Higher Flow Capability of Direct Drive Pilot Valve for Highest Dynamic Valve Design.
The high natural frequency of the Direct Drive pilot stage (300 Hz ± 10%) in conjunction with the its high flow capability results in one of the highest dynamic servo-proportional valves on the market.

Direct Drive Pilot Valve for Dynamic Performance Independent of System Pressure
The electro-mechanical design of the direct drive pilot valve results in dynamic performance of the valve that is nearly independent of system pressure.

High Pressure Gain of Direct Drive Pilot Valve for Reliable Operation
The pilot valve's high pressure gain improves the spool driving forces of the main stage. This ensures enhanced main stage spool position control even in situations with high internal flow forces and contaminated fluids.

Improved Resistance to Contamination Reduces Down Time
The Direct Drive pilot stage valves have high spool driving forces offering greater chip shearing forces, making the valve more tolerant to contamination.

2-Stage Poroportional Control Valve

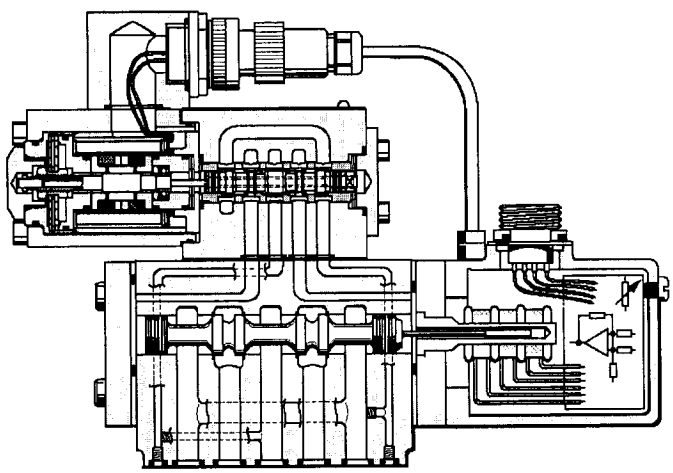

OPERATING PRINCIPLE OF THE DIRECT DRIVE PILOT STAGE

The D633 Series pilot valve consists of a permanent magnet linear force motor, a drive rod connecting motor armature and the spool, guided within a bushing. The linear force motor contains a coil, permanent magnets, pole pieces, an armature and a centering spring. The 4-way spool controls fluid flow from the pressure port to one of the load ports and also from the other load port to return. Deflection of the centering spring, due to spool displacement, provides a return force for the armature. An electric current applied to the coil of the linear force motor produces an electromagnetic flux dependent on the current polarity and amplitude. This electromagnetic flux is superimposed on the permanent magnetic flux in the airgaps between armature and pole pieces. This results in a polarity dependent displacement of the armature against the centering spring force. The spool being connected to the armature by a rod shares the armature motion. Flow forces acting on the spool due to the fluid flow through the valve and friction forces between spool and bushing due to contaminated fluid are also overcome by the force motor. The position of the spool is approximately proportional to the coil current. Spring force and motor force work together in the same direction when the valve spool travels back to center position. At centered position the linear force motor requires no current.

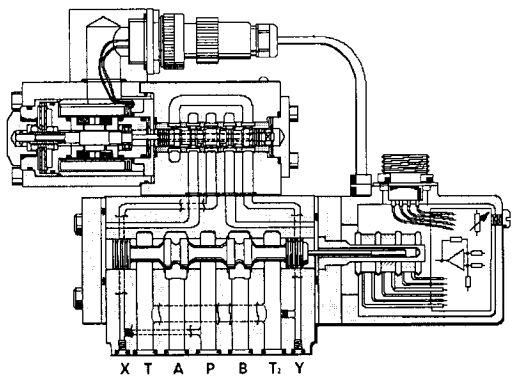

Hydraulic symbol:
Symbol shown with pilot pressure and electric supply on and zero command signal.

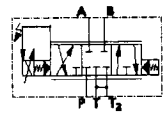

D681 Series, 2-Stage Proportional Control Valve
with D633-7 Series Pilot Valve

OPERATING PRINCIPLE OF THE TWO-STAGE VALVE

The main stage spool position control loop, consisting of main stage spool, position transducer and pilot valve, is closed by the integrated electronics.
An electric command signal (flow rate set point) is applied to the integrated position controller which drives the current in the pilot valve coil. The position transducer (LVDT) which is excited via an oscillator measures the position of the main spool (actual value, position voltage). This signal is then demodulated and fed back to the controller where it is compared with the command signal. The controller drives the pilot valve until the error between command signal and feedback signal is zero. Thus the position of the main spool is proportional to the command signal.

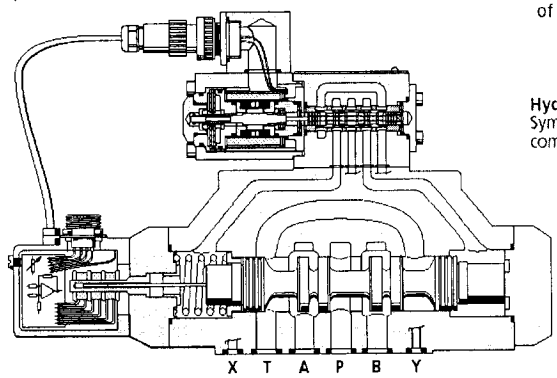

Hydraulic symbol:
Symbol shown with pilot pressure and electric supply on and zero command signal.

D683 Series 2-stage Proportional Valve with D633-7 Series Pilot Valve

PERFORMANCE SPECIFICATIONS FOR STANDARD MODELS

Operating pressure Range	
Ports P, A and B	up to 5,000 psi [350 bar]
Port T	see data of individual series
Temperature Range	
Ambient	-4 °F to +140 °F [-20°C to +60°C]
Fluid	-4 °F to +176 °F [-20°C to +80°C]
Seal Material	NBR, FPM and others on request
Operating Fluid	mineral oil based hydraulic fluid (DIN 51524, part 1 to 3), other fluids on request
Viscosity	
Recommended	15 to 45 centistrokes
Allowable	5 to 400 centistrokes

System Filtration

Pilot stage or pilot valve: high pressure filter (without bypass, but with dirt alarm) mounted in the main flow and if possible directly upstream of the valve.

Main stage: high pressure filter as for the pilot stage. When used in combination with a fast regulating VD-pump a bypass filter is recommended.

Class of Cleanliness

The cleanliness of the hydraulic fluid greatly effects the performance (spool positioning, high resolution) and wear (metering edges, pressure gain, leakage) of the valve.

Recommended Cleanliness Class	
For normal operation	ISO 4406 < 16 / 13
For longer life	ISO 4406 < 14 / 11
Filter Rating recommended	
For normal operation	$\beta_{10} \geq 75$ (10 µm absolute)
For longer life	$\beta_5 \geq 75$ (6 µm absolute)
Installation Options	any position, fixed or movable
Vibration	30 g, 3 axes
Degree of Protection	EN60529: class IP 65, with mating connector mounted
Shipping Plate	Delivered with an oil sealed shipping plate under the mounting surface.

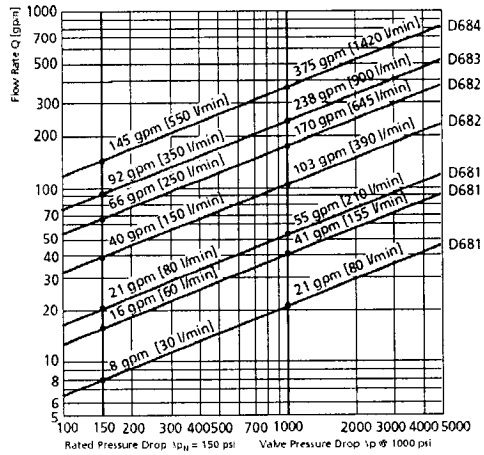

Valve Flow Diagram
Valve flow for maximum valve opening (100% command signal) as a function of the valve pressure drop

VALVE FLOW CALCULATIONS

A valve's flow is dependent upon its electrical command signal and valve pressure drop. The flow for a given valve pressure drop can be calculated using the square root function for sharp edged orifices as follows:

$$Q = Q_N \sqrt{\frac{\Delta p}{\Delta p_N}}$$

Q [gpm] = calculated flow
Q_N [gpm] = rated flow
Δp [psi] = actual valve pressure drop
Δp_N [psi] = rated valve pressure drop

If large flow rates with high valve pressure drop are required an appropriate higher pilot pressure has to be selected in order to overcome the flow forces. An approximate value can be calculated as follows:

$$P_x \geq .012 \times \frac{Q}{A_K} \times \sqrt{\Delta p}$$

Q [gpm] = max. flow
Δp [psi] = valve pressure drop with Q
A_K [in²] = spool drive area
P_x [psi] = pilot pressure

The pilot pressure p_x has to be at least 215 psi [15 bar] above the return pressure of the pilot stage.

GENERAL REQUIREMENTS FOR VALVE ELECTRONICS

- Supply 24 VDC, min. 18 VDC, max. 32 VDC. Current consumption max. 800 mA
- All signal lines, also those of external transducers, shielded
- Shielding connected radially to ⊥ (0 V), power supply side and connected to the mating connector housing (EMC)
- **EMC**: Meets the requirements of EN 55011:1998 class B, EN 50082-2:1995, performance criteria class A
- Protective grounding lead ≥ .75 mm²[18 AWG]
  Consider voltage losses between cabinet and valve.
- Note: When making electrical connections to the valve (shield, protective earth), appropriate measures must be taken to ensure that locally different earth potentials do not result in excessive ground currents. See also Moog Application Note AM 353 E.

FAIL-SAFE VALVE ELECTRONICS WITH SUPPLY VOLTAGE 24 VOLT AND 11+PE POLE CONNECTOR

Command signal
0 to ±10 mA floating, Valves with current command input
The spool stroke of the valve is proportional to I4 = –I5.
100 % valve opening P ◗ A and B ◗ T is achieved at I4 = +10 mA.
At 0 mA command, the spool is in its center position. The input pins 4 and 5 are inverting. Either pin 4 or 5 is used according to the required operating direction. The other pin is connected to signal ground at cabinet side.

Command signal
0 to ±10 V Valves with voltage command input
The spool stroke of the valve is proportional to (U4 – U5). 100 % valve opening P ◗ A and B ◗ T is achieved at (U4 – U5) = +10 V. At 0 V command the spool is in its center position. The input stage is a differential amplifier. If only one command signal is available, pin 4 or 5 is connected to signal ground at cabinet side, according to the required operating direction.

Actual value 4 to 20 mA
The actual spool position value can be measured at pin 6 (see diagram below). This signal can be used for monitoring and fault detection purposes. The spool stroke range corresponds to 4 to 20 mA. The centred position is at 12 mA. 20 mA corresponds to 100 % valve opening P ◗ A and B ◗ T.

The position signal output 4 to 20 mA allows to detect a cable break when I_6 = 0 mA.

For failure detection purposes it is advised to connect pin 6 of the mating connector and route this signal to the control cabinet.

CIRCUIT DIAGRAM

Circuit diagram for measurement of actual I_6 (position of main spool) for valves with 11+PE pole connector

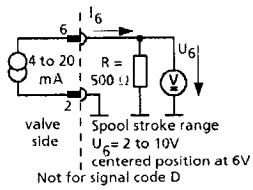

Note: Enable Input
With enable signal off, the main spool will move to a safe position.
a) Centered position (unbiased pilot valve function code G[1])
b) End position (biased pilot valve function code H[1])

[1]) see type designation

CONNECTOR WIRING

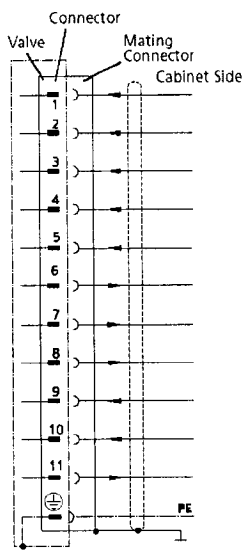

Wiring for valves with 11+PE pole connector to EN 175201 (Part 804[1]) and mating connector (type E, metal shell) with leading protective earth connection ⏚.

Function	Voltage Command	Current Command
Supply	24 VDC (min. 18 VDC, max. 32 VDC)	Static: I_{max}: 200 mA Dynamic: I_{max}: 800 mA
Supply/Signal Ground	(0 V)	
Enabled Not Enabled	U_{3-2} > 8.5 VDC U_{3-2} < 6.5 VDC	I_6 = 2.0 mA at +24 VDC (see note above)
Input Rated Command (differential)	U_{4-5} = 0 to ±10 V R_e = 10 kΩ	Input Command $I_4 = -I_5$: 0 to ±10 mA (R_e=200 Ω) Input Command (inverted) $I_5 = -I_4$: 0 to ±10 mA Inputs U_{4-2} and U_{5-2} for both signal types limited to min. -15 V and max. +32 V
Output Actual Value Spool Position	I_{6-2} = 4 to 20 mA. At 12 mA spool is in centered position. R_L = 100 to 500 Ω Signal code D: U_{6-2} = 2 to 10 V. At 6 V spool is in centered position. R_L = 500 Ω	
Auxiliary Signal	Spool position U_{7-2} = 13 to 3 V. At 8 V spool is in centered position. R_L = 5 kΩ	
Valve Ready	U_{8-2} > 8.5 VDC:Enable and supply ok U_{8-2} < 6.5 VDC:Not enabled or supply not ok	Output I_{max}: 20 mA
Supply, 4/2-way solenoid valve	24 VDC (min. 22.8 VDC, max. 26.4 VDC)	
Supply, 4/2-way solenoid valve, signal ground	(0 V)	
Position Error, Logic	U_{11-2} > 8.5 VDC: < 30% U_{11-2} < 6.5 VDC: > 30%	Output I_{max}: 20 mA
Protective Earth		

[1]) formerly DIN 43651

TECHNICAL DATA

PERFORMANCE SPECIFICATIONS FOR STANDARD MODELS

		English [Metric]	D681 -P. . H.UO/W	D681 -P. . H.UF
Mounting Pattern	ISO with additional 2nd T port		ISO 4401 - 05 - 05 - 0 - 94	ISO 4401 - 05 - 05 - 0 - 94
Valve Body Version			4-way, 2 x 2-way and 5-way 2-stage, standard spool O/W (spring centered)	4-way, 2 x 2-way and 5-way 2-stage, standard spool F spring A ◗ T
Pilot Valve	Q_n (±10%) at Δp_n = 1,015 psi [70 bar]	gpm [l/min]	0.92 [3.5]	0.97 [3.7]
Series	D633-7...		Standard	Biased
Pilot Connection			X and Y	X and Y
Mass		lb [kg]	O = 15 [6.8] / W = 17.6 [8.0]	15 [6.8]
Rated Flow	(±10%) at Δp_N = 75 psi [5 bar] per land	gpm [l/min]	8 [30] / 16 [60] / 21[80]	8 [30] / 16 [60] / 20 [80]
Operating Pressure	max.			
	port P, A, B, T and X with Y external	psi [bar]	5,075 [350]	5,075 [350]
	port T with Y internal and Y (pressure peaks 3,045 psi [210 bar])	psi [bar]	1,015 [70]	1,015 [70]
Response Time*	for 0 to 100% stroke	[ms]	11.0	11.0
Threshold*		[%]	< 0.03	< 0.03
Hysteresis*		[%]	< 0.20	< 0.20
Null Shift*	with ΔT = 100°F [38°C]	[%]	< 1.5	< 1.5
Null Leakage Flow*	total max. (~ critical lap)	gpm [l/min]	0.58 [2.2]	0.58 [2.2]
Null Leakage Flow*	pilot stage only, max.	gpm [l/min]	0.11 [0.40]	0.11 [0.40]
Pilot Flow*	max., for 100% step input	gpm [l/min]	1.6 [6.0]	1.7 [6.5]
Main Spool Stroke		in [mm]	± 0.12 [± 3.0]	± 0.12 [± 3.0]
Spool Drive Area		in²[cm²]	0.31 [2.0]	0.31 [2.0]

* measured at 3,000 psi [210 bar] pilot or operating pressure, respectively, fluid viscosity of 32 mm²/s and fluid temperature of 104°F [40°C]

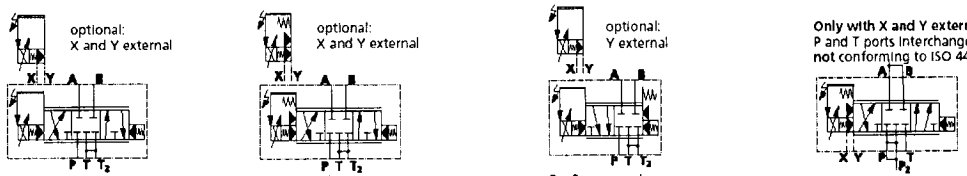

4-way version
no fail safe position

4-way version
fail safe position A ◗ T

2 x 2-way version
fail safe centered position

5-way version

PERFORMANCE SPECIFICATIONS FOR STANDARD MODELS

Flow vs. Signal Curve
at Δp_N = 75 psi [5 bar] per land

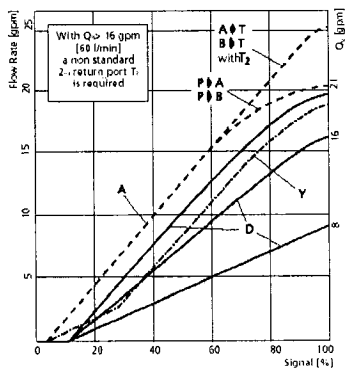

Spool version A: **-critical lap, linear characteristic (21)**
Spool version D: **10% overlap, linear characteristic**
Spool version Y: **-critical lap, curvilinear characteristic (21)**

Typical characteristic curves measured at 3,000 psi [210 bar] pilot or operating pressure, fluid viscosity of 32 mm2/s and fluid temperature of 104°F [40°C]

D681 - P. . H.UO/W
Step Response

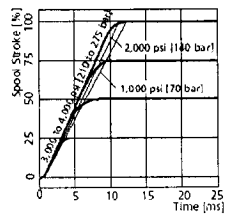

D681 - P. . H.UF

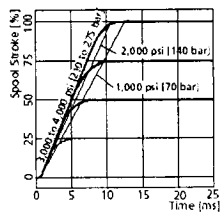

Frequency Response

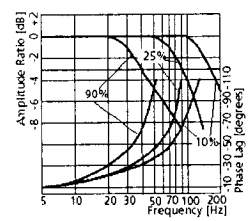

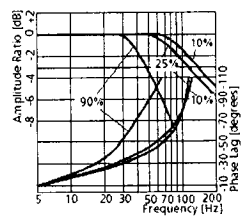

TECHNICAL DATA

INSTALLATION DIAGRAM

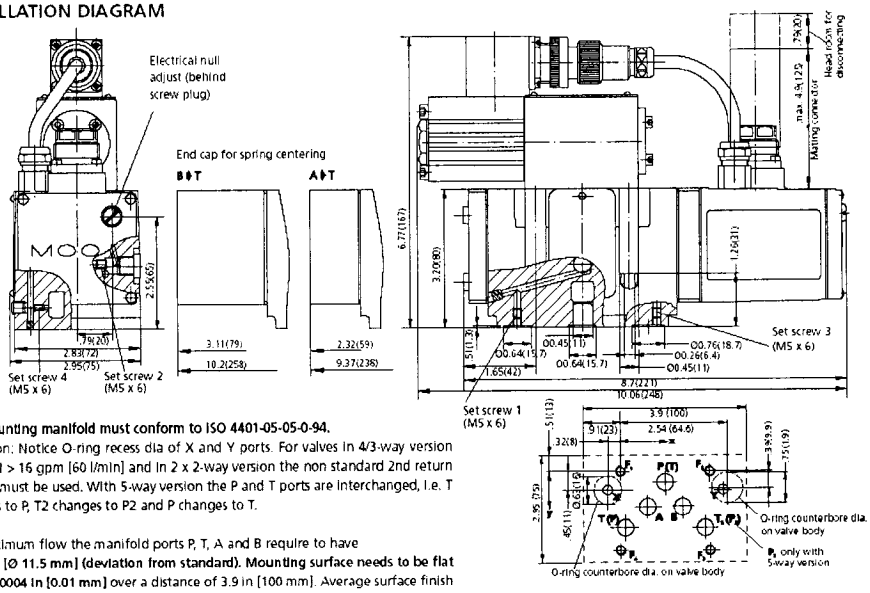

The mounting manifold must conform to ISO 4401-05-05-0-94.
Attention: Notice O-ring recess dia of X and Y ports. For valves in 4/3-way version with QN > 16 gpm [60 l/min] and in 2 x 2-way version the non standard 2nd return port T2 must be used. With 5-way version the P and T ports are interchanged, i.e. T changes to P, T2 changes to P2 and P changes to T.

For maximum flow the manifold ports P, T, A and B require to have **Ø .45 in [Ø 11.5 mm] (deviation from standard). Mounting surface needs to be flat within .0004 in [0.01 mm]** over a distance of 3.9 in [100 mm]. Average surface finish value, Ra, better than √

	P	A	B	T	T_2	X	Y	F_1	F_2	F_3	F_4
	Ø0.45 [11.5]	Ø0.45 [11.5]	Ø0.45 [11.5]	Ø0.45 [11.5]	Ø0.45 [11.5]	Ø0.25 [6.3]	Ø0.25 [6.3]	M6	M6	M6	M6
x	1.1 [27.0]	0.66 [16.7]	1.5 [37.3]	0.15 [3.2]	2.0 [50.8]	-0.32 [-8.0]	2.4 [62.0]	0	2.1 [54.0]	2.1 [54.0]	0
y	0.25 [6.3]	0.84 [21.4]	0.84 [21.4]	1.3 [32.5]	1.3 [32.5]	0.43 [11.0]	0.43 [11.0]	0	0	1.8 [46.0]	1.8 [46.0]

CONVERSION INSTRUCTION

for main stage operation with internal or external pilot connection	Pilot Flow Supply	Set Screw M5 x 6 bore 1	bore 2	Pilot Flow Return	Set Screw M5 x 6 bore 3	bore 4
	Internal P	closed	open	Internal T	closed	open
	External X	open	closed	External Y	open	closed

SPARE PARTS AND ACCESSORIES

O-rings (included in delivery)			NBR 85 Shore	FPM 85 Shore
for P, T, T_2, A, B, X	6 pieces ID 0.49 [12.4] x Ø 0.07 [1.8]		45122-004	42082-004
for Y	1 piece ID 0.61 [15.6] x Ø 0.07 [1.8]		45122-011	42082-011
Mating connector, waterproof IP65 (not included in delivery)			for cable diameter	
6+PE pole	B97007-061	DIN 43563	min. Ø 0.39 [10.0] max. Ø 0.47 [12.0]	
11+PE pole	B97067-111	DIN 43651	min. Ø 0.43 [11.0] max. Ø 0.51 [13.0]	
Flushing plates	for P, A, B, T, T_2, X, Y	for P, T, T_2, X, Y	for P, T, T_2, and X, Y	
	B67728-001	B67728-002	B67728-003	
Mounting manifolds	see special data sheet			
Mounting bolts (not included in delivery)		required torque	required	
M6 x 40 DIN EN ISO 4762-10.9	A03665-060-040	115 in-lb [13 Nm]	4 pieces	

TECHNICAL DATA FAIL-SAFE VERSIONS

OPERATING PRINCIPLE OF THE FAIL-SAFE VALVE

Application safety is dependent on the application itself, local safety requirements and design preferences. For applications where certain safety regulations are applicable, a defined metering spool position is needed in order to avoid potential damage. Various fail-safe versions are available for Moog servo-proportional control valves. To define the fail-safe version in a D680 Series Valve, a complete understanding of the hydraulic circuit and country specific safety regulations is required.

With fail-safe valves it is possible to check whether the main spool is in its predefined position. If the main spool is within its defined range, the logic output signal at pin 11 is > + 8.5 V. If this signal is < + 6.5 V, then the main spool is outside the defined range. This logic signal may be delayed up to 500 ms. To reduce the fail-safe switching time it is advised to both switch off the supply of the 4/2-way valve and the enable signal at the same time.

The following information applies to W, U and V electrically controlled fail-safe functionality. Contact Moog for additional information.

Fail Safe Functionality
After switching off the 24 V supply to the safety solenoid valve, this fail-safe function creates a defined metering spool position: overlapped centered position or fully opened A ◗ T.

Fail-Safe Version W or U
In order to move the spool to the safe centered position with D680 Series fail-safe valves, the two control chambers of the main stage are hydraulically short circuited by a 4/2-way solenoid valve. The spring force moves the spool into the overlapped centered position.

Fail-Safe Version V
In order to reach the fully opened position A ◗T with D680 Series fail-safe valves , the spring force (after the control chambers have been short circuited) pushes the spool to the end position A ◗ T.

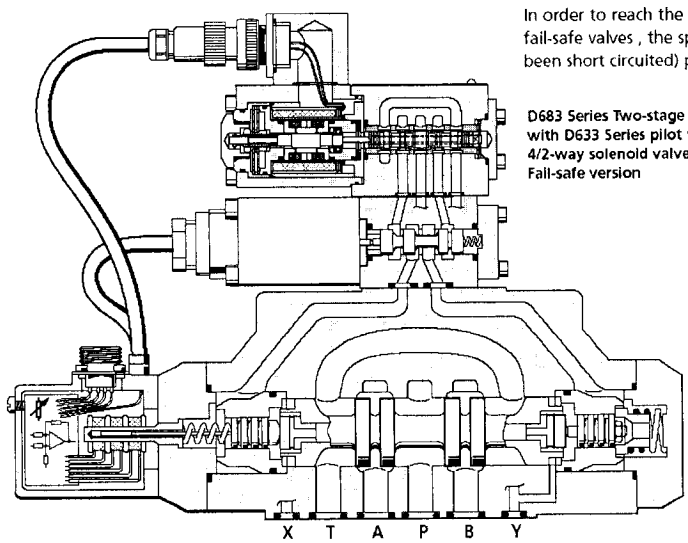

D683 Series Two-stage Proportional Control Valve with D633 Series pilot valve and 4/2-way solenoid valve for the Fail-safe version

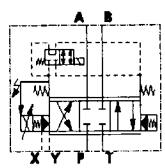

Hydraulic symbol:
Symbol shown with pilot pressure and electric supply on and solenoid off.

Note:
According to EN 954-1, a higher safety category can be achieved if a fail-safe valve is used.

ELECTRICAL CHARACTERISTICS

Electrical characteristics of the 4/2-way solenoid valve for the fail-safe version.

Valve version	4/2-way solenoid valve
Function	electromagnetic
Nominal voltage U_N	24 VDC (min 22.8 VDC, max 26.4 VDC)
Nominal current, I_N	1.35 A
Nominal power, P_{II}	33 W

Connector wiring

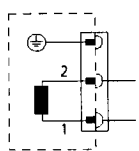

DIN 43650-1
Form A: 2+PE - PG9

TECHNICAL DATA FAIL-SAFE VERSION

INSTALLATION DIAGRAM

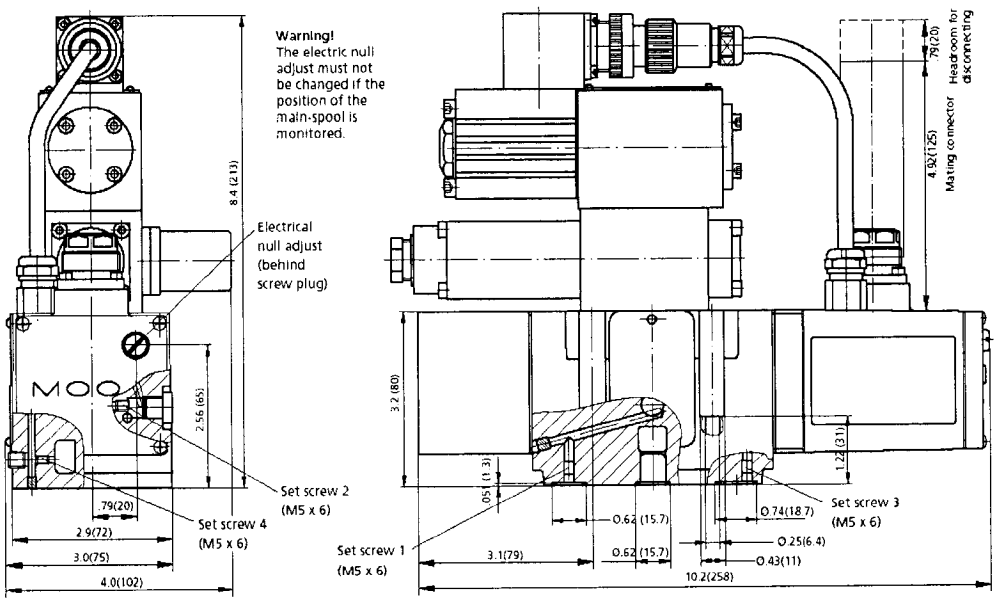

The mounting manifold must conform to ISO 4401-05-05-0-94 (see page 11).

Fail-safe
Centered position

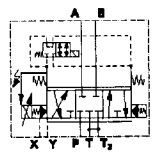

Fail-safe
Centered position by mechanical spool stop

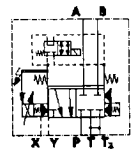

CONVERSION INSTRUCTION

for main stage operation with internal or external pilot connection	Pilot Flow Supply	Set Screw M5 x 6 bore 1	bore 2	Pilot Flow Return	Set Screw M5 x 6 bore 3	bore 4
	Internal P	closed	open	Internal T	closed	open
	External X	open	closed	External Y	open	closed

SPARE PARTS AND ACCESSORIES

Spare parts and accessories: Page 11

ORDERING INFORMATION

Model Number

D681 to D684 [. . . . . .]

Type Designation

[. . . . . 2 - -]

Specification Status	
-	Series specification
E	Preseries specification
Z	Special specification

Model Designation	
	Assigned at the factory

Factory Identification

Valve Version		Series
P	Standard spool	D681 and D682
N	Stub shaft spool	D683 and D684

Rated Flow			
	Q [gpm]	[l/min] at Δp = 150 psi [10 bar]	Series
30	8	30	D681
60	16	60	D681
80	21	80	D681
01	40	150	D682
02	67	250	D682
03	94	350	D683
05	148	550	D684

Maximum Operating Pressure p_P		
B	1,000 psi [70 bar]	Pilot valve D633-7...,$p_{P\ max}$ = 5,000 psi [350 bar]
H	4,000 psi [280 bar]	The integrated valve electronics is adapted
K	5,000 psi [350 bar]	to the pilot pressure

Main Spool Type	
A	4-way: ~ critical lap, linear characteristic
D	4-way: 10% overlap, linear characteristic
P	4-way: P ◗ A, A ◗ T: ~ critical lap, curvilinear characteristic P ◗ B: 60% overlap, curvilinear characteristic B ◗ T: 50% underlap, linear characteristic
U	5-way: P ◗ A, P ◗ B, A ◗ T: ~ critical lap, curvilinear characteristic (D681 only)
R	4-way: 10% overlap, curvilinear characteristic
Y	4-way: ~ critical lap, curvilinear characteristic
Z	2x2-way: A ◗ T, B ◗ T: ~ critical lap, linear characteristic
X	Special spool on request

Direct Drive Pilot Valve	
U	D633-7...
X	Special valve version on request

Function Code		Connector
O	No enable input. Pin C not used	S
A	Without enable signal applied the spool moves to adjustable centered position	S
B	Without enable signal applied the spool moves into defined end position A ◗ T or B ◗ T (see page 8)	S
E	Without enable signal applied the spool moves to adjustable centered position. Position error monitored (see page 9)	E
F	Without enable signal applied the spool moves into defined end position A ◗ T or B ◗ T Position error monitored (see page 9)	E
G	Without enable signal applied the spool moves to adjustable centered position. Spool position monitored (see page 19)	E
H	Without enable signal applied the spool moves into defined end position A ◗ T or B ◗ T Spool position monitored (see page 19)	E

Supply Voltage		
2	24 VDC	(18 to 32 VDC)

Signals for 100% Spool Stroke			
	Command	Output	Connector
A	±10 V	±10 V(diff.)	E
D	±10 V	2 to 10 V	E/S
F	±10 V	2.5 to 13.5 V, with enable input	S
M	±10 V	4 to 20 mA	E/S
T	±10 V	±10 V with dead band compens. (diff.)	E
X	±10 mA	4 to 20 mA	E/S
Y	others on request		

Valve Connector		
E	11+PE pole	DIN 43651
S	6+PE pole	DIN 43563

Seal Material	
N	NBR (Buna) Standard
V	FPM (Viton) optional
X	Other materials on request

Pilot Connections and Pilot Pressure			
	Supply X	Return Y	
4	internal	internal	Parameters of the control electronics are adapted to the pilot pressure. See operating pressure on the nameplate and in this ordering information.
5	external	internal	
6	external	external	
7	internal	external	

Spool Position of Main Stage with/without Electrical or Hydraulic Supply					
O	Undefined				
	Mechanical fail-safe version				
	Position	p [psi]	px external [psi]		
F	P ◗ B, A ◗ T	≥ 145	≥ 145		
		< 145	< 15		
D	P ◗ A, B ◗ T	≥ 145	≥ 145		
		< 145	< 15		
	Electrically controlled fail-safe version				
	Position	p_P [psi]	p_X ext	WV*	VEL**
W	Centered position defined	≥ 15	≥ 15	off	on
	undefined	≥ 145	≥ 145	on	off
U	Centered position defined	≥ 15	≥ 15	off	on
	P ◗ B, A ◗ T	≥ 145	≥ 145	on	off
S	P ◗ A, B ◗ T	≥ 15	≥ 15	off	on
	P ◗ A, B ◗ T	≥ 145	≥ 145	on	off
V	P ◗ B, A ◗ T	≥ 15	≥ 15	off	on
	P ◗ B, A ◗ T	≥ 145	≥ 145	on	off
X	Special versions on request				

*WV: Solenoid Valve
**VEL: Valve Electronics

15 psi = 1 bar, 145 psi = 10 bar

Preferred configurations are highlighted. Options may increase price.
Technical changes are reserved.
All combinations may not be available. For special options, letters not on the information above may be applied.
Please contact Moog.

Appendix H - Circuit Diagram for Servo-Valve Module

The 24 VDC supply and ground is sent to pin 1 and 2, respectively, of the servo-valve, and also to the fail-safe solenoid valve, pin 10 and 11, respectively. The command signal from the controller is provided to the module via the input BNC. The LT1007 operational amplifier is used to drive the long cables connecting the module to the servo-valve. The monitor BNC shows the output of the op amp. The enable/disable switch sends a ready signal to pin 3 of the servo-valve. If the 24VDC is being supplied to the valve and the enable switch is on, the LED will light up. If the valve is disabled it should return to its center or closed position. If the supply to the valve is cut, the fail-safe solenoid will cause the valve to move to the center position. The spool position BNC shows the actual spool position output from the valve. Pins 7 (auxiliary spool position signal from valve) and 11 (position error signal from valve) are left unconnected. The details of the 11+PE connections to the servo-valve are in the Appendix G.

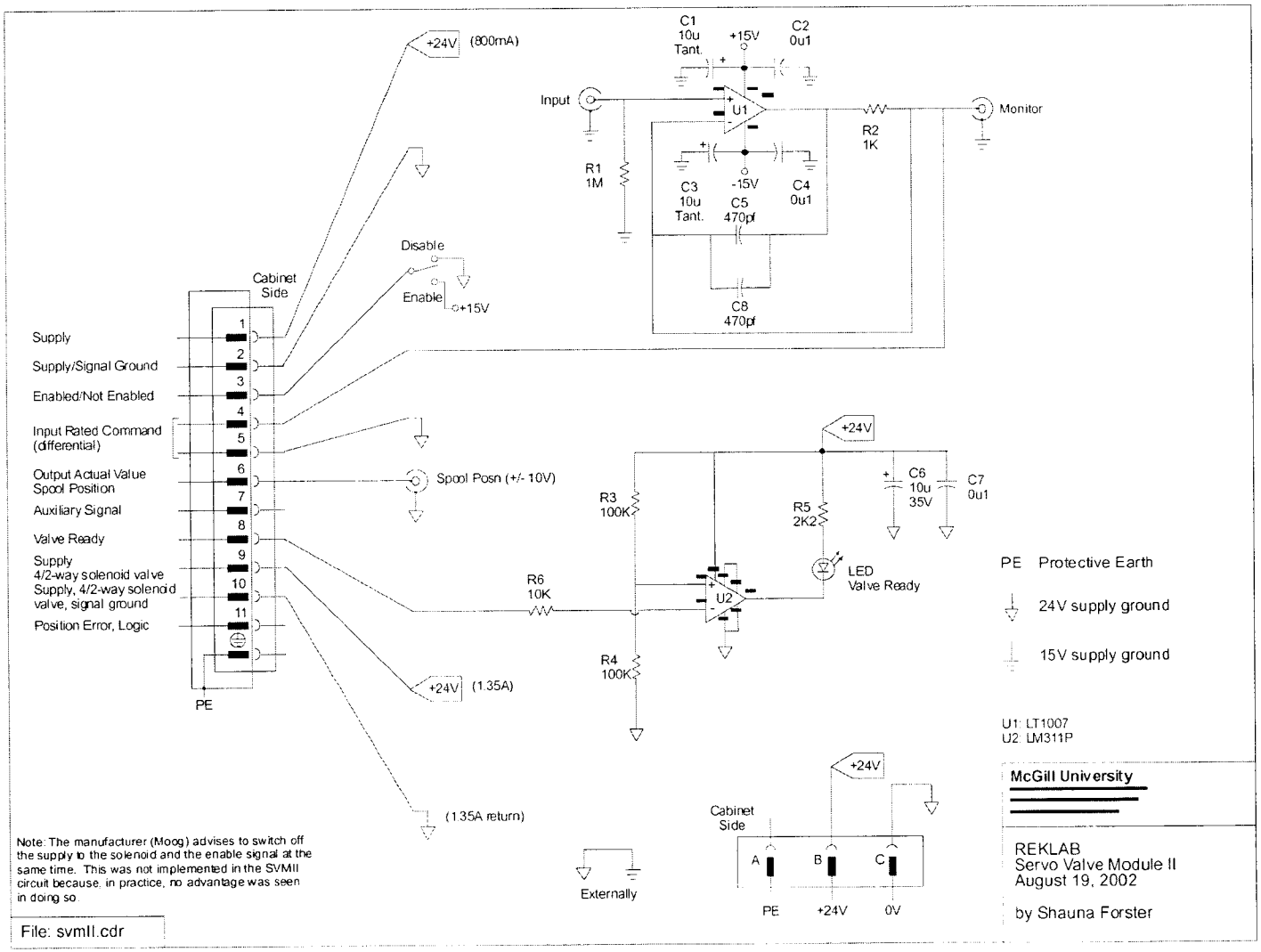
+24V (800mA)
C1
10u
Tant.
+15V
C2
0u1
Input
U1
Monitor
R2
1K
R1
1M
C3
10u
Tant.
-15V
C5
470pf
C4
0u1
C8
470pf
Disable
Enable
+15V
Cabinet
Side
Supply
Supply/Signal Ground
Enabled/Not Enabled
Input Rated Command
(differential)
Output Actual Value
Spool Position
Auxiliary Signal
Valve Ready
Supply
4/2-way solenoid valve
Supply, 4/2-way solenoid
valve, signal ground
Position Error, Logic
1
2
3
4
5
6
7
8
9
10
11
PE
Spool Posn (+/- 10V)
+24V (1.35A)
(1.35A return)
+24V
R3
100K
R5
2K2
C6
10u
35V
C7
0u1
LED
Valve Ready
R6
10K
U2
R4
100K
Externally
+24V
Cabinet
Side
A
B
C
PE
+24V
0V
PE Protective Earth
24V supply ground
15V supply ground
U1: LT1007
U2: LM311P
McGill University
REKLAB
Servo Valve Module II
August 19, 2002
by Shauna Forster
Note: The manufacturer (Moog) advises to switch off the supply to the solenoid and the enable signal at the same time. This was not implemented in the SVMII circuit because, in practice, no advantage was seen in doing so.
File: svmII.cdr

Appendix I - Data Sheet for Torque Transducer

(model #2110-5k)

TORQUE SENSORS

REACTION

FEATURES:

- High torsional stiffness
- Higher resistance to bending moments
- Minimal friction error
- Low end sensitivity due to absence of moving parts

Safety Considerations: *"It would be unsafe to operate Lebow® Torque Sensors and Load Cells beyond static overload or ultimate extraneous load limits as defined in the glossary of terms eg, when applicable higher than maximum speed. When in doubt, consult the factory. Lebow® Products is not responsible for any property damage or personal injury which may result because of the misapplication of the Transducer."*

PERFORMANCE SPECS:

2110-2116 AND 2320-2404

SPECIFICATIONS

Actual performance average:	
Nonlinearity:	0.026%
Hysteresis:	0.029%
Nonlinearity: *of rated output*	±0.1%
Hysteresis: *of rated output*	±0.1%
Output at rated capacity:* *millivolts per volt, nominal*	2
Repeatability: *of rated output*	±0.05%
Zero balance: *of rated output*	±1.0%
Bridge resistance: *ohms nominal*	350*
Temperature range, compensated: °F	+70 to +170
Temperature range, compensated: °C	+21 to +77
Temperature range, usable: °F	-65 to +200
Temperature range, usable: °C	-54 to +93
Temperature effect on output: *of reading per °F*	±0.002%
Temperature effect on output: *of reading per °C*	±0.0036%
Temperature effect on zero: *of rated output per °F*	±0.002%
Temperature effect on zero: *of rated output per °C*	±0.0036%
Excitation voltage, maximum: *volts DC or AC rms*	20
Insulation resistance, bridge/case: *megohms at 50 VDC*	>5,000
Number of bridges	1

*Model 2404 output at rated capacity is 1.5 mV/V nominal and bridge resistance 700 ohms.

MODEL 2110-2116

Flanged reaction torque sensors

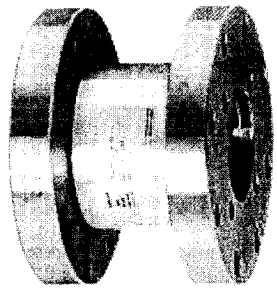

MODEL 2320 AND 2404

Hollow reaction torque sensors

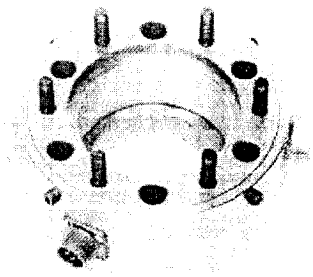

VISIT OUR WEB SITE: www.lebow.com

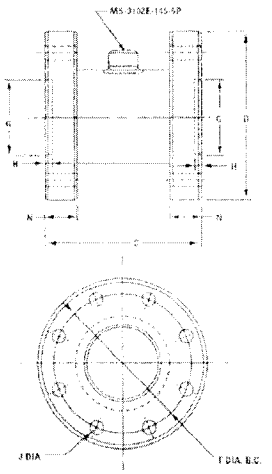

2110-2K, 5K	IN.	CM.
C	3	7.62
D	4	10.16
F	3.25	8.25
G*	1.50	3.81
H	0.13	0.32
N	0.50	1.27
J†	0.33	0.83

2111-10K, 20K	IN.	CM.
C	3.50	8.89
D	5	12.70
F	4.25	10.80
G*	2.00	5.08
H	0.25	0.64
N	0.75	1.91
J†	0.39	0.99

2112-50K, 100K	IN.	CM.
C	7.38	18.73
D	8	20.32
F	6.62	16.81
G*	3.50	8.89
H	0.31	0.79
N	1.00	2.54
J†	0.55	1.40

2113-200K	IN.	CM.
C	8.50	21.59
D	9.75	24.77
F	8	20.32
G*	4	10.16
H	0.40	0.79
N	1.00	2.54
J†	0.77	1.96

2114-300K‡, 500K‡	IN.	CM.
C	10.50	26.67
D	13	33.02
F	11	27.94
G*	6	15.24
H	0.31	0.79
N	2	5.08
J†	1.02	2.59

2115-600K‡, 750K‡	IN.	CM.
C	13.50	34.29
D	15	38.10
F	12	30.48
G*	6	15.24
H	0.31	0.79
N	2	5.08
J†	1.52	3.85

2116-1200K‡, 2400K‡	IN.	CM.
C	16	40.64
D	20	50.80
F	16	40.64
G*	8	20.32
H	0.50	1.27
N	2	5.08
J††	1.52	3.85

* Diameter tolerance +.002–.000.

† 8 equally spaced holes are located within .005 of true position.

†† 16 equally spaced holes.

‡ Calibration performed to 300,000 lbs. in. maximum.

2320

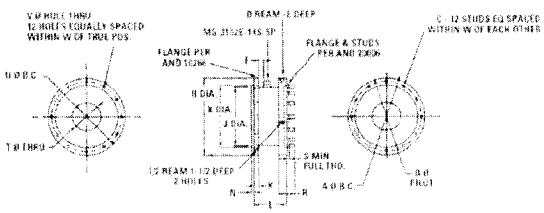

2320	IN.	CM.
A	10	25.40
B	9.00	22.86
C	8.24	-
D	0.38	0.94
E	0.28	0.64
F	1.25	3.17
G	0.75	0.64
H	1.00	2.53
J	8.49	21.57
K	0.63	1.58
L	4.25	10.79
N	0.32	0.80
P	1.53	3.89
R	1.13	2.85
S	0.81	2.06
T	4.15	10.47
U	10.00	25.40
V	0.41	1.03
W	0.01	0.02
X	8.49	21.93

2404

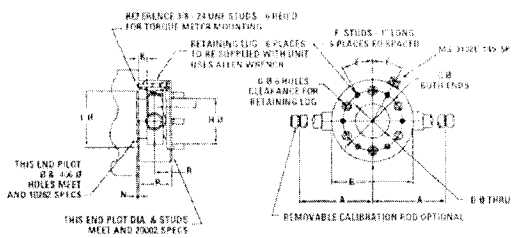

2404	IN.	CM.
A	10	25.40
B	6.44	16.35
C	5.00	12.70
D	3.00	7.62
E	60°	60°
F	8.75	
G	0.64	1.62
H	1.38	3.51
J	0.41	1.04
K	0.64	1.62
L	4.75	12.07
N	0.19	0.47
P	2.25	5.72
R	1.94	4.93
S	3.81	9.68
T	-	-
U	-	-
V	-	-
W	-	-
X	-	-

LOAD CARRYING CAPACITY

W = weight of test device

W x S = overhung moment

S = distance to center of gravity of test unit

Do not exceed moment (**W x S**) or shear (**W**), whichever value is attained first. **P** = thrust.

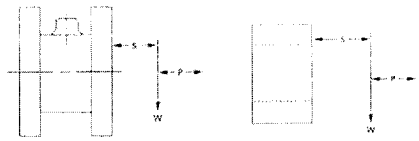

SENSOR CHARACTERISTICS: 2110-2116, 2320 AND 2404

MODEL NUMBER	CAPACITY lbs. in (N • m)	OVERLOAD lbs. in (N • m)	TORSIONAL STIFFNESS lbs. in/rad (N • m/rad)	MAX. OVERHUNG MOMENT W x S lbs. in. (N • m)	MAX. SHEAR W lbs. (N)	MAX. THRUST P lbs. (N)
2110-2K	2,000 (25)	3,000 (340)	184,000 (48,384)	1,000 (113)	1,500 (6,675)	2,000 (8,896)
2110-5K	5,000 (565)	7,500 (845)	920,000 (103,941)	2,000 (226)	2,000 (8,896)	4,000 (17,792)
2111-10K	10,000 (1,130)	15,000 (1,690)	2,680,000 (302,784)	5,000 (565)	4,000 (17,800)	6,000 (26,688)
2111-20K	20,000 (2,250)	30,000 (3,380)	5,750,000 (649,630)	10,000 (1,130)	6,500 (28,900)	10,000 (44,480)
2111-30K	30,000 (3,390)	45,000 (5,080)	10,000,000 (1,129,720)	15,000 (1,695)	8,500 (37,813)	13,000 (57,824)
2112-50K	50,000 (5,650)	75,000 (8,475)	8,000,000 (903,833)	24,000 (2,704)	12,000 (53,375)	16,000 (71,040)
2112-100K	100,000 (11,300)	150,000 (16,950)	20,000,000 (2,259,584)	50,000 (5,650)	20,000 (89,000)	30,000 (133,440)
2113-200K	200,000 (22,600)	300,000 (33,900)	33,400,000 (3,773,505)	90,000 (10,170)	30,000 (133,440)	40,000 (177,920)
2114-300K	300,000 (33,900)	450,000 (50,850)	60,000,000 (6,778,752)	150,000 (16,950)	42,000 (186,800)	60,000 (266,880)
2114-500K*	500,000 (56,500)	750,000 (84,750)	114,000,000 (12,879,628)	200,000 (22,600)	55,000 (244,640)	80,000 (355,840)
2115-600K*	600,000 (67,796)	900,000 (101,695)	160,000,000 (18,079,096)	200,000 (22,600)	95,000 (422,560)	90,000 (400,320)
2115-750K*	750,000 (84,745)	1,125,000 (127,119)	210,000,000 (23,728,814)	250,000 (28,250)	110,000 (489,280)	105,000 (467,040)
2116-1200K*	1,200,000 (135,593)	1,800,000 (203,375)	180,000,000 (20,338,983)	350,000 (39,550)	140,000 (622,720)	130,000 (578,240)
2116-2400K*	2,400,000 (271,186)	3,600,000 (406,800)	430,003,000 (48,587,570)	700,000 (79,096)	225,000 (1,000,800)	210,000 (934,080)
2404-50	50 (5)	250 (25)	17,000 (1,920)	200 (22)	50 (222)	200 (889)
2404-100	100 (10)	300 (30)	40,000 (4,519)	300 (34)	100 (445)	300 (1,333)
2404-200	200 (20)	500 (55)	100,00 (11,298)	400 (44)	150 (667)	400 (1,779)
2404-500	500 (55)	750 (85)	250,000 (28,246)	700 (77)	300 (1,334)	600 (2,668)
2404-1K	1,000 (115)	1,500 (170)	500,000 (56,490)	1,000 (113)	400 (1,779)	1,000 (4,448)
2404-2K	2,000 (225)	3,000 (340)	1,250,000 (141,224)	2,000 (226)	500 (2,224)	1,500 (6,672)
2404-5K	5,000 (565)	7,500 (850)	3,500,00 (395,427)	4,000 (3.88)	600 (2,669)	2,500 (11,120)
2320-12K	12,000 (1,350)	18,000 (2,030)	6,000,000 (677,826)	6,500 (676)	1,600 (6,672)	6,000 (26,688)
2320-36K	36,000 (4,060)	54,000 (6,085)	30,000,000 (3,389,370)	15,000 (1,694)	3,500 (13,344)	16,000 (71,200)

*Calibration performed to 300,000 lbs. in.; consult factory for higher calibrations.

VISIT OUR WEB SITE: www.lebow.com

Appendix J - Circuit Diagram for Torque Transducer Module

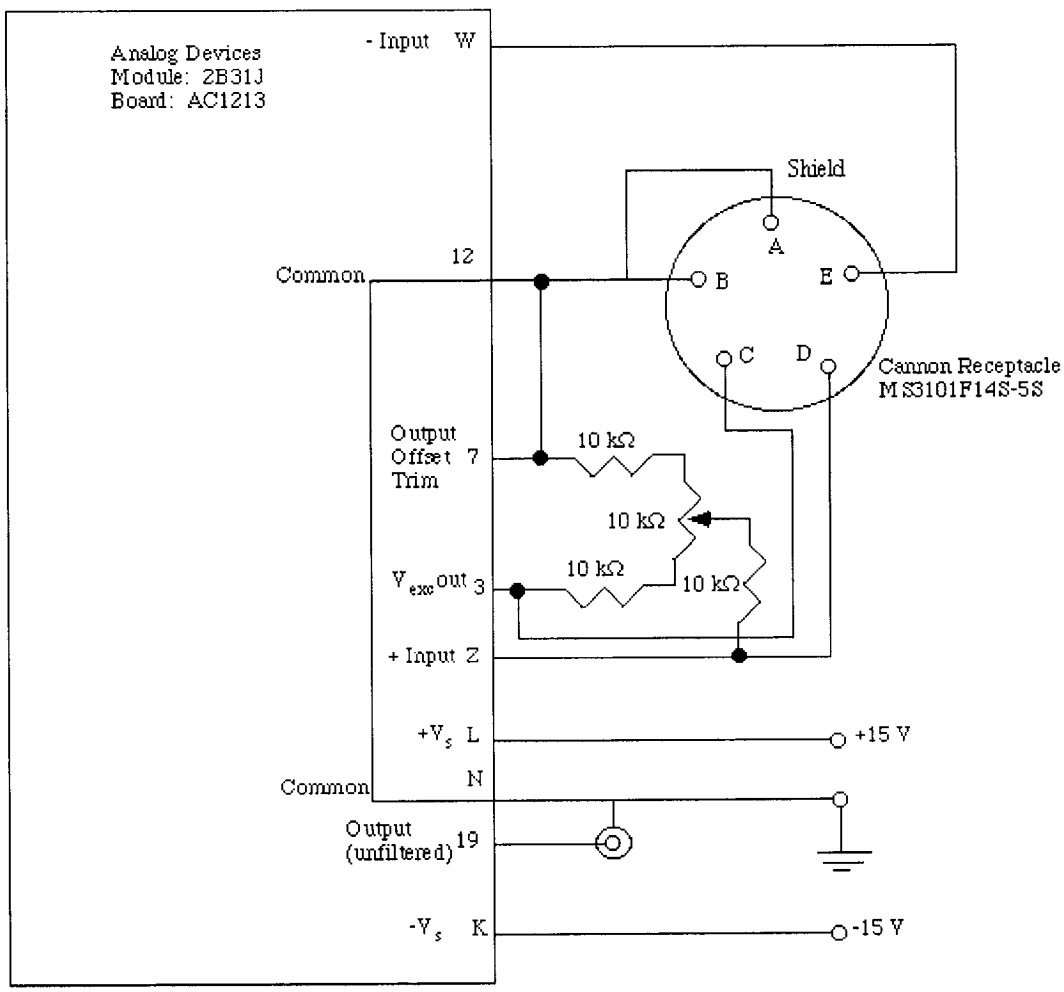

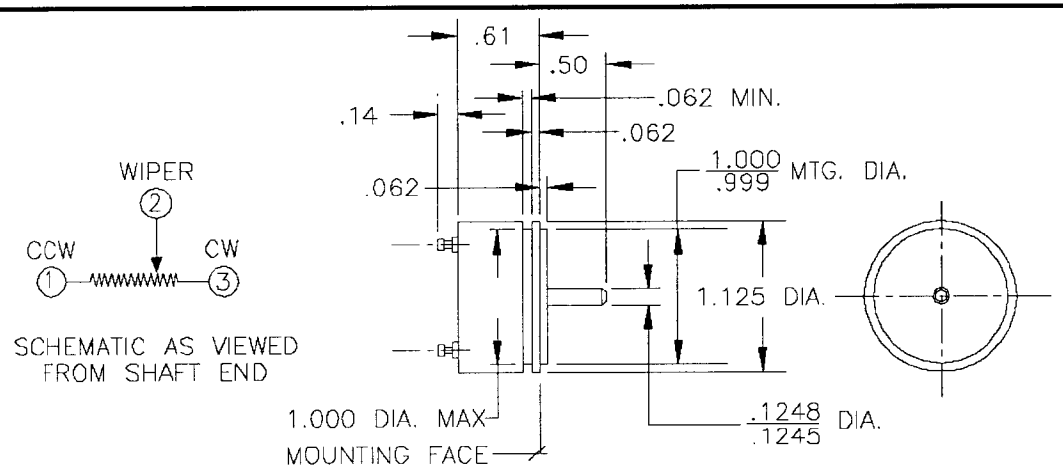

No. DASH	(OHMS) RESISTANCE
251	250
501	500
102	1,000
202	2,000
252	2,500
502	5,000
103	10,000
203	20,000
253	25,000
503	50,000

11. LIFE: 20,000,000 REV. AT 40 RPM.
10. DIELECTRIC STRENGTH: 750 VOLTS AC FOR 60 SECONDS.
9. POWER RATING: 1.0 WATT AT 85° DERATED TO ZERO AT 105°.
8. OPERATING TEMPERATURE RANGE: −55° TO +105°C.
7. TEMP. COEFFICIENT OF RESISTANCE: 500 PPM/°C.
6. TOTAL MECHANICAL TRAVEL: 360° CONTINUOUS.
5. THEORETICAL ELECTRICAL TRAVEL: 340° ±3°.
4. INDEPENDENT LINEARITY: ±0.5%.
3. THEORETICAL RESOLUTION: INFINITE.
2. TOTAL RESISTANCE: TOLERANCE: ±10%.
1. TOTAL RESISTANCE: SEE CHART (OTHER VALUES ON REQUEST).

17. GOLD PLATED TERMINALS.
16. PRECIOUS METAL CONTACTS.
15. STAINLESS STEEL BALL BEARINGS.
14. STAINLESS STEEL SHAFT.
13. OUTPUT SMOOTHNESS: 1%.
12. SHAFT ROTATIONAL TORQUE: .35 OUNCE−INCHES MAX.

C/L	BY	APP'D	DATE
J	MARTIN CORONA	B	08/09/96
H	D.HORN	EM	8/18/81
G	DM	EM	6/30/78
F	DM	EM	10/18/77
E	G	EM	6/11/77
D	DN	EM	4/13/77

REVISION

TOLERANCES
UNLESS OTHERWISE SPECIFIED
FRACTIONS ±1/64 DECIMALS .XX ± .010 .XXX ± .005
ANGLES ±1/2°

PART NO. X112−P19
NEXT ASSY.

MAUREY INSTRUMENT CORP.
4555 W 60th ST. CHICAGO, ILL. 60629

POTENTIOMETER, SERVO, CONDUCTIVE PLASTIC

CUSTOMER:

DRAWN BY	SCALE		
R.O.L.	1:1	112−P19	J
APP'D	DATE		
EM	4−4−77		

Appendix L - Circuit Diagram for Potentiometer Module

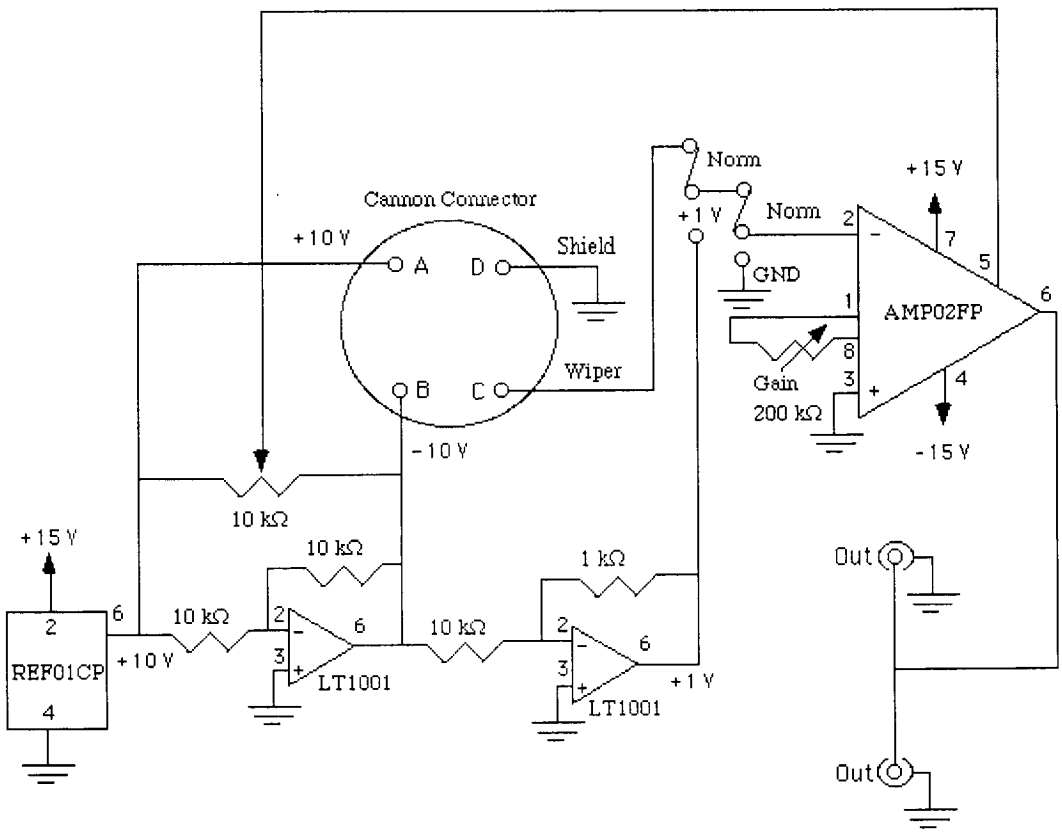

Appendix M - Data Sheet for EMG System

Bagnoli-4 EMG System
Specifications

All electrodes and systems are tested and calibrated before shipment to ensure that manufacturing specifications have been met. Performance according to specifications is guaranteed for environments devoid of noise sources. Examples of common noise sources include electric motors (such as those found on treadmills and fans) and high current power supplies. Performance according to specifications cannot be guaranteed if DelSys devices are used in conjunction with other equipment that has not been reviewed and approved by DelSys Inc. Examples include proprietary A/D cards and electric exercise equipment. DelSys reserves the right to change specifications without notice.

Electrode Specs>> **DETAILS** A/D Pinout>> **DETAILS**

Main Amplifier Unit

Electrical

Amplification/ Channel (overall)	100, 1000, 10000 V/V (±1%)
Frequency Response	20±5 Hz - 450±50 Hz, 40 dB/dec.
System Noise (R.T.I)	< 1.2 µV over specified BW
Maximum Output Voltage	±5 Volts
Isolation	3750 Vrms, 1 minute
Power Supply Leakage	< 100 µA
System Leakage Current	< 10 µA
Power Requirements	12 VDC, 60 mA (quiescent)
Signal Quality Check	50/60 Hz interference ±4.8 V saturation threshold

Mechanical

Number of Channels	4
Output Connectors	4 BNC, DSub-37F (click for pinout>>)
Operating Temperature	15°C to 40°C (59°F to 104°F)
Case Dimension	20 x 11 x 4 cm (7.9 x 4.3 x 1.6")
Weight	0.50 Kg (1.1 lbs)
Signal Quality Warning	Red LED, selectable audible buzzer

I/O Unit

Number of Electrode Inputs	4
Electrode Input Connectors	Hypertronics Corporation
Output connector	RJ-45 Modular Jack
Length of Tether	25 FT

Case Dimensions	6.0 x 6.0 x 2.5 cm (2.4 x 2.4 x 1.0")
Weight	71 g (2.5 Oz)

Appendix N - Data Sheet for EMG Electrodes

Bagnoli Electrodes
Specifications

The Bagnoli-Series Electrodes are specifically designed to be used with Bagnoli EMG Systems. Using these electrodes with equipment other than the Bagnoli EMG Systems may result in damage to the electrodes, and will void the warranty.

All electrodes are tested and calibrated before shipment to ensure that manufacturing specifications have been met. Performance according to specifications is guaranteed for environments devoid of noise sources. Examples of common noise sources include electric motors (such as those found on treadmills and fans) and high current power supplies. Performance according to specifications cannot be guaranteed if DelSys devices are used in conjunction with other equipment that has not been reviewed and approved by DelSys Inc. Examples include proprietary A/D cards and electric exercise equipment. DelSys reserves the right to change specifications without notice.

	DE 2.1	DE-3.1
Mechanical		
Number of Contacts	2	3
Contact Dimension (mm)	10.0x1.0	10.0x1.0
Contact Spacing (mm)	10.0	10.0, 10.0
Contact Material	99.9% Ag	99.9% Ag
Case Dimensions (mm)	41x20x5	41x20x5
Cable Length (m)	1.5	1.5
Connector	Hypertronics	Hypertronics
Temperature Range	0-40 °C	0-40 °C
Electrical		
Gain (V/V)	10 +2%	10 +2%
Bandwidth High Pass	DC	DC
Bandwidth Low Pass	open	open
Bandwidth Rolloff	N/A	N/A
Noise (RMS, R.T.I.)	1.2 µV	1.2 µV
CMRR @ 60 Hz (dB)	>80 dB	>80 dB
Supply Voltage	±4.5 - ±15 V	±4.5 - ±15 V
Supply Current	± 1 mA	± 2.5 mA
Input Impedance (ohm//pF)	$>10^{15}$//0.2	$>10^{15}$//0.2

Revised December, 2000.

Appendix O - Data Sheet for Angular Sensors

FAS-G Specifications

Range	Single axis (roll): 360 degrees
A/D Resolution	12 bits
D/A Resolution (output voltage)	12 bits
Dynamic Compensation	Closed loop digital control (0 to 50 Hz)
Angle Resolution	Roll: < 0.1 degrees (angle resolution specs. taken at most aggressive filter setting) (static)
Temperature Drift	Single axis: ±0.025 %/deg.C (temperature specs. represent 95% confidence intervals)
Nonlinearity	0.23% full scale (static)
Repeatability	0.10 degrees
Accuracy	Roll: ±1.0 degrees typical (accuracy specs. taken at constant ambient temp., tested with known sine and step inputs including angular rates to 300 deg/s)
Output Data Rate	6.5535 ms update interval (152.6 Hz)
Analog Output Modes	Gravity Inclination Angle- 0-360 deg 0-4096 v Gyro Compensated Inclination Angle- +/-300 deg/sec max 0-4096v Angular Rate- ax, ay bits 0-5 v
Digital Output Format	RS-232 serial (see appendix for Data Communications Protocol)
Transmission Rate	19200 bits/sec
Supply Voltage	5.2 volts DC min.
Supply Current	30 milliamps

Connector	8 pin mini DIN; mating connector available from MicroStrain or Digi-Key P/N CP-2080-ND or CUI Stack P/N MD-80
Operating Temperature	-40 to 85 deg Celsius
Enclosure (w/ tabs)	64 mm by 90 mm by 25 mm; 2.5" by 3.5" by 1.0"
Shock limit	1000g (unpowered); 500g (powered)

Appendix P - Data Sheet for Ultrasonic Sensor

Ultrasonic analog sensors, rectangular

UNDK 20U6914/S35A

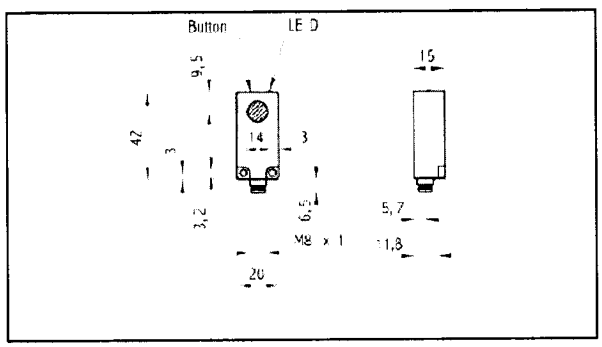

Technical Data	
scanning range Sd	20 - 200 mm
resolution	0.3 mm
output circuit	analog voltage output
housing style	rectangular
width /diameter	20 mm
height	42 mm
depth	15 mm
housing material	polycarbonate
connection	connector
scanning range close limit Sdc (Teach-in)	20 - 150 mm
scanning range far limit Sde (Teach-in)	20 - 150 mm
sonic beam angle	6°
sonic frequency	380 kHz
voltage supply range +Vs	15 - 30 VDC
residual ripple	< 10% Vs
supply current	< 35 mA
max. switching current	< 20 mA
output	0 - 10 V / 10 - 0 V
load resistance at +Vs>15V	-
load resistance at +Vs>24V	-
short circuit protection	yes
reverse polarity protection	yes
response time ton/toff	< 30 ms
linearity L	-
repeatability	< 0,5 mm
temperature drift	< 2% of distance to target Sd
temperature range	-10 ... +60 °C
protection class	IP 67
output indicator	yellow LED / red LED
adjustment	teach-in
adjustment aid	target display flashing
connector type	-
connector options	ESW 31A, ESG 32A

photo

connection diagram

internal and external Teach-in
compact housing

Appendix Q – Actuator Coupling

ACCESSORIES (CONTINUED)

COUPLINGS (See actuator model sections for SAE, ASA spline specifications.)

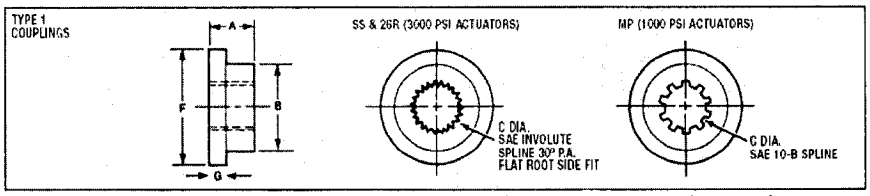

	Part No.	Model	A	B	C	F	G
For "SS" Models	451498 001	SS-1	1.00	1.75	20T 20/40P 1.0000PD.	3.50	0.50
	451498 002	SS-4	1.50	2.50	24T 16/32P 1.5000PD.	5.25	0.62
	451498 008	SS-8	2.00	3.00	30T 16/32P 1.8750PD.	6.00	0.75
	451498 003	SS-12	2.25	3.50	26T 12/24P 2.1667PD.	7.00	0.75
	451498 004	SS-40	3.50	5.00	26T 8/16P 3.2500PD.	10.50	1.00
	451498 006	SS-65	3.88	6.00	30T 8/16P 3.7500PD.	12.00	1.38
	451498 005	SS-130	5.50	8.00	34T 6/12P 5.1667PD.	16.00	1.38
For "MP" Models	26-11-241	MP 11	0.50	0.92	* 18T 40/80P 0.4500PD.	2.00	0.25
	26-11-240	MP 22	0.75	1.12	* 29T 40/80P 0.7250PD.	2.25	0.31
	26-11-176	MP 32 MP 34	1.03	2.31	1.25	4.75	0.50
	26-11-177	MP 63	1.75	3.63	2.00	5.25	0.63
	26-11-178	MP 84	2.13	4.13	2.50	6.00	0.75
	26-11-179	MP 105	2.50	5.25	3.00	7.25	0.88
	26-11-180	MP 116	3.00	6.25	3.50	8.50	1.00
	26-11-181	MP 128	4.25	7.25	4.00	10.00	1.25
For "26R" Models	26-11-5034	26R 2	1.63	2.31	26T 20/40P 1.3000PD.	3.75	0.50
	26-11-5035	26R 5	1.75	3.63	26T 16/32P 1.6250PD.	5.25	0.63
	26-11-5036	26R 10	2.13	4.13	26T 12/24P 2.1667PD.	6.00	0.75
	26-11-5037	26R 17	2.50	5.25	26T 10/20P 2.6000PD.	7.25	0.88
	26-11-5038	26R 31	3.00	6.25	32T 10/20P 3.2000PD.	8.50	1.00
	26-11-5039	26R 62	4.25	7.25	32T 8/16P 4.0000PD.	10.00	1.25
	26-11-5040	26R 124	5.25	8.75	38T 8/16P 4.7500PD.	12.25	1.75

*Involute Serration

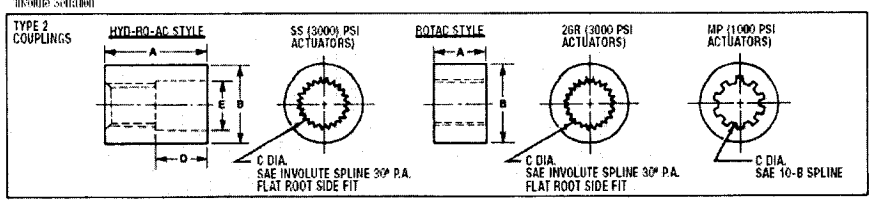

	Part No.	Model	A	B	C	D	E
For "SS" Models	451497 010	SS-2A	1.75	1.00	18T 32/64P 0.5625PD.	0.88	0.626
	451497 009	SS-3A	2.00	1.25	22T 32/64P 0.6875PD.	1.00	0.751
	451497 001	SS-1	2.00	1.75	20T 20/40P 1.0000PD.	1.00	1.126
	451497 002	SS-4	3.00	2.50	24T 16/32P 1.5000PD.	1.50	1.751
	451497 008	SS-8	4.00	3.00	30T 16/32P 1.8750PD.	2.00	2.126
	451497 003	SS-12	4.50	3.50	26T 12/24P 2.1667PD.	2.25	2.501
	451497 004	SS-40	6.00	5.00	26T 8/16P 3.2500PD.	3.50	3.754
	451497 006	SS-65	8.00	6.00	30T 8/16P 3.7500PD.	3.88	4.376
	451497 005	SS-130	10.00	8.00	34T 6/12P 5.1667PD.	5.50	6.001
For "MP" Models	26-11-182	MP 32 MP 34	1.63	2.00	1.25	—	—
	26-11-183	MP 63	2.13	3.25	2.00	—	—
	26-11-184	MP 84	2.50	3.75	2.50	—	—
	26-11-185	MP 105	3.00	4.75	3.00	—	—
	26-11-186	MP 116	4.25	5.75	3.50	—	—
	26-11-187	MP 128	4.25	5.75	4.00	—	—
For "26R" Models	26-11-5041	26R 2	1.63	2.00	26T 20/40P 1.3000PD.	—	—
	26-11-5042	26R 5	1.75	2.75	26T 16/32P 1.6250PD.	—	
	26-11-5043	26R 10	2.13	3.25	26T 12/24P 2.1667PD.	—	
	26-11-5044	26R 17	2.50	3.75	26T 10/20P 2.6000PD.	—	
	26-11-5045	26R 31	3.00	4.75	32T 10/20P 3.2000PD.	—	
	26-11-5046	26R 62	4.25	5.75	32T 8/16P 4.0000PD.	—	—
	26-11-5047	26R 124	5.25	7.00	38T 8/16P 4.7500PD.	—	—

OA-6

Appendix R – Safety Cam

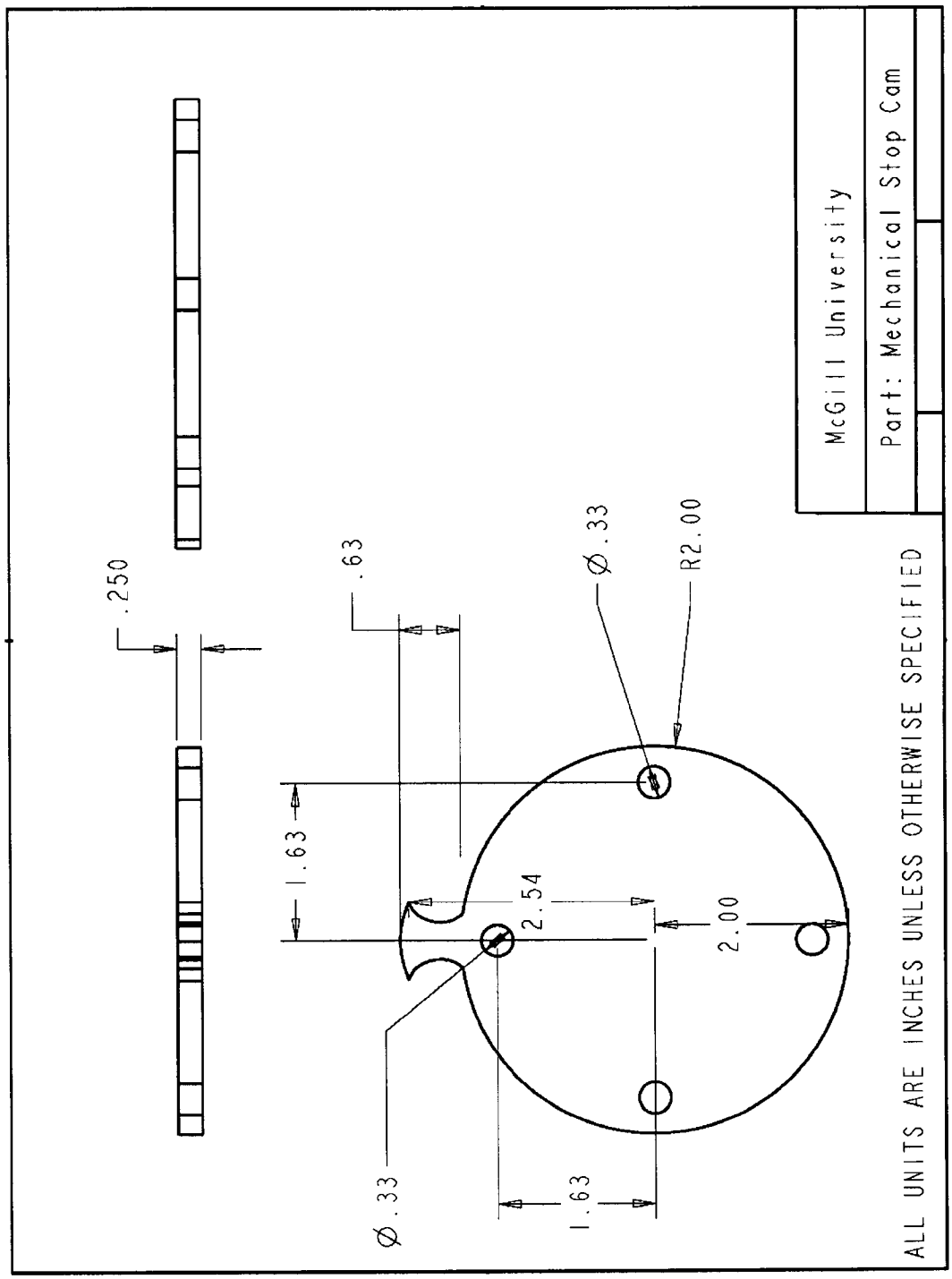

Appendix S - Foot Pedal End

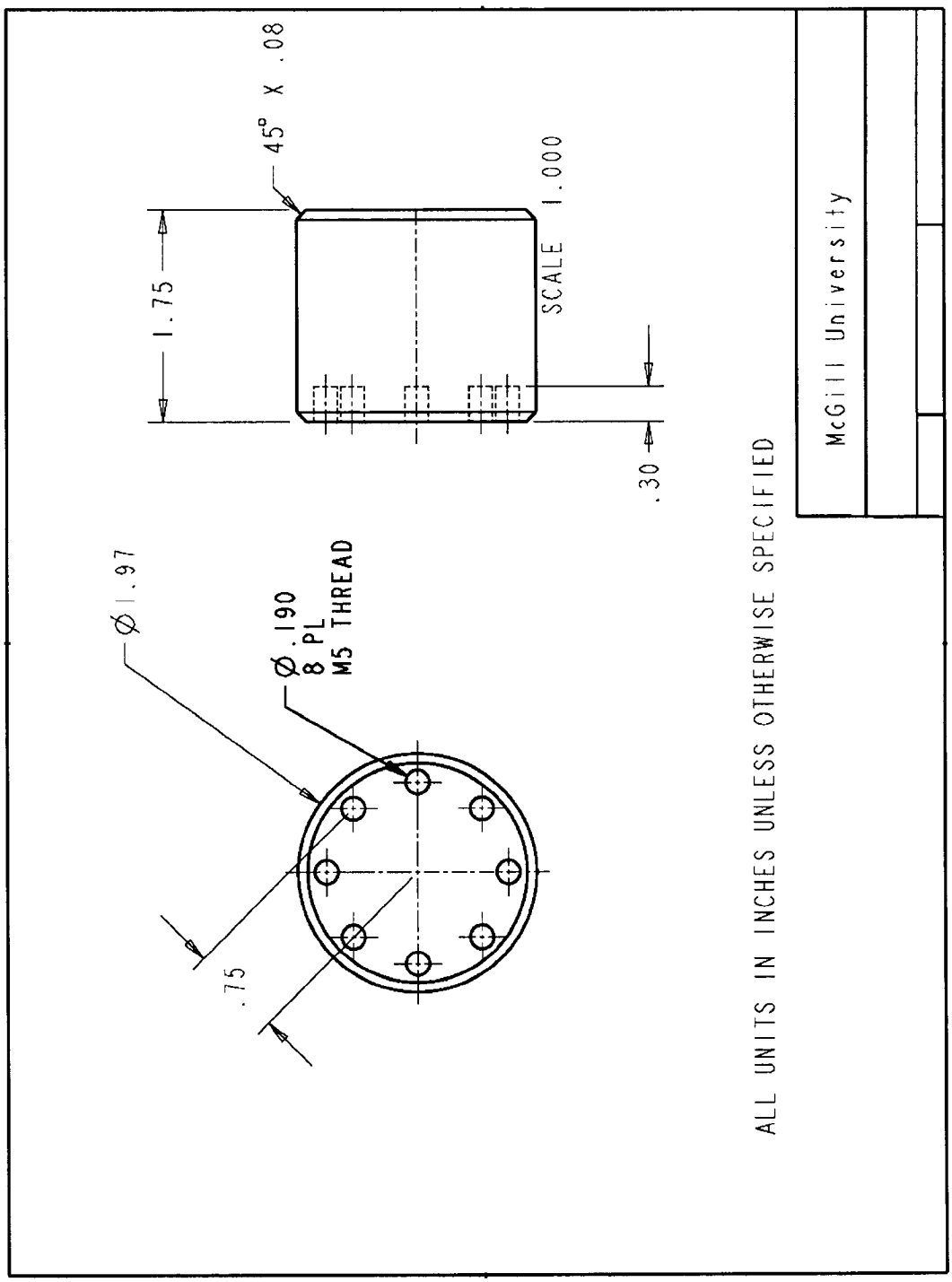

Appendix T – Torque Transducer / Foot Pedal Coupling